NUMERICAL MODELING OF THE COUPLED MECHANISMS UNDERLYING SALT ACCUMULATION IN AGRICULTURAL SOILS

by

Mehmet Tuna Arıcan

B.Sc. in Mechanical Engineering, Boğaziçi University, 2017

Submitted to the Institute of Environmental Sciences
in partial fulfillment of the requirements for the degree of
Master of Science
in
Environmental Technology

Boğaziçi University

2022

NUMERICAL MODELING OF THE COUPLED MECHANISMS UNDERLYING SALT ACCUMULATION IN AGRICULTURAL SOILS

APPROVED BY:

Prof. Dr. Nadim K. Copty (Thesis Advisor)	. . . . .
Prof. Dr. Ali Kerem Saysel	. . . . .
Assoc. Prof. Dr. Sezar Gülbaz	. . . . .

DATE OF APPROVAL: 27.01.2022

ACKNOWLEDGEMENTS

First of all, I would like to express my endless thanks and gratitude to my supervisor, Prof. Dr. Nadim K. Copty. The guidance and mentorship he provided me during this difficult process is the biggest factor in my writing this thesis. Thanks to him, I was able to overcome many of the problems I encountered. I am very lucky to have a professor like him. I will always remember his contributions to me.

I would like to thank my committee members Prof. Dr. Ali Kerem Saysel and Assoc. Prof. Dr. Sezar Gülbaz for spending their time for me and giving valuable suggestions for my thesis.

I would like to express my gratitude to Ahmet Ege İlhan, who helped me with all these challenging code development steps and doubled my energy every time when I needed it. I also would like to thank Elif Bal for her help and support.

I would like to say thank you to each and every member of my family for the respect and patience they have shown and for their continued support in completing this thesis.

And most importantly, I express my ultimate gratitude to İrem Özgüç for being there for me in every high and low moments, for looking after our love and friendship, for supporting and encouraging me when things got tough and for always believing in me more than myself.

Finally, financial support provided by TÜBİTAK BİDEB 2210-A is appreciated.

ABSTRACT

NUMERICAL MODELING OF THE COUPLED MECHANISMS UNDERLYING SALT ACCUMULATION IN AGRICULTURAL SOILS

Sodicity is a widespread significant threat to agricultural soils with adverse impact on soil properties and crop yields. The main processes underlying this environmental hazard is the excessive accumulation of sodium ions within the soil due to the use of saline groundwater for irrigation along with high rates of evaporation. This situation naturally puts agricultural soils in arid and semi-arid regions into that risk and therefore understanding the mechanisms behind it gains importance. Although, there have been numerous studies to understand and model the problem, a detailed modeling of the coupled processes can provide further insight into the different mechanisms and their interactions. The main processes included in the model include liquid and vapor water flow, solute transport and sorption, heat transport, and evapotranspiration assess, and according to that, a numerical 1D model code is developed using an explicit finite difference method. The model is applied to a series of different cases with crop and meteorological data adopted from the Konya Closed Basin a significant agricultural region of Turkey and under the risk of sodicity with increasing drought in recent years. The factors tested in assessing soil sodicity are irrigation water quality, crop type and climate change. The importance of including heat and vapor transport during such calculations are presented and discussed.

ÖZET

TARIMSAL TOPRAKLARDA TUZ BİRİKİMİNE DAYALI BİRLEŞTİRİLMİŞ MEKANİZMALARIN SAYISAL MODELLENMESİ

Sodisite, toprak özellikleri ve mahsul verimi üzerinde olumsuz etkisi olan tarım toprakları için yaygın ve önemli bir tehdittir. Bu çevresel tehlikenin altında yatan ana süreçler, yüksek buharlaşma oranları ile birlikte tuzlu yeraltı suyunun sulama için kullanılması nedeniyle toprakta aşırı sodyum iyonlarının birikmesidir. Bu durum doğal olarak kurak ve yarı kurak bölgelerdeki tarım topraklarını bu riske sokmakta ve bu nedenle arkasındaki mekanizmaları anlamak önem kazanmaktadır. Sorunu anlamak ve modellemek için çok sayıda çalışma olmasına rağmen, birleştirilmiş süreçlerin ayrıntılı bir modellemesi, farklı mekanizmalar ve bunların etkileşimleri hakkında daha fazla bilgi sağlayabilir. Modele dahil edilen ana süreçler, sıvı ve buhar su akışı, çözünen taşınımı ve sorpsiyon, ısı akışı ve evapotranspirasyon değerlendirmesini içerir ve buna göre, açık bir sonlu farklar yöntemi kullanılarak sayısal bir tek boyutlu model kodu geliştirilmiştir. Model, Türkiye'nin önemli bir tarım bölgesi olan ve son yıllarda artan kuraklık ile sodisite riski altında olan Konya Kapalı Havzası'ndan alınan mahsul ve meteorolojik verilerle bir dizi farklı duruma uygulanmıştır. Toprak sodisitesinin değerlendirilmesinde test edilen faktörler, sulama suyu kalitesi, ürün tipi ve iklim değişikliğidir. Bu tür hesaplamalar sırasında ısı ve buhar taşınımının dahil edilmesinin önemi sunulmuş ve tartışılmıştır.

TABLE OF CONTENTS

ACKNOWLEDGEMENTS iii
ABSTRACT iv
ÖZET v
TABLE OF CONTENTS vi
LIST OF FIGURES viii
LIST OF TABLES xii
LIST OF SYMBOLS xiii
LIST OF ABBREVIATIONS xvi
1. INTRODUCTION 1
2. LITERATURE REVIEW 10
3. METHODOLOGY 19
3.1. Water/Vapor Flow Equations 19
3.2. Heat Flow Equations 22
3.3. Solute Transport Equations 24
3.4. Numerical Discretization 27
3.5. Initial and Boundary Conditions 28
3.5.1. Boundary Conditions 28
3.5.2. Initial Conditions 33
4. MODEL VALIDATION 34
4.1. Water Flow Validation 34
4.2. Water Flow Coupled with Heat Flow Validation 38
4.3. Water Flow with Solute Transport Validation 40
5. RESULTS AND DISCUSSION 45
5.1. Ambient Conditions 45
5.2. Base Run 50
5.3. Case 1 – Non-Saline Groundwater Non-Sodic Soil 61
5.4. Case 2 – Climate Change Effects 66
5.5. Case 3 – Crop Type Effects 68
5.6. Case 4 – Vapor Flow Effects 70

6. CONCLUSIONS AND FUTURE RESEARCH.....76

REFERENCES.....79

LIST OF FIGURES

Figure 1.1. Schematic diagram of the vadose zone 2

Figure 1.2. Electrical conductivity and ionic strength relation for natural waters 4

Figure 1.3. Concentration of ions with distance from clay platelet 5

Figure 1.4. Water and vapor flow mechanisms 6

Figure 1.5. Solute transport mechanism with water flow 7

Figure 1.6. Geographical location of Konya along with annual rainfall contours 9

Figure 2.1. Van Genuchten and Brooks & Corey water retention curve comparison 11

Figure 2.2. Temperature effects on water flow 13

Figure 2.3. Simulated and measured distribution of water content θ (m^3 m^{-3}) 17

Figure 2.4. Simulated and measured distribution of temperature T (°C) 18

Figure 2.5. Simulated and measured distribution of electrical conductivity (EC) (S m^{-1}) 18

Figure 3.1. Schematic demonstration of water and heat flow 24

Figure 3.2. Relation of activity coefficients and ionic strength for ions in natural waters 25

Figure 4.1. Validation results of 1st run 36

Figure 4.2. Validation results of 2nd run 38

Figure 4.3. Validation results for temperature comparison 40

Figure 4.4. Validation results for solute concentration comparison 42

Figure 4.5. Validation results for solute adsorption 43

Figure 4.6. % Difference of adsorbed concentrations (daily basis) 43

Figure 5.1. Soil Temperatures as a function of time at different depths 46

Figure 5.2. Air Temperature and relative humidity as a function of time 46

Figure 5.3. Average wind speed and precipitation as a function of time 47

Figure 5.4. Daily distributed generated solar radiation from Table 5.1 47

Figure 5.5. Hourly distributions of air temperature, relative humidity and soil temperature at bottom boundary (Start Time: DOY: 130 Hour: 00:00) 48

Figure 5.6. Hourly distributions of incoming shortwave radiation, outgoing longwave radiation and net radiation 49

Figure 5.7. Hourly temperature, relative humidity and radiation (data are from Figure 5.5 and 5.6) 49

Figure 5.8. Irrigation scheduled from expected rain and evapotranspiration, actual precipitation ... 52

Figure 5.9. ESP and SAR values for the Base Run 53

Figure 5.10. Changes in hydraulic conductivity as a function of time at two different elevations for the Base Run 53

Figure 5.11. Soluble concentrations as a function of time for the Base Run 55

Figure 5.12. Exchangeable cation concentrations (sorbed concentrations) as a function of time for the Base Run 55

Figure 5.13. Soluble concentrations as a function of time and depth for the Base Run 56

Figure 5.14. Exchangeable cation concentrations as a function of depth and time for the Base Run 57

Figure 5.15. Cation fluxes at bottom of column as a function of time for the Base Run.....57

Figure 5.16. Water content as a function of time for the Base Run 58

Figure 5.17. Pressure head as a function of time for the Base Run 58

Figure 5.18. Liquid Water and vapor content over the entire column as a function of time for the Base Run 59

Figure 5.19. Water Content as a function of time and depth for the Base Run 60

Figure 5.20. Subsurface evaporation rates as a function of time and depth for the Base Run.....60

Figure 5.21. Temperature variations as a function of time for the Base Run 61

Figure 5.22. ESP and SAR values for Case 1 62

Figure 5.23. Hydraulic conductivities as a function of time at two depths for Case 1 63

Figure 5.24. Soluble concentrations for Case 1 64

Figure 5.25. Exchangeable cation concentrations for Case 1 64

Figure 5.26. Solute bottom flux for Case 1.....65

Figure 5.27. Liquid water and vapor content of the entire column as a function of time for 65

Figure 5.28. ESP and SAR as a function of time for Case 2.....66

Figure 5.29. Liquid water and vapor content of the entire column as a function of time for 67

Figure 5.30. Water flux at the bottom of the domain for the Base Run and Case 2 68

Figure 5.31. Water content as a function of depth and time for Case 2 68

Figure 5.32. Irrigation and precipitation of Case 3 69

Figure 5.33. ESP and SAR values for Case 3 70

Figure 5.34. ESP and SAR values for Case 4 71

Figure 5.35. Water content as a function of time for Case 4 71

Figure 5.36. Flux distributions over depth before and after irrigation event on day 191 in Base Run for given time 72

Figure 5.37. Flux distributions over depth before and after irrigation event on day 191 for Case 4 72

Figure 5.38. Total surface flux, liquid surface flux and vapor surface flux for the Base Run 73

Figure 5.39. Total surface flux, liquid surface flux and vapor surface flux for Case 4 73

Figure 5.40. Changes in temperature at different levels for Case 4 74

Figure 5.41. Subsurface evaporation / condensation in Case 4 74

Figure 5.42. Liquid water and vapor content of entire column as a function of time for Case 4 75

Figure 5.43. Relative humidity values for the Base Run and Case 4 75

LIST OF TABLES

Table 1.1. Classification for sodium hazard of soil....3

Table 1.2. Guidelines for saline-sodic water quality suitable for irrigation in terms of reduction potential of irrigation 4

Table 2.1. Penman-Monteith calculation constants of ASCE....16

Table 3.1. Extended Debye-Hückel Formula parameters 26

Table 3.2. Average total monthly rainfall (1929-2020) 33

Table 4.1. Water flow validation input parameters....34

Table 5.1. Average Monthly Solar Radiation 46

Table 5.2. Soil hydraulic parameters used in Base Run....50

Table 5.3. Irrigation Water Parameters 51

Table 5.4. Average maize height during growth season 51

Table 5.5. Evapotranspiration values of maize in 10 days interval....51

Table 5.6. Irrigation water parameters in Case 1 62

Table 5.7. Evapotranspiration rates of sugar beet in 10 days interval 69

LIST OF SYMBOLS

Symbol	Explanation	Unit
α	Van Genuchten Parameter	1/m
α	Enhancement Factor Calibration Parameter	-
c	Cloud Cover Fraction	-
C	Concentration in Aqueous Phase	mg/L
$\bar{C}$	Adsorbed Concentration	mg/g soil
C_0	Total Salt Concentration of The Aqueous Phase	meq/L
C_a	Volumetric Heat Capacity of Air	J/ (m^3 K)
C_n	Volumetric Heat Capacity of Solids	J/ (m^3 K)
C_p	Volumetric Heat Capacity of Porous Media	J/ (m^3 K)
C_{ppt}	Precipitated Phase	mg/g soil
C_v	Volumetric Heat Capacity of Vapor	J/ (m^3 K)
C_w	Volumetric Heat Capacity of Water	J/ (m^3 K)
$\overline{C_T}$	CEC	meq/g soil
d_r	Inverse Relative Distance Between Earth and Sun	-
D	Dispersion Coefficient	m^2/s
D_a	Diffusivity of Vapor in Air	m^2/s
D_v	Diffusivity of Vapor in Soil	m^2/s
e_{act}	Actual Vapor Pressure	kPa
e_{sat}	Saturated Vapor Pressure	kPa
E	Evaporation	m/s
ET_0	Evapotranspiration	m/s
f	Calibration Constant for Hourly Radiation	-
f_c	Clay Fraction of Soil	-
G	Soil Heat Flux	W/m^2
G_{sc}	Global Solar Constant	MJ/(m^2 min)
G_{wT}	Gain Factor	-
h	Pressure Head	m

H	Sensible Heat Flux	W/m^2
I	Ionic Strength	moles/L
K	Hydraulic Conductivity of Liquid Phase	m/s
K_{13}	Gapon Selectivity Constant	-
K_{14}	Gapon Selectivity Constant	-
K_{15}	Gapon Selectivity Constant	-
K_{LT}	Thermal Hydraulic Conductivity of Liquid Phase	m/s
K_r	Relative Hydraulic Conductivity	m/s
K_s	Saturated Hydraulic Conductivity	m/s
K_{vh}	Isothermal Hydraulic Conductivity of Vapor	m/s
K_{vT}	Thermal Hydraulic Conductivity of Vapor	m/s
l	Van Genuchten Parameter	-
L_0	Volumetric Latent Heat of Evaporation	J/m^3
m	Van Genuchten Parameter	-
n	Van Genuchten Parameter	-
q_c	Solute Flux	$mg/ (m^2 s)$
q_H	Heat Flux	W/m^2
q_L	Liquid Water Flux	m/s
q_v	Vapor Flux	m/s
q_w	Total Water Flux	m/s
r	Reduction Term of Hydraulic Conductivity	-
r_a	Aerodynamic Resistance	s/m
r_s	Soil Surface Resistance	s/m
R_n	Net Radiation	W/m^2
R_{nl}	Net Outgoing Longwave Radiation	W/m^2
R_{ns}	Net Incoming Shortwave Radiation	W/m^2
R_s	Measured Radiation	$MJ/ (m^2 d)$
R_{s0}	Extraterrestrial Radiation	$MJ/ (m^2 d)$
RH	Relative Humidity	-
RH_{air}	Relative Humidity of Air	-
S_e	Effective Water Saturation	-
S_h	Heat Storage	J/m^3

T	Temperature	° C
T_a	Air Temperature	° C
T_s	Surface Temperature	° C
T_t	Ratio of Shortwave Radiation	-
u_2	Wind Speed at 2 m	m/s
α	Surface Albedo	-
γ_i	Activity Coefficient	-
γ	Surface Tension	g/s^2
δ	Solar Declination	-
ε_a	Atmospheric Emissivity of Clear Sky	-
ε_s	Soil Surface Emissivity	-
η_e	Enhancement Factor	-
θ_a	Volumetric Soil Air Content	m^3/m^3
θ_L	Volumetric Water Content	m^3/m^3
θ_n	Volumetric Solid Content	m^3/m^3
θ_r	Residual Water Contend	m^3/m^3
θ_s	Saturated Water Content	m^3/m^3
θ_v	Volumetric Vapor Content	kg/m^3
λ	Soil Thermal Conductivity	W/ (m K)
ρ_a	Atmospheric Density of Air	kg/m^3
ρ_b	Soil Bulk Density	kg/m^3
ρ_v	Vapor Density	kg/m^3
ρ_{vs}	Saturated Vapor Density	kg/m^3
ρ_w	Liquid Water Density	kg/m^3
τ	Tortuosity Factor	-
φ	Latitude	radians
ω_s	Sunset Hour Angle	-

LIST OF ABBREVIATIONS

Abbreviation	Explanation
CEC	Cation Exchange Capacity
EC	Electrical Conductivity
ESP	Exchangeable Sodium Percentage
ET	Evapotranspiration
PDE	Partial Differential Equations
SAR	Sodium Adsorption Ratio
TAGEM	General Directorate of Agricultural Research and Policies of Turkey
TSMS	Turkish State Meteorological Service

1. INTRODUCTION

Sustainable crop production is increasingly being threatened as conditions such as climate, water availability and demand by increasing population change. To increase crop yield and income, farmers often tend to increase their water usage which inevitably is leading to depletion of water resources in numerous regions of the world. In many arid or semi-arid regions, farmers mostly rely on groundwater as their primary irrigation source because traditionally it is the most available water resource. According to previous studies 43% of total irrigation in the world is from groundwater (S. Siebert, 2010). However, as the water flows through rocks, minerals and salt ions are dissolved into the water and at the same time some of these minerals can be adsorbed or deposited onto soil particles especially when soil water is lost shortly by evaporation. Therefore, using groundwater as an irrigation source should be managed effectively as the high salt content, particularly sodium ions, can significantly reduce soil permeability (H. Frenkel, 1978) and limit water availability for plant uptake (M. Seilsepour, 2009). Consequently, mismanagement of groundwater for irrigation can reduce food security as well as the farmers' income in return. In this context, groundwater use and its effects on the soil should be examined to manage the risk mentioned. This type of hazard is commonly referred as "sodicity".

Soil has a porous structure consisting of solid soil particles (mix of silt, clay etc.), and cavities or voids. These voids are fully saturated with water below the water table and filled with air and water above it. The portion of the subsurface above the water table is called the unsaturated zone or vadose zone. As expected, the cavities, soil particles and fluids are not distributed uniformly along its depth. A schematic showing the different compartments of the subsurface is shown in Figure 1.1.

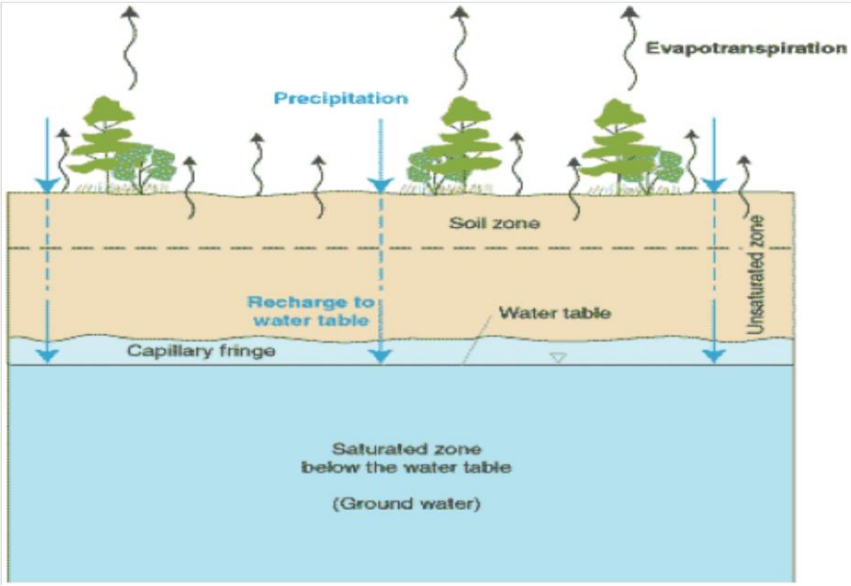


Figure 1.1. Schematic diagram of the vadose zone (Alley, Reilly, & Franke, 1999)

Mineral-rich groundwater carries various types of ions depending on its location. For assessing sodicity risk which relates to the accumulation of sodium in the soil, the most common cations are taken into account namely: calcium (Ca^{2+}), magnesium (Mg^{2+}), sodium (Na^{+}) and potassium (K^{+}) and hydrogen (H^{+}) as pH. In general, soil particles are negatively charged so cations tend to accumulate or adsorb on the surface of these particles according to their affinities. Sodicity is related to the accumulation of sodium ions, but it is affected by the presence of other ions and their relative affinity to the soil surface. Hence, to determine the adsorbed sodium, other cations should be considered as well. The ratio of adsorbed Na^{+} relative to the other adsorbed cations are expressed as a term called Exchangeable Sodium Percentage (ESP) and it is calculated as follows (Simunek & Suarez, 1994).

$$ESP = \frac{\overline{Na}^{+}}{CEC} \tag{1}$$

where $\overline{Na}^{+}$ is adsorbed sodium, also called as exchangeable sodium (meq/100g soil), and CEC is Cation Exchange Capacity (meq/100g soil). CEC represents the total number of sites available for cation adsorption. In general, sodic soil is classified by ESP greater than %15 and electrical conductivity (EC) lower than 4 (dS m^{-1}) as shown in Table 1.1 (Davis, Waskom, & Bauder, 2007).

Table 1.1. Classification for sodium hazard of soil

Classification	**EC (dS m^{-1})**	**ESP**	**Soil pH**	**Soil Physical Condition**
Sodic	<4	>15	>8.5	Poor
Saline-Sodic	>4	>15	<8.5	Varies
Slightly Saline	2-4	<15	<8.5	Normal
Saline	>4	<15	<8.5	Normal
High pH	<4	<15	>7.8	Varies

In practice, determining CEC is not an easy option as it is time consuming and costly. So, to decide whether the soil is sodic or not, other approaches are also given in the literature. In this context, sodium presence in soil moisture is taken as a key parameter. As a result, the ratio of the Na^+ concentration relative to the other cations in the solution is proposed and referred to as the Sodium Adsorption Ratio (SAR), calculated as (Richards, 1954):

$$SAR = \frac{Na^+}{\left(0.5\ (Ca^{+2} + Mg^{+2})\right)^{\frac{1}{2}}} \tag{2}$$

where the ionic concentrations are given in meq per liter. Once the SAR is calculated, the state of the soil can be decided by evaluating the SAR value, a common relationship between SAR and ESP is used which is given as follows (Richards, 1954):

$$ESP = 100\ \left(\frac{-0.0126 + 0.01475\ SAR}{1 + [-0.0126 + 0.01475\ SAR]}\right) \tag{3}$$

Instead of calculating SAR for soil water, it can also be calculated for irrigation water as well. By doing this, it allows for assessing sodicity risk of using the area specific groundwater directly onto the agricultural soil. As a common practice, there are widely used charts to predict if a type of groundwater has the potential for sodicity and soil clogging. It is used via direct measurement of irrigation water in terms of cations and electrical conductivity. One example to that is given in Table 1.2.

Table 1.2. Guidelines for saline-sodic water quality suitable for irrigation in terms of reduction potential of irrigation (Ayers & Tanji, 1981)

	EC dS/m		
SAR	NO PROBLEM	SLIGHT TO MODERATE	SEVERE PROBLEM
0 to 3	> 0.9	0.9 to 0.2	< 0.2
3 to 6	> 1.3	1.3 to 0.25	< 0.25
6 to 12	> 2.0	2.0 to 0.35	< 0.35
12 to 20	> 3.1	3.1 to 0.9	< 0.9
20+	> 5.6	5.6 to 1.8	< 1.8

Obviously, for these calculations EC is required and if there is a sample it is generally easy to measure it with a probe. But for numerical calculation purposes, it is not easy to determine accurately. As different models for estimating EC are proposed, most of them are related to total ion content of water or soil water. For this calculation, a widely used relationship is given in Figure 1.2 (Griffin & Jurinak, 1973) and according to this, EC can be found by Eq.4.

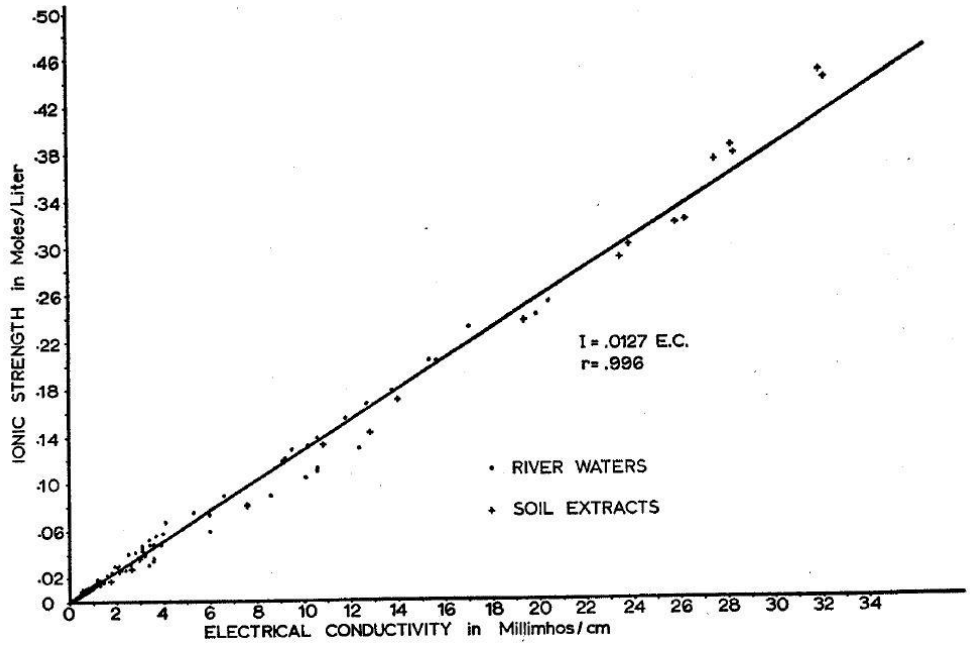


Figure 1.2. Electrical conductivity and ionic strength relation for natural waters (Griffin & Jurinak, 1973)

$$EC = 77 \times I \tag{4}$$

where I is ionic strength (mol/L), and although a wider range of I is shown on Figure 1.2, it is generally utilized for ionic strength between 0.0001 – 0.1 moles per liter for groundwater (Hem, 1961). Calculation of I is also given in Section 3.3.

Soil sodicity is a state of soil characterized by swelled clay particles which decrease the soil's infiltration rate. This infiltration rate is an important aspect for agricultural soil as the plant water uptake and growth is directly related to the water movement in the soil and especially in the root zone during the critical plant growth season. As seen from Eq. (2), while (Na^+) ions increase SAR value, calcium (Ca^{2+}) and magnesium (Mg^{2+}) ions reduce it. To understand the physics behind it, a closer look to clay behavior is required. Monovalent ions causes clay dispersion, which causes the soil pores to decrease. This in turn leads to lower permeability and infiltration rate. On the other hand, divalent ions create clay flocculation which increases average pore size and hence the permeability and infiltration rate. These effects of different ions on clay particles are depicted in the Figure 1.3.

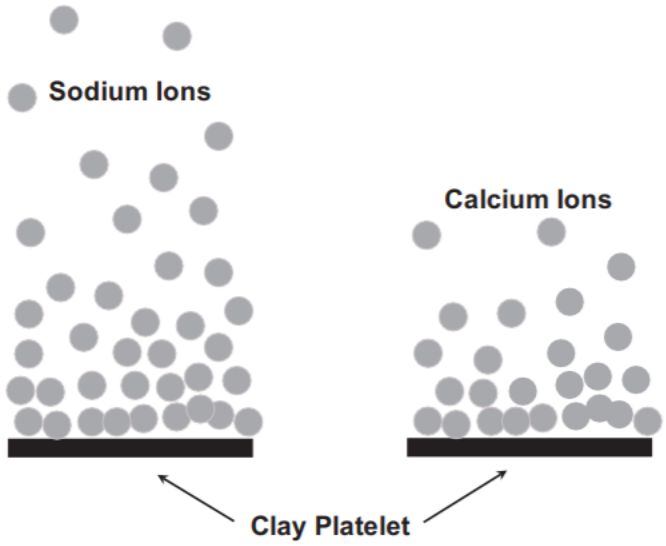


Figure 1.3. Concentration of ions with distance from clay platelet
(Hanson, Grattan, & Fulton, 1999)

The concentrations of solutes through the soil is an important aspect of sodicity. However, calculating concentration distributions is a complicated process which depends on water movement as well as heat transport. Change in water content at any depth alters the concentrations. However, change in water content may be caused by water flow and phase changes. Hence, heat becomes a significant player for determining water distribution as it changes liquid water transport parameters and its availability. Similarly, the generated vapor influences heat transport which makes this water-

vapor-heat balance, a coupled and complex mechanism. The schematic diagram in Figure 1.4 illustrates these processes.

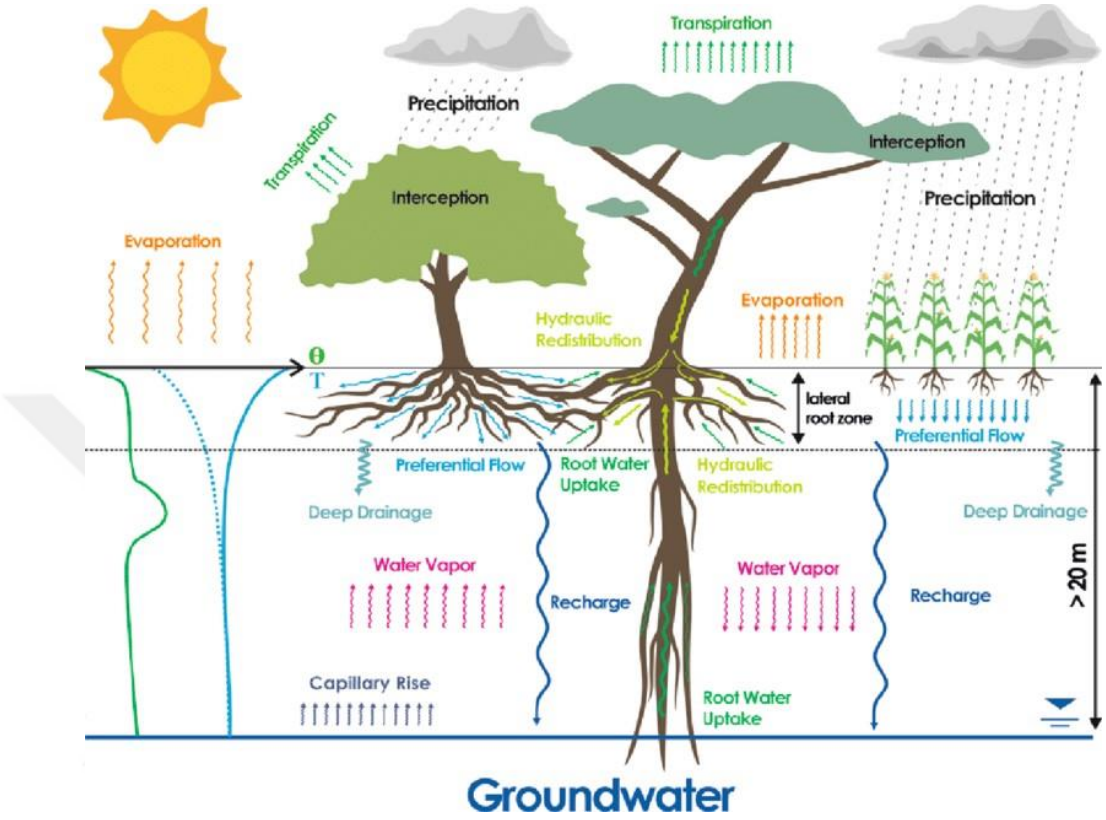


Figure 1.4. Water and vapor flow mechanisms (Beyer, 2016)

Apart from this, temperature influences solute absorption rates which also changes solute concentration distributions. Concentration distribution can also directly change water movement due to osmotic pressure. Therefore, modeling the water flow and solute transport in actual soils is governed by complex coupled processes that must be modeled together due to their strong interactions. These interactions are represented in the Figure 1.5 below.

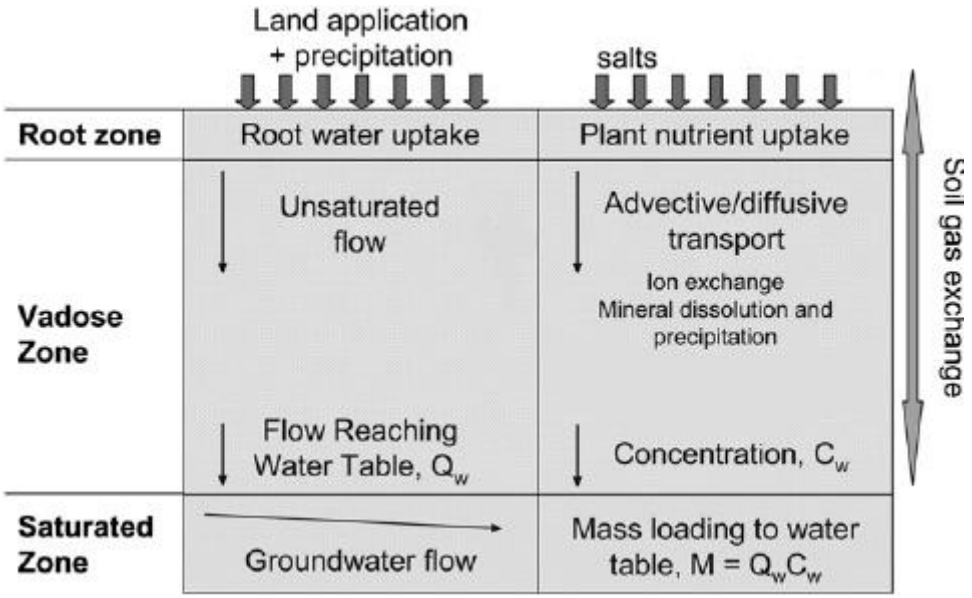


Figure 1.5. Solute transport mechanism with water flow (Miller, Rubin, Mayer, & Benito, 2008)

In examining real-world problems, like a field irrigated with groundwater, one should consider meteorological conditions, seasonal effects as well as crop properties, particularly its growth and water uptake characteristics. Diurnal variations of temperature, humidity, wind as well as water usage of crop types create significant fluctuations in soil-atmosphere interface on hourly basis. High temperature on the surface during summer with vegetation or significant rainfall during winter with non-to-short crop are good examples for such conditions. Implementing these highly variable conditions into the complex mechanisms mentioned above, makes the situation even more complicated.

Another important aspect in arid and semi-arid regions is the long periods of dry conditions along with high evaporation potential. The low discontinuous water content in the soil lowers the hydraulic conductivity of the soil while increasing the water vapor transport.

The high evaporation potential in arid and semi-arid regions, high levels of salinity and sodicity and the demand for increased food production has placed available water resources under significant stress. Indeed, numerous studies have shown that groundwater levels are being rapidly depleted. Many regions in Turkey and elsewhere have been experiencing unsustainable groundwater level drops of several meters per year. Anticipated climate change is likely to place even further burden on groundwater resources. There is a need therefore to develop effective tools for managing this vital resource. Numerical modeling has become a valuable and indispensable tool for calculated the soil water budget as well as for predicting solute transport within the vadose zone. To provide reliable predictions, models must somehow accurately simulate the coupled complex water flow and

solute transport. This is particularly true for the harsh conditions present in arid regions. These models typically represent the governing processes in terms of a series of differential equations that need to be solved jointly using accurate and efficient numerical schemes.

The model developed in this study will be applied, for demonstration purposes, to the Konya basin. The Konya basin located in the middle of the Anatolian peninsula consisting of wide plains mostly used for agricultural purposes (Figure 1.6). However, due to its geographical location, Konya is susceptible to drought which can adversely affect food security. According to recent studies, rainfall has decreased by about 10% in recent years, with increased temperatures (Berke, Dıvrak, & Sarısoy, 2014). Precipitation is expected to decrease further in the coming decades due to climate change. Uneducated irrigation alongside low drainage due to flat structure have brought sodicity to a significant level in Konya. Due to the sodicity, farmers have increased their irrigation as short-term measures which actually has made the long-term situation even worse. This excessive irrigation has led to total or partial loss of wetlands such as Salt Lake, the second largest lake of Turkey well known for being a habitat for wildlife. Because of the loss in water resources, quality and quantity of crop production deteriorated (Berke, Dıvrak, & Sarısoy, 2014).

Traditionally, local farmers of that area apply surface or flood irrigation (Dıvrak, İş, & Ayas, 2007). However, as groundwater resources get depleted, problems regarding water availability have arisen. Consequently, State Water Works (DSİ) and other agencies have tried to develop possible alternative solutions to alleviate water demands in corporation with farmers. For instance, applying drip irrigation techniques is more widely used these days. Producing crops with lower water consumption is also being suggested.

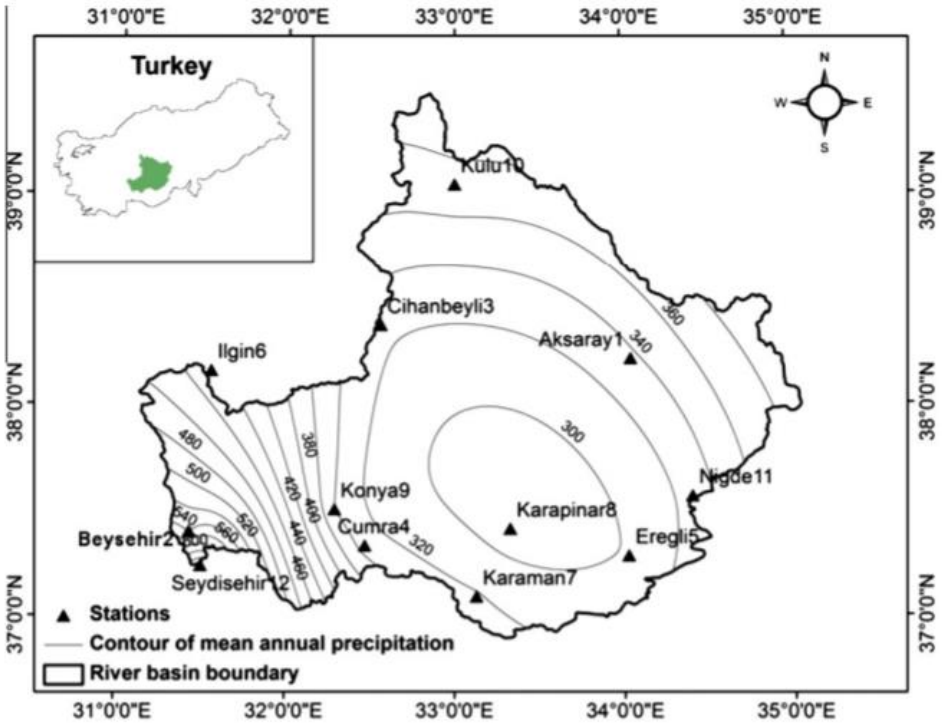


Figure 1.6. Geographical location of Konya along with annual rainfall contours (Dogan, Berktay, & Singh, 2012)

2. LITERATURE REVIEW

Subsurface flow has always been an interest for various fields of science and engineering including groundwater remediation activities, subsurface construction and investigation of agriculture dynamics which is the focus of this study. Understanding how crops are utilizing soil moisture and combining their behavior with soil characteristics is crucial to assure food security as well as soil productivity. Darcy's Law which describes one-dimensional (1D) flow in saturated porous media proposed by Henry Darcy in 1856 is also recognized as a starting point for subsurface flow theoreticians (Whitaker, 1985). As time goes by, interest expanded to water behavior within the unsaturated soil above the water table especially for agricultural sciences. Initially, the term "capillary flow" was used in attempt to explain the relationship between this capillary effect and water content (Narasimhan, 2005). A few decades later, in 1931, Richards, by examining the pressure field and water accumulation observed in soil, offered the most common equation of water flow in variably saturated porous media which, to this date, constitutes the backbone of soil-related numerical studies. This equation describes relationship between water content and unsaturated water flow including capillary and gravitational action and is given as (Richards, 1931):

$$\frac{\partial \theta}{\partial t} = \left[K \left(\frac{\partial h}{\partial x} + 1 \right) \right] \tag{5}$$

where, K is hydraulic conductivity for unsaturated zone [LT^{-1}], h is pressure head [L], θ is volumetric water content [L^3L^{-3}], t and x are temporal and spatial variables, respectively. The flux term of this equation is given as:

$$q = K \left(\frac{\partial h}{\partial x} + 1 \right) \tag{6}$$

where q is water flux density [LT^{-1}]. As it is seen above, volumetric water content is the common variable for such computations as it represents the moisture distribution within the soil relative to the pore volume which makes it more meaningful than expressing water volume only while comparing soils. The volumetric water content, θ, is calculated as:

$$\theta = \frac{(W_{wet\ soil} - W_{dry\ soil})}{W_{dry\ soil}} \frac{\rho_b}{\rho_w} \tag{7}$$

where $W_{wet\ soil}$ and $W_{dry\ soil}$ are the weights of wet and dry soil extracts [M], ρ_b is soil dry bulk density (kg m^{-3}), ρ_w is the water density (kg m^{-3}).

A few decades after these findings, scientists started to examine ways to solve Richards' equation more robustly in order to predict agricultural soil water more practically. For this purpose, the relationships between the variables seen in Eq. (5) are required. This led to more detailed studies and the development of various models based on the examination soil samples at macroscopic scale. Two widely used examples of these models are Brooks and Corey (Brooks & Corey, 1964) and Van Genuchten (Genuchten, 1980) relationships. The former one is said to be more valid for coarse textured soil and characterized by "J" shaped water retention curve while the latter is more valid for a wider range of soil including fine textured and characterized by "S" shaped water retention curve (Valiantzas, 2011). An example for these retention curves are given in Figure 2.1 for comparison purposes.

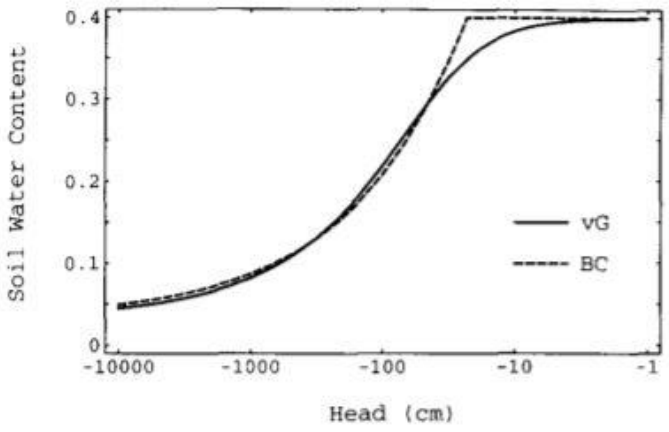


Figure 2.1. Van Genuchten and Brooks & Corey water retention curve comparison (Stankovich & Lockington, 1995)

According to Van Genuchten, when air entry is considered, θ becomes,

$$\theta = \theta_r + \frac{\theta_s - \theta_r}{(1 + (|ah|)^n)^m} \tag{8}$$

θ_r is residual volumetric water content and θ_s is saturated water content, h is pressure head [L], a is inverse of air entry value [L^{-1}] and n and m are some independent empirical constants. θ_r, θ_s, n and m can be found empirically from experimentally a derived soil water retention curve. The

unsaturated zone hydraulic conductivity (also called capillary conductivity), K, is expressed in terms of the saturated state value as follows.

$$K(h,x) = K_s(x)K_r(h,x) \tag{9}$$

where, K_r is the dimensionless relative hydraulic conductivity and K_s is the saturated zone hydraulic conductivity [LT^{-1}]. For calculating K_r, Van Genuchten used Mualem's statistical analysis for pore size-permeability relation and came up with the formula given as (Genuchten, 1980),

$$K_r = S_e^l\left[1 - (1 - S_e^{1/m})^m\right]^2 \tag{10}$$

where S_e is effective water saturation, m and l are model parameters. S_e is calculated as,

$$S_e = \frac{\theta - \theta_r}{\theta_s - \theta_r} \tag{11}$$

Early scientists tried to solve the water transport equation algebraically. However, it became apparent from the complex highly non-linear relationship depicted in Figure 2.1 that this is not possible except for selected simplified problems. As digital computers become available, numerical methods became more popular and for soil scientists it was inevitable that this opportunity will also be used to solve water transport problems (Cass, Campbell, & Jones, 1984). This development encouraged the relevant scientists to go on more challenging and complex transport mechanisms. As research about water flow in soil continued, temperature dependence of flow characteristics gained importance. In 1957, De Vries, included temperature effects in the calculation of the flux and introduced the vapor phase and its interaction with liquid phase (Philip & Vries, 1957).The impacts of these developments are described in detail in the Methodology chapter of this thesis. Grifoll and Josep Ma Gaspo (2005) conducted a study to show temperature and evaporation effects in water flow. Figure 2.2 shows how water flow and water content changes with temperature, for the case of surface temperature around 50°C most of the water flows as vapor near the surface.

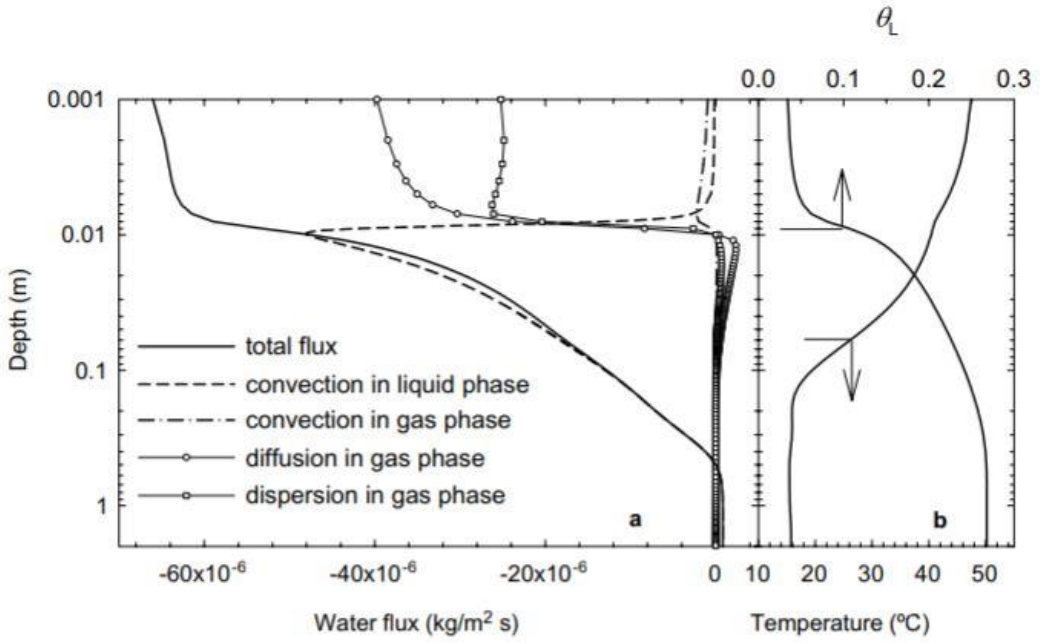


Figure 2.2. Temperature effects on water flow (Arrows indicate corresponding axis for the line atop) (Grifoll & Josep Ma. Gasto, 2005)

In lab experiments, it is practical to maintain surface temperature constant (Sakai, Toride, & Simunek, 2009) (Grifoll & Josep Ma. Gasto, 2005) which allows temperature effect to be observed more clearly. However, in real applications, the surface temperature is dynamic, determined by energy transfer occurring at soil-atmosphere interface, hence the need for a mass conservation equation. The energy balance at the surface is given as follows (van Bavel & Hillel, 1976).

$$R_n - H - L_0E - G = 0 \tag{12}$$

where R_n is the net radiation (Wm^{-2}), H is the sensible heat flux (Wm^{-2}), L_0E is the latent heat flux (Wm^{-2}), L_0 is the volumetric latent heat of evaporation (Jm^{-3}), E is the rate of evaporation (ms^{-1}) and G is the surface heat flux (Wm^{-2}). In cases where vegetation is present, evaporation is replaced by evapotranspiration term which will be described later. According to this energy balance, heat supplied by the sun to the surface is converted to other forms of energy such as longwave outgoing terrestrial radiation, convection, conduction and surface evaporation. For solving Eq. (13), each term is calculated separately. These terms are given as (van Bavel & Hillel, 1976),

$$R_n = R_{ns} + R_{nl} = (1 - a)R_s + \{[(1 - 084c)\varepsilon_a + 0.84c]\sigma T_a^4 - \varepsilon_s \sigma T_s^4\} \tag{13}$$

$$H = C_a \frac{T_s - T_a}{r_s + r_a} \tag{14}$$

$$G = \lambda \frac{\partial T}{\partial x} \tag{15}$$

$$L_0 E = L_0 \times \left(\frac{RH_{surface} \times \rho_{sat}(T_{surface}) - RH_{air} \times \rho_{sat}(T_{air})}{r_a + r_s} \right) \tag{16}$$

where C_a is the volumetric heat capacity of air (=1200 J m^{-3} K^{-1}), r_s is the surface resistance to heat transfer (sm^{-1}), r_a is the aerodynamic resistance to heat transfer (sm^{-1}), $RH_{surface}$ and RH_{air} are relative humidity of soil surface and air, $\rho_{sat}(T)$ is saturated vapor density at a given temperature (kg m^{-3}), R_{ns} is the net short wave radiation (Wm^{-2}), R_{nl} is the net longwave radiation (W m^{-2}), a is the surface albedo, R_s is the incoming shortwave solar radiation (W m^{-2}), ε_a is the atmospheric emissivity of clear sky, ε_s is the emissivity of soil which represents reflection of longwave radiation from soil surface, c is the fraction of cloud cover, σ is Stefan-Boltzmann Constant (=4.90×10^{-9} MJm^{-2} K^{-4} d^{-1}), T_a is the ambient air temperature (K), T_s is the soil surface temperature (K).

As it is seen above, all four variables are function of surface temperature. In literature, for numerical methods, there are two ways of using these equations. In the first approach, the only unknown variable is the surface temperature, T_s, which is computed iteratively. The second method is to use *G* as a boundary condition surface flux and determine surface temperature correspondingly (Campbell & Norman, 1998).

Evaporation is a term which defines the case where bare soil conditions are prevailing. However, vegetation presence can change water heat and solute transport significantly. Specifically, plants draw water along with ions as root uptake and their body and leaves create shade which interferes with heat balance over surface. Most of the water taken by plants are evaporated from their leaves, which is called transpiration, and relatively low portion remains within the plant (Cass, Campbell, & Jones, 1984). Accordingly, total evaporation over a vegetated surface, in other words evapotranspiration, is different than evaporation. Calculating this term, ET_0, was obviously challenging but Penman made a set of experiments for computing this term. The experiments were bare soil and grass surface soil are measured and a consequently a rate of evapotranspiration is given as (Penman, 1948),

$$ET_0 = \frac{mR_n + \rho_a c_p \delta_e g_a}{\lambda_v (m + \gamma)} \tag{17}$$

where m is slope of saturation vapor pressure curve (Pa K^{-1}), R_n net irradiance (W m^{-2}), ρ_a is the water vapor density in the atmosphere (kg m^{-3}),c_p heat capacity of air (J kg^{-1} K^{-1}) ,δ_e is specific humidity (Pa), g_a surface aerodynamic conductance (m s^{-1}), λ_v is latent heat of vaporization (J kg^{-1}), γ is psychrometric constant (Pa K^{-1}). In the following years this model was improved by Monteith, and the combined Penman-Monteith Equation is proposed (Monteith, 1965).

$$ET_0 = \frac{m(R_n - G) + \frac{\rho_a c_p \delta_e}{r_a}}{\lambda_v \left(m + \gamma \left(1 + \frac{r_s}{r_a} \right) \right)} \tag{18}$$

However, calculating evapotranspiration is still challenging as it involves many terms which require quite intense prework. To make this approach more practical, Food and Agricultural Organization (FAO) published a step-by-step calculation manual in 1998 (Allen, Pereira, Raes, & Smith, 2006). Similarly, to standardize this calculation for wider acceptance, American Society of Civil Engineering (ASCE) published in 1999 their version of Penman-Monteith Equation which is given as follows:

$$ET_{sz} = \frac{0.408m(R_n - G) + \gamma \frac{C_n}{T + 273} u_2 ({e_s}^0 - e_a)}{m + \gamma(1 + C_d u_2)} \tag{19}$$

where ETsz = the standardized reference evapotranspiration (ms^{-1}), C_n is the numerator constant for the reference crop type and C_d is the denominator constant for the reference crop type, u_2 is wind measured at height of 2m, ${e_s}^0$ saturated vapor pressure and e_a is ambient air vapor pressure. ASCE divides crop types into two as long crop and short crop (i.e., clipped grass). The constants for these crop types are given in Table 2.1.

Table 2.1. Penman-Monteith calculation constants of ASCE

Calculation Time Step	**Short Reference Crop ET**		**Tall Reference Crop ET**		**Units of ET**	**Units of R_n and G**
	C_n	C_d	C_n	C_d		
Daily	900	0.34	1600	0.38	mm d^{-1}	MJ m^{-2} d^{-1}
Hourly, Daytime	37	0.24	66	0.25	mm h^{-1}	MJ m^{-2} h^{-1}
Hourly, Nighttime	37	0.96	66	1.7	mm h^{-1}	MJ m^{-2} h^{-1}

Solute transport studies are also a significant part of understanding plant growth mechanisms. For this purpose, the processes which ions went through were closely examined and their presence in soil is classified in three phases cited as precipitation, adsorption and aqueous (Simunek & Suarez, 1994). From conservation of mass, the transport equation can be written as:

$$\frac{\partial(\theta C)}{\partial t} + \rho_b \frac{\partial \bar{C}}{\partial t} + \rho_b \frac{C_{ppt}}{\partial t} = \frac{\partial}{\partial x}\left(\theta D \frac{\partial C}{\partial x} - q_L C\right) \tag{20}$$

where C is solute concentration in aqueous phase (mg/L), $\bar{C}$ is adsorbed concentration (mg/g soil), C_{ppt} is precipitated phase (mg/g soil), ρ_b is bulk density (kg/m^3), D is dispersion coefficient (m^2/s). To solve this equation, $\bar{C}$ and C_{ppt} are calculated as a function of C. At this point, different approaches have been made in literature.

Two common examples to these approaches are using partition coefficient which is more widely utilized for single ion and using selectivity coefficients for multi-ion problems. The former one offers several isotherms for the modelling of solute adsorption such as the linear, Freundlich and Langmuir. A general formula of these isotherms is (Simunek, Genuchten, & Sejna, 2006),

$$\bar{C} = \frac{k_d C^{\beta}}{1 + \eta_f C} \tag{21}$$

where k_d is the distribution coefficient [L^3M^{-1}], η_f and β are empirical constants. When $\beta = 1$, Eq. (21) becomes the Langmuir equation; when $\eta_f = 0$, it is Freundlich Equation and when $\beta = 1$ and $\eta_f = 0$, the equation represents linear adsorption. When more than one solute is considered, this equation is required to be solved for each ion. However, soil has a total adsorption capacity which it

can accommodate, referred to as cation exchange capacity CEC, and therefore the adsorbed concentrations of these ions are not independent from each other. To overcome this problem, a popular approach is using Gapon selectivity coefficients (Šimůnek, Šejna, Saito, Sakai, & Genuchten, 2013). At the end ESP and SAR values are calculated as a variable indicating combined effects of different ions. Details can be found in section 3.3, Solute Transport Equations.

Once the solute distributions are obtained, including the change in hydraulic conductivity (or permeability) is needed for observing clogging effect in numerical models. Numerous studies have been made for this purpose and some relations have been offered. For example, in some studies, linear relationships between permeability and SAR value are given (Chaudhari, 2001). In one experiment, pH and total electrolyte concentration are also found as influencing factors (Quirk & Schofield, 1955).

Apart from SAR, electrical conductivity is also a required value for assessing sodicity. As electrical conductivity can be a measurement, it can also be determined from calculated solute distributions. In the literature, there are very few work that have included all these effects while calculating solute transport. However, a good work conducted by Noborio, showed how solute concentrations variate with respect to environmental conditions (Noborio, McInnes, & Heilman, 1996b). In the figures below, it can be seen that when the surface is dry and temperature is high, concentrations (expressed as electrical conductivity) get higher. The vertical axis is depth; the left figure is simulated, the middle is measured, and right column is the difference.

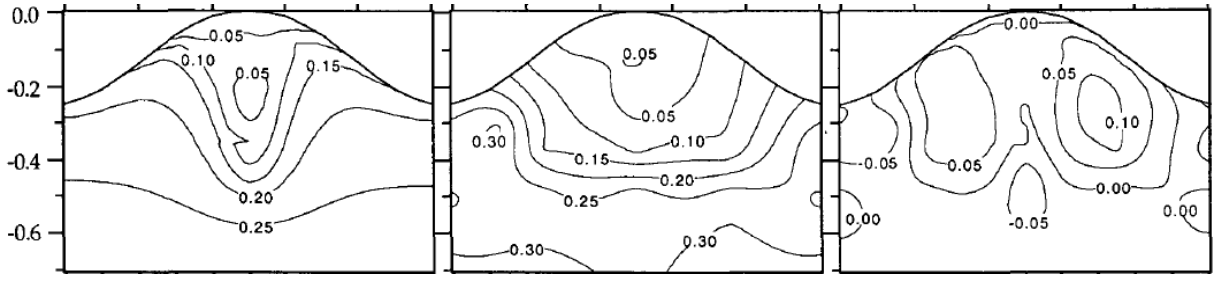


Figure 2.3. Simulated and measured distribution of water content θ (m^3 m^{-3})
(Noborio, McInnes, & Heilman, 1996b)

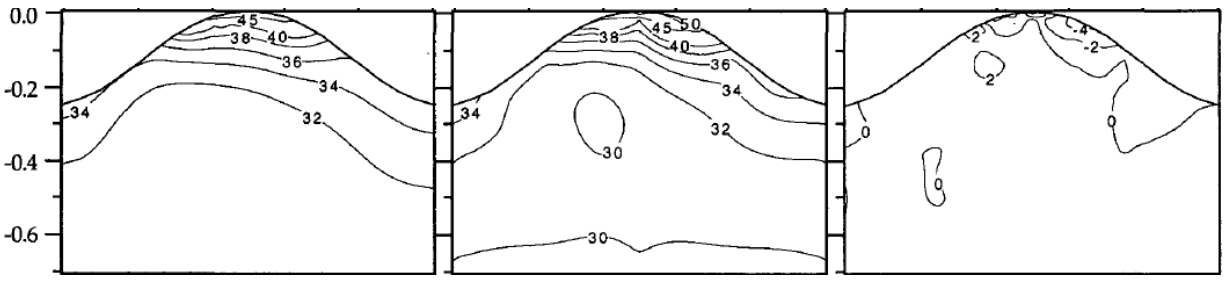


Figure 2.4. Simulated and measured distribution of temperature T (°C)

(Noborio, McInnes, & Heilman, 1996b)

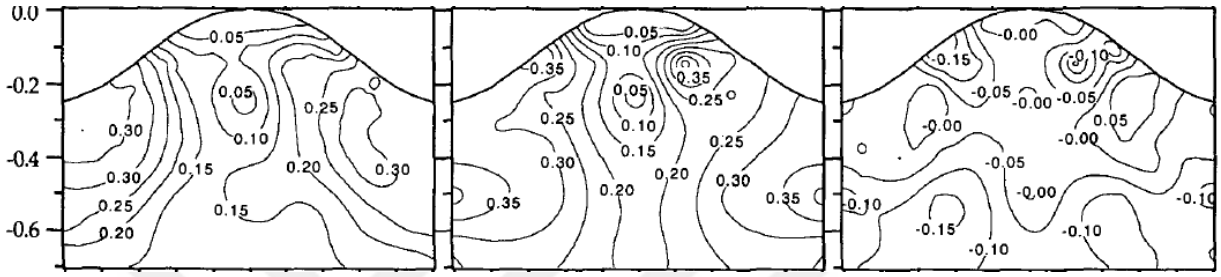


Figure 2.5. Simulated and measured distribution of electrical conductivity (EC) (S m^{-1})

(Noborio, McInnes, & Heilman, 1996b)

3. METHODOLOGY

This section describes the numerical model developed to simulate water flow and solute transport through a soil column. The model in this work consists of coupled mechanisms which should be solved simultaneously. However, the highly non-linear characteristic of each Partial Differential Equation (PDE), creates a challenge for building the model structure. As there exists no convenient commercial tool to solve the problem as described in this work, a new code is developed in MATLAB. However, a widely used public domain program, HYDRUS, is used for model validation of certain modules of the code by comparing a hypothetical soil in both programs.

The model consists of four separate PDEs that must be solved jointly. Two of them are combined relate to water and vapor flow. Heat and solute transports are the other two. The following sections present in detail the equations incorporated in the model and the numerical scheme used to solve these highly non-linear equations.

3.1. Water/Vapor Flow Equations

For water retention model, Van Genuchten equations are used as described in Eq. (8-11). Also, as sodicity can cause reduced permeability and possibly clogging of the soil, an additional factor is applied to Eq. (9) that reduces the hydraulic conductivity with the accumulation of or adsorbed sodium ion concentration as given in Eq. (22). This factor is explained in more detailed at the end of Section 3.3, Solute Transport Equations.

$$K(h,x) = r \times K_s(x) K_r(h,x) \tag{22}$$

where r is a reduction factor depending on adsorbed ions.

Volumetric water content, θ, changes as the water evaporates. Although Richards equation could be enough for some cases, it should be expanded by adding thermal effects and resulting vapor flow for obtaining more realistic results especially for dry soils such as the Konya basin in the summer months which is being used in this study for demonstration. First, total water content, θ_T, is defined as follows (Saito, Simunek, & Mohanty, 2006).

$$\theta_T = \theta + \theta_v \tag{23}$$

where, θ_v is the water vapor content [L^3L^{-3}]. Thus, the expanded version of Richards equation becomes (Saito, Simunek, & Mohanty, 2006),

$$\frac{\partial \theta_T}{\partial t} = \frac{\partial}{\partial x}\left[(K_{Lh} + K_{vh})\left(\frac{\partial h}{\partial x} + 1\right) + (K_{LT} + K_{vT})\frac{\partial T}{\partial x}\right] \tag{24}$$

where K_{Lh} is the isothermal hydraulic conductivity of liquid phase [LT^{-1}], K_{vh} is the isothermal hydraulic conductivity of vapor [LT^{-1}], K_{LT} is the thermal hydraulic conductivity of liquid phase [$L^2T^{-1}K^{-1}$] and K_{vT} is the thermal hydraulic conductivity of vapor [$L^2T^{-1}K^{-1}$]. The isothermal flow combined with gravitational and thermal effect will be considered for modelling the 1D flow in porous media. Moreover, q_L, q_v and q_w are the liquid, vapor and total water flux densities, respectively [LT^{-1}], which can be expressed as follows (Philip & Vries, 1957).

$$q_v = -K_{vh}\left(\frac{\partial h}{\partial x} + 1\right) - K_{vT}\frac{\partial T}{\partial x} \tag{25}$$

$$q_L = -K_{Lh}\left(\frac{\partial h}{\partial x} + 1\right) - K_{LT}\frac{\partial T}{\partial x} \tag{26}$$

$$q_w = q_v + q_L \tag{27}$$

The term of K_{LT} can be written as (Saito, Simunek, & Mohanty, 2006),

$$K_{LT}(T) = K_{Lh}(h)\left(hG_{wT}\frac{1}{\gamma_0}\frac{d\gamma}{dT}\right) \tag{28}$$

where G_{wT} is the gain factor, taken as 7 for sand (Noborio, McInnes, & Heilman, 1996a), which shows temperature dependence of water retention, γ is the surface tension [MT^{-2}], and γ_0 is the surface tension at 25°C (= 71.89 g s^{-2}) and when T in °C, γ is found as follows in g/s^2 and,

$$\gamma = 75.6 - 0.1425T - 2.38 \times 10^{-4}T^2 \tag{29}$$

The vapor conductivities, K_{vh} and K_{vT} , account for the vapor transport due to diffusion through air within the soil particles. So, an expanded Fick's Law combined with ideal gas approach is applied (Noborio, McInnes, & Heilman, 1996b).

$$K_{vh} = \frac{D_v}{\rho_w}\rho_{vs}\frac{M_w g}{RT}RH \tag{30}$$

$$K_{vT} = \frac{D_v}{\rho_w}\eta_e RH\frac{d\rho_{vs}}{dT} \tag{31}$$

where D_v is the vapor diffusivity in soil [L^2T^{-1}], ρ_w is the water density (=1000 kg/m^3), ρ_{vs} is saturated vapor density [ML^{-3}], M_w is the molecular weight of water (=0.018015 kg/mol), g is gravitational acceleration (=9.81 m/s^2), R is the universal gas constant (=8.314 J/mol/K), η_e is the enhancement factor (Cass, Campbell, & Jones, 1984) and RH is the relative humidity. The soil vapor diffusivity, D_v, is calculated as follows from the vapor diffusivity in free air (Saito, Simunek, & Mohanty, 2006).

$$D_v = \tau a_v D_a \tag{32}$$

$$D_a = 2.12 \times 10^{-5}\left(\frac{T}{273.15}\right)^2 \tag{33}$$

where τ is tortuosity factor, a_v is the porosity filled with air, D_a is the diffusivity of vapor in air (m^2s^{-1}) at temperature T in Kelvin. And saturated vapor density, ρ_{vs}, in kg/m^3 is found as follows (Saito, Simunek, & Mohanty, 2006),

$$\rho_{vs} = 10^{-3}\left(\frac{\exp\left(31.3716 - \frac{6014.79}{T} - 7.92495 \times 10^{-3}T\right)}{T}\right) \tag{34}$$

The relative humidity, RH can be computed as (Philip & Vries, 1957),

$$RH = \exp\left(\frac{hM_w g}{RT}\right) \tag{35}$$

Since evaporation is assumed to happen rapidly, the water and vapor are generally in equilibrium. As they are expressed in density terms, the equilibrium is obtained as follows.

$$\rho_v = \rho_{vs} RH \tag{36}$$

And finally, the volumetric water vapor content, θ_v, is expressed in terms of volumetric water content (Saito, Simunek, & Mohanty, 2006).

$$\theta_v = \rho_v \frac{\theta_s - \theta}{\rho_w} = \rho_{vs} RH \frac{\theta_s - \theta}{\rho_w} \tag{37}$$

The enhancement factor, η_e, in Eq. (38) is used to express increases in thermal vapor flux due to liquid island formation and increased temperature gradients in the air phase. To illustrate for clay, it is calculated as follows (Cass, Campbell, & Jones, 1984).

$$\eta_e = a + 3\frac{\theta}{\theta_s} - (a-1)\exp\left(-\left(\left(1 + \frac{2.6}{\sqrt{f_c}}\right)\frac{\theta}{\theta_s}\right)^4\right) \tag{38}$$

where f_c is the mass fraction of clay in the soil, a is a calibration parameter commonly taken as 9.5 (Cass, Campbell, & Jones, 1984).

Instead of solving equation Eq. (24) directly, flux terms are found separately and used for the next time steps' θ calculation. New h values are found by inverse calculation using the Van Genuchten relation.

3.2. Heat Flow Equations

Heat flows through the porous media due to vaporization, conduction and convection within the liquid phase, conduction through solid particles and convection within the vapor phase can be written as (Nassar & Horton, 1992),

$$C_p(\theta)\frac{\partial T}{\partial t} + L_0\frac{\partial \theta_v}{\partial t} = \frac{\partial}{\partial x}\left(\lambda(\theta)\frac{\partial T}{\partial t}\right) - C_w\frac{\partial q_L T}{\partial x} - C_v\frac{\partial q_v T}{\partial x} - L_0\frac{\partial q_v}{\partial x} \tag{39}$$

where L_0 is latent heat of evaporation [$ML^{-1}T^{-2}$], $\lambda(\theta)$ is the soil thermal conductivity [$MLT^{-3}K^{-1}$], $C_p(\theta)$ is the porous media heat capacity [$ML^{-1}T^{-2}K^{-1}$], C_w is the liquid phase heat capacity and C_v is the heat capacity of vapor phase.

λ is calculated as (Chung & Horton, 1987),

$$\lambda(\theta) = b_1 + b_2\theta + b_3\theta^{0.5} \tag{40}$$

where b_1, b_2 and b_3 are some empirical parameters ($Wm^{-1}K^{-1}$). Heat flux q_H is calculated as follows (Sakai, Toride, & Simunek, 2009).

$$q_H = -\lambda\frac{\partial T}{\partial x} + C_v(T - T_r)q_v + C_w(T - T_r)q_L + L_0 q_v \tag{41}$$

where T_r is an arbitrary reference temperature taken as 15 °C. Heat storage within the soil is calculated as follows (Sakai, Toride, & Simunek, 2009).

$$S_h = C_s(T - T_r)\theta_n + C_v(T - T_r)\theta_v + C_w(T - T_r)\theta_w + L_0\theta_v \tag{42}$$

where S_h is heat storage (Jm^{-3}). C_s (=1.92 MJ m^{-3} K^{-1}) is the volumetric heat capacities of dry soil particles. θ_n is volumetric solid content [L^3L^{-3}]. C_p term in Eq. (39) is calculated as (Sakai, Toride, & Simunek, 2009),

$$C_p = C_s\theta_n + C_v\theta_v + C_w\theta_L \tag{43}$$

so, the conservation of energy equation is (Sakai, Toride, & Simunek, 2009),

$$\frac{\partial S_h}{\partial t} = -\frac{\partial q_H}{\partial x} \tag{44}$$

and instead of solving equation Eq. (39), Eq. (41-44) are solved separately in order to get heat flux terms at any time step. After that, S_h values are calculated for next time step and next T values are found by inverse calculation of Eq (36).

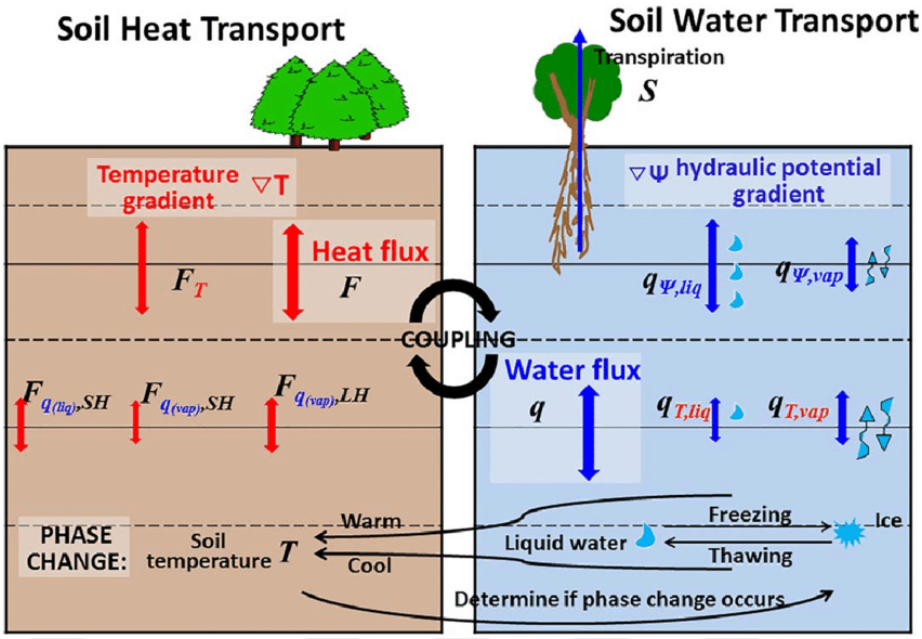


Figure 3.1. Schematic demonstration of water and heat flow (Wang & Yang, 2018)

3.3. Solute Transport Equations

For problems involving soil sodicity, the main solutes of concern are Na^+, Ca^{2+}, Mg^{2+} and K^+ which are carried by liquid water. It is assumed that Na^+, Ca^{2+}, Mg^{2+} and K^+ ions do not undergo any degradation or precipitation. Moreover, gas phase partitioning is neglected. Hence, the solute is just transported according to the 1D advection-dispersion model though the aqueous phase with sorption on porous media. Indeed, the adsorbed concentration distribution over the time and space domains is one of the main interests of this study. Briefly, the transient form of the solute transport equation, which is a reduced form of Eq. (20), in porous media can be expressed as (Ingrid Y. Padill & Conklin, 1999),

$$-\frac{\partial q_L c_w}{\partial x}+\frac{\partial}{\partial x}\left(\theta D\frac{\partial c_w}{\partial x}\right)=\frac{\partial \theta c_w}{\partial t}+\frac{\partial \rho_b \bar{c}}{\partial t} \tag{45}$$

where c_w is solute concentration in the aqueous phase [ML^{-3}], $\bar{c}$ is solute concentration adsorbed to the soil [MM^{-1}], D is hydrodynamic dispersion coefficient [L^2T^{-1}] which includes molecular diffusion as well, and ρ_b is the soil bulk density [ML^{-3}]. ρ_b is assumed to be constant.

Eq. (45) should be solved for the four ions of concern. For determining the effects of other ions' presence, CEC is taken into account and Gapon Selectivity Coefficients are used by assuming no site

remains empty. Implementing these coefficients requires solving of a system of algebraic equations which are given below (Šimůnek, Šejna, Saito, Sakai, & Genuchten, 2013).

$$\overline{C_T} = \overline{Ca}^{2+} + \overline{Mg}^{2+} + \overline{Na}^{+} + \overline{K}^{+} \tag{46}$$

$$K_{13} = \frac{\overline{Mg}^{2+}}{\overline{Ca}^{2+}} \frac{(Ca^{2+})^{\frac{1}{2}}}{(Mg^{2+})^{\frac{1}{2}}} \tag{47}$$

$$K_{14} = \frac{\overline{Ca}^{2+}}{\overline{Na}^{+}} \frac{(Na^{+})}{(Ca^{2+})^{\frac{1}{2}}} \tag{48}$$

$$K_{15} = \frac{\overline{Ca}^{2+}}{\overline{K}^{+}} \frac{(K^{+})}{(Ca^{2+})^{\frac{1}{2}}} \tag{49}$$

where $\overline{C_T}$ is the CEC (meq/g soil), (Ca^{2+}), (Mg^{2+}), (K^{+}) and (Na^{+}) are ion activities calculated assuming ionic strength of 0.01M. For calculating ion activities, an activity coefficient is needed (=1 for ideal solution) for each ion. Figure 3.2 can be used for rapid determination of activity coefficient.

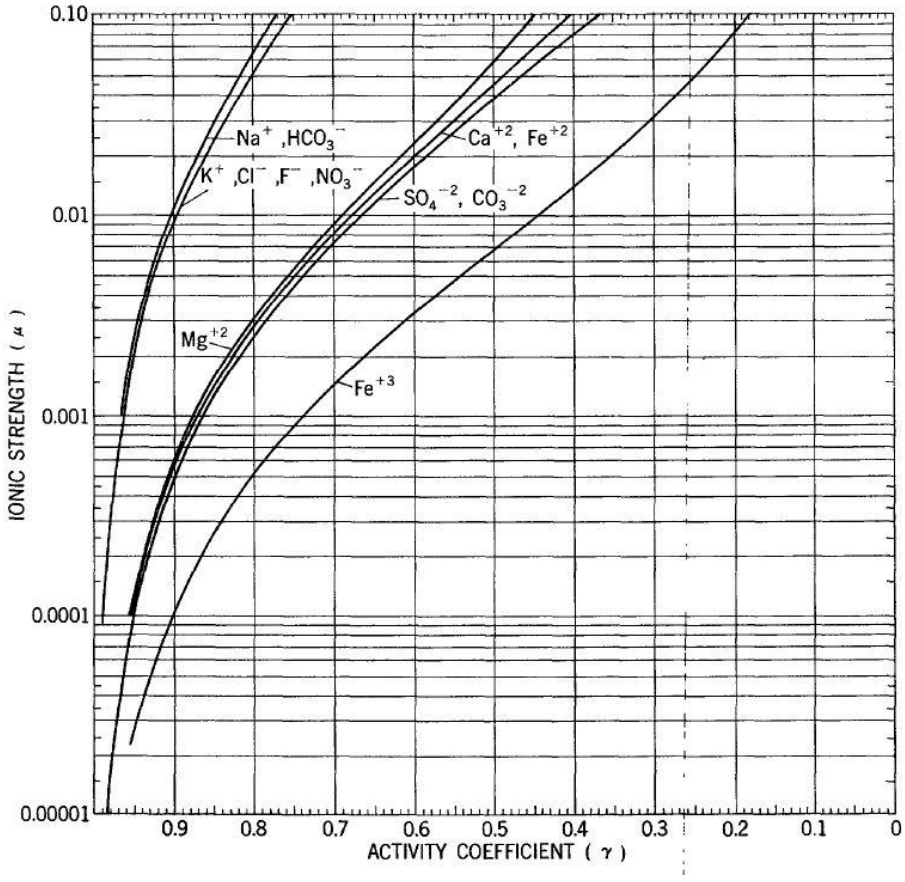


Figure 3.2. Relation of activity coefficients and ionic strength for ions in natural waters (Hem, 1961)

Another option, which adopted in this study, is to calculate activity coefficients from Extended Debye-Hückel Formula, given as (Truesdell & Jones, 1974),

$$ln\gamma = -\frac{A\,z^2\sqrt{I}}{1 + Ba\sqrt{I}} \tag{50}$$

where A ($M^{-1/2}$) and B ($M^{-1/2}$ nm^{-1}) are constants depending only upon the dielectric constant, density, and temperature, z is the ionic charge in protonic units, a (nm) is two adjustable parameters, and I is the ionic strength (M). The parameters for applying Eq. (50) to different ions are given in Table 3.1 and ion activities are found as given in Eq. (51).

$$\left(C_i{}^{z+}\right) = \gamma_i C_i \qquad i = Ca, Mg, Na, K \tag{51}$$

Table 3.1. Extended Debye-Hückel Formula parameters

	Ca	**Mg**	**Na**	**K**
A ($M^{-1/2}$)	0.5085			
B ($M^{-1/2}$ nm^{-1})	3.281			
a (nm)	0.6	0.8	0.4	0.3
z(+)	2	2	1	1

Solving Eq. (45) for each ion is not independent from each other so solving the four equations is required. However, since these equations are nonlinear, reaching a solution is not trivial. For simplicity, at the beginning of a timestep, the sorption term is neglected. After calculating the concentration from Eq. (45), new adsorbed values are determined using Eq. (46-49) and these adsorbed masses are subtracted from the aqueous concentrations. This sequential approach introduces some error, but it can be neglected for short time steps. The Gapon Selectivity Coefficients are found from initial distributions.

After calculating the concentration distributions, its effect on hydraulic conductivity reduction must be determined. This is done as described above (r term in Eq. (22)) assuming no pH effect. This term is calculated as (McNeal, 1968),

$$r = 1 - \frac{cx^n}{1 + cx^n} \tag{52}$$

$$x = f_{mont}\, 3.6 \times 10^{-4} ESP^{*} d^{*} \tag{53}$$

$$ESP^{*} = \max\left(0, ESP - (1.24 + 11.63\, log C_0)\right) \tag{54}$$

$$ESP = 100\, \frac{\overline{Na}}{CEC} \tag{55}$$

$$d^{*} = \begin{cases} 0 & C_0 \geq 300 \dfrac{meq}{L} \\ 356.4\, {C_0}^{-\frac{1}{2}} + 1.2 & C_0 < 300 \dfrac{meq}{L} \end{cases} \tag{56}$$

$$n = \begin{cases} 1 & ESP < 25 \\ 2 & 25 \leq ESP \leq 50 \\ 3 & ESP > 50 \end{cases} \tag{57}$$

$$c = \begin{cases} 35 & ESP < 25 \\ 932 & 25 \leq ESP \leq 50 \\ 25000 & ESP > 50 \end{cases} \tag{58}$$

where c and n are empirical parameters, and x is a swelling factor, f_{mont} is fraction of montmorillonite in the soil (=0.1) (McNeal, 1968), ESP^{*} is the adjusted exchangeable sodium percentage, d^{*} is the adjusted interlayer spacing [L], ESP is Exchangeable Sodium Percentage, C_0 is total salt concentration of the aqueous phase (meq/L). As seen from Eq. (55), reduction factor is proportional to sorbed concentration of sodium and hence SAR.

3.4. Numerical Discretization

These set of PDEs are solved numerically by using an explicit finite difference method assuming that changes in natural systems do not occur significantly on the order of seconds. For this purpose, the 1 m long soil column is considered as a 1D workspace. The length is divided into 25 cells and time increments are taken to be between 10 and 30 seconds, depending on the variation of the governing parameters such as the hydraulic conductivity and computation stability.

3.5. Initial and Boundary Conditions

3.5.1. Boundary Conditions

For water flow, the bottom of the column is set to water table which means pressure head, h, is zero. The bottom temperature is also fixed. It is set to a constant value of 15°C for validation runs. However, during this model's application to the Konya plain, the fixed bottom temperature is taken from the data given by meteorological service of Turkey for a specific day of the year. For solutes, the cation concentrations at the bottom of the column are fixed to groundwater quality data observed in Konya (Bozdağ, 2014).

For the upper boundary, water evaporates from bare soil or evapotranspiration takes place when there is crop on top. For bare soil surface evaporation is calculated as follows (Daamen & Simmonds, 1996),

$$E = \frac{\rho_s - \rho_a}{r_a + r_s} \tag{59}$$

where ρ_a is the water vapor density in the atmosphere (kg m^{-3}), ρ_s is the water vapor density at surface (kg m^{-3}), r_s is the soil surface resistance to vapor flow (sm^{-1}) and r_a is the aerodynamic resistance to vapor flow (s m^{-1}). r_s is calculated as follows (Griend & Owe, 1994).

$$r_s = 10 \exp\left(35.63\left(0.15 - \theta_{top}\right)\right) \tag{60}$$

where θ_{top} is near-surface moisture content. r_a is a bit more complex parameter calculated as follows (Allen, Pereira, Raes, & Smith, 2006).

$$r_a = \frac{\ln((z_m - d)/z_{om}) * \ln((z_h - d)/z_{oh})}{u_2\, k^2} \tag{61}$$

where z_m is wind measurement height (m), z_{om} is surface roughness for momentum (m), z_h is temperature and humidity measurement height (m), z_{om} is surface roughness for heat and vapor transport (m), d is zero place displacement for wind, u_2 is wind corrected for 2 meters and k is von Karman constant (=0.41). The calculation of these variables requires plant height, h_c (m), and once it is known they are calculated as follows (Allen, Pereira, Raes, & Smith, 2006).

$$d = 0.67 \times h_c \tag{62}$$

$$z_{om} = 0.123 \times h_c \tag{63}$$

$$z_{oh} = 0.1 \times z_{om} \tag{64}$$

And u_2 (m/s) is given as,

$$u_2 = u_z * \frac{4.87}{\ln(67.8\, z_m - 5.42)} \tag{65}$$

where u_z is measured wind (m/s) at the height of z_m (m).

On the other hand, evapotranspiration is calculated by using the Penman-Monteith formula, given in Eq. (18), as discussed in (Allen, Pereira, Raes, & Smith, 2006). Evapotranspiration values are calculated for three different crop types. Apart from evaporation and evapotranspiration, precipitation, which is defined based on meteorological data and an assumed irrigation pattern are applied additionally. The sum of these 4 time-dependent terms gives the total water flux. For validation runs, upper surface water flux is set to a constant value for different time intervals.

For temperature at the upper boundary, energy balance must be considered. The energy balance equation is given in (Noborio, McInnes, & Heilman, 1996a) as follows.

$$R_n - H - L_0(E \; or \; ET_0) - G = 0 \tag{66}$$

where R_n is the net radiation (Wm^{-2}), H is the sensible heat flux (Wm^{-2}), L_0E is the latent heat flux (Wm^{-2}), L_0 is the latent heat of evaporation, G is the surface heat flux (Wm^{-2}). From this equation, G value is applied as boundary heat flux. R_n and H are calculated by using meteorological data measurements such as incoming solar radiation and air temperature, T_a, and geographical location of Konya.

Recall net radiation is calculated as (Brutsaert, 1982),

$$R_n = R_{ns} + R_{nl} = (1 - a)R_s + \{[(1 - 084c)\varepsilon_a + 0.84c]\sigma T_a^4 - \varepsilon_s \sigma T_s^4\} \quad (67)$$

T_a and R_s are generally measured data but the rest of the variables, if not given as measurements, are usually calculated. Surface albedo, a, calculated as (van Bavel & Hillel, 1976),

$$\begin{matrix} a = 0.25 & \theta_0 < 0.1 \\ a = 0.35 - \theta_0 & 0.1 \leq \theta_0 \leq 0.25 \\ a = 0.10 & \theta_0 > 0.25 \end{matrix} \quad (68)$$

where θ_0 is the water content at soil surface and for simplicity it is sometimes taken as 0.23 which represents the value for short grass (Allen, Pereira, Raes, & Smith, 2006). Soil surface emissivity, ε_s, is calculated as (van Bavel & Hillel, 1976),

$$\varepsilon_s = \min(0.9 + 0.18\theta, 0) \quad (69)$$

and atmospheric emissivity of clear sky, ε_a, is calculated as (Brutsaert, 1982),

$$\varepsilon_a = 1.24\left(\frac{e_{act}}{T_a}\right)^{\frac{1}{7}} \quad (70)$$

$$e_{act} = RH_{air} \times e_{sat} \quad (71)$$

$$e_{sat} = 0.6108e^{17.27\left(\frac{T_a}{T_a + 237.3}\right)} \quad (72)$$

where e_{act} is the actual vapor pressure (kPa), e_{sat} is saturated vapor pressure (kPa) calculated from air temperature, T_a(°C). Like T_a, RH_{air} is relative humidity of air and also a measured meteorological data. As last term in Eq. (67), cloud cover, c, is calculated as (Cass, Campbell, & Jones, 1984),

$$c = (0; 2.33 - 3.33T_t; 1) \quad (73)$$

where T_t is ratio of shortwave radiation. c has minimum value of zero which means clear sky and maximum value of 1 representing overcast. T_t is calculated as,

$$T_t = \frac{R_s}{R_{s0}} \tag{74}$$

where R_s is measured value and R_{s0} is extraterrestrial radiation (Wm^{-2}), in other words potential irradiance a geographical site can get theoretically. In this context, R_a is calculated as (Allen, Pereira, Raes, & Smith, 2006),

$$R_a = \frac{24(60)}{\pi} G_{sc} d_r [(\omega_s sin\varphi sin\delta) + (cos\varphi cos\delta sin\omega_s)] \tag{75}$$

where R_a is extraterrestrial radiation on plane over spherical globe, G_{sc} is solar constant (=0.0820 $MJm^{-2}min^{-1}$ or 1366 Wm^{-2}), d_r is inverse relative distance between earth and sun, ω_s is sunset hour angle, φ is the latitude in radians and δ is solar declination. As expected, d_r and δ are changing with day of the year. Their expressions are given as,

$$d_r = 1 + 0.033 \cos\left(\frac{2\pi}{365} J\right) \tag{76}$$

$$\delta = 0.409 \sin\left(\frac{2\pi}{365} J - 1.39\right) \tag{77}$$

where J is the number of the day of the year between 1st of January to 31st of December, 1 to 365, respectively. Sunset hour angle, ω_s, calculated as follows.

$$\omega_s = \arccos(-tan\varphi tan\delta) \tag{78}$$

Once R_a is calculated, to find R_{s0} the only thing remaining is to adjust R_a according to elevation. This relation is given in Eq. (79).

$$R_{s0} = (0.75 + 2 \times 10^{-5} z) R_a \tag{79}$$

where z is elevation above sea level (m). By using these equations, in Eq. (67), R_n becomes a function of T_s. Generally, radiation, relative humidity and temperature measurements are given as daily values. But in some cases, for which hourly data are needed, they are calculated by using the distribution equations given below.

$$sine = sin\varphi sin\delta + cos\varphi cos\delta \cos\left(\frac{2\pi}{24}(t - 12)\right) \tag{80}$$

$$S_t = f \times \max(R_s sine, 0) \tag{81}$$

$$T_{air} = T_{air_{daily}} + \left(\frac{T_{max} - T_{min}}{2}\right) \cos\left(\frac{2\pi}{24}(t - 13)\right) \tag{82}$$

$$RH_{air} = RH_{daily} + \left(\frac{RH_{max} - RH_{min}}{2}\right) \cos\left(\frac{2\pi}{24}(t - 1)\right) \tag{83}$$

$$RH_{\min} = \frac{e_{day}}{e_{max}} \tag{84}$$

$$RH_{\min} = min\left(2RH_{min} - RH_{daily}; 1\right) \tag{85}$$

where t is time in hours, e_{day} and e_{max} are calculated by using mean and maximum values of Eq. (72), f is a calibration parameter to equalize sum of hourly radiation values to daily total.

H is calculated as follows (van Bavel & Hillel, 1976).

$$H = C_a \frac{T_{surface} - T_a}{r_a + r_s} \tag{86}$$

where C_a is the volumetric heat capacity of air (=1200 J m^{-3} K^{-1}), r_a is the aerodynamic resistance to heat transfer (s m^{-1}) and r_s is the soil surface resistance to heat transfer (s m^{-1}). For the validation runs, the surface temperature of the column is assumed to be a constant value or a sinusoidal distribution.

Solutes are added to the soil through irrigation assuming that the local groundwater is used for irrigation (Bozdağ, 2014). Thus, their flux are calculated according to water balance at the surface. When there is no irrigation, the solute flux reduces to zero. In the presence of irrigation, more evaporation leads to higher solute concentration at the surface. On the other hand, precipitation which is assumed to be free of any ions lower the solute concentrations in the soil. In the validation runs no surface solute flux is assumed at top the top boundary while saline water table is assumed to be present at the bottom.

Irrigation scheduling needs to be defined as well. A general approach to plan irrigation is to utilize published evapotranspiration values for a certain crop. Thus, the irrigation rate is defined by subtracting the expected rainfall from the published evapotranspiration values for the given period and particular crop. For this purpose, evapotranspiration values are taken from (TAGEM, 2017) for 10 days of intervals and precipitation values are taken from Meteorological Service of Turkey and given in Table 3.2. As a result, the water applied to the surface is calculated by their difference assuming irrigation takes place once in every ten days. Apart from this, observed precipitation taken from measurements, is also applied to the surface separately.

Table 3.2. Average total monthly rainfall (1929-2020) (Meterological Service Of Turkey, 2021)

Months	**Jan**	**Feb**	**Mar**	**Apr**	**May**	**June**	**July**	**Aug**	**Sep**	**Oct**	**Nov**	**Dec**
Rainfall(mm)	37.8	28.5	29.1	32.1	43.4	25.7	7.0	6.3	13.4	29.8	32.5	43.6

3.5.2. Initial Conditions

During the validation runs, for water transport, the initial hydraulic pressure is assumed to be constant over the entire soil column. This translates to a zero-pressure head distribution at the water table and an initial pressure head of $-x$ where x is elevation relevant to the water table, and for temperature, the whole soil column is set to a constant value equal to soil temperature at the bottom. Initial solutes concentrations in aqueous and adsorbed phase, are taken from preliminary runs performed using the 1D HYDRUS model. For initial conditions of Konya runs, soluble concentrations and exchangeable concentrations are distributed equally along the depth of soil column.

Another option would be selecting the initial conditions of Konya runs after a run is done for some period of time (e.g., 1 day) by specifying Gapon Constants at the beginning. The obtained values of pressure head, temperature, concentrations of aqueous phase and adsorbed concentrations could be set as initial values for subsequent runs. However, it is more realistic to use measured concentrations as initial conditions than using Gapon Coefficients.

4. MODEL VALIDATION

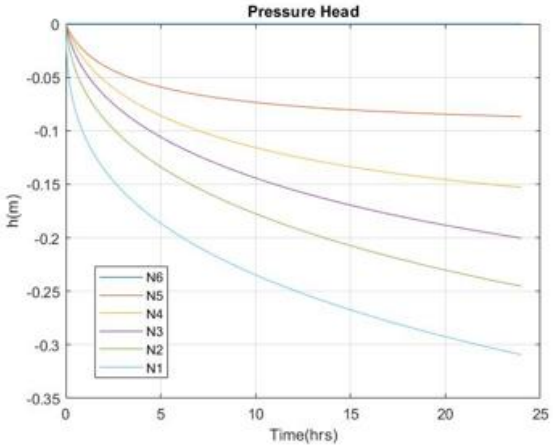
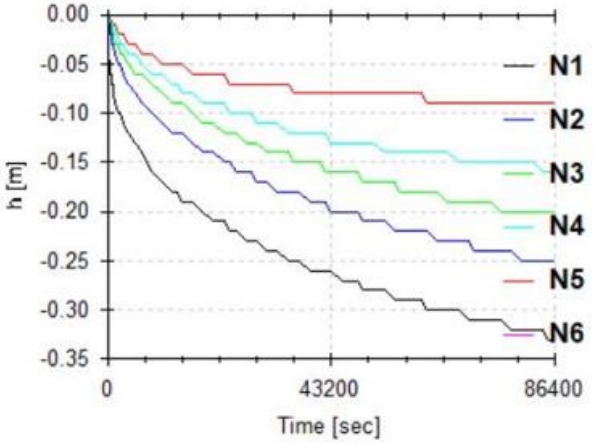
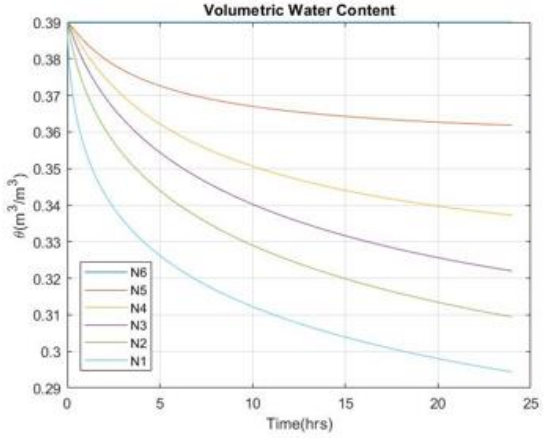
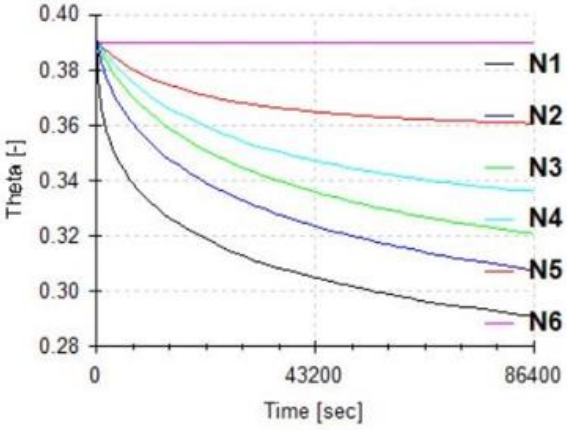
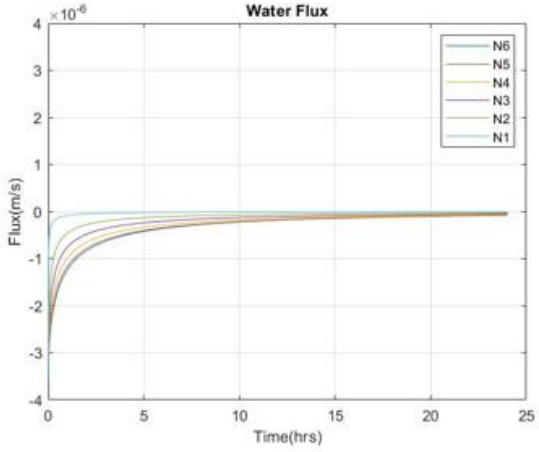
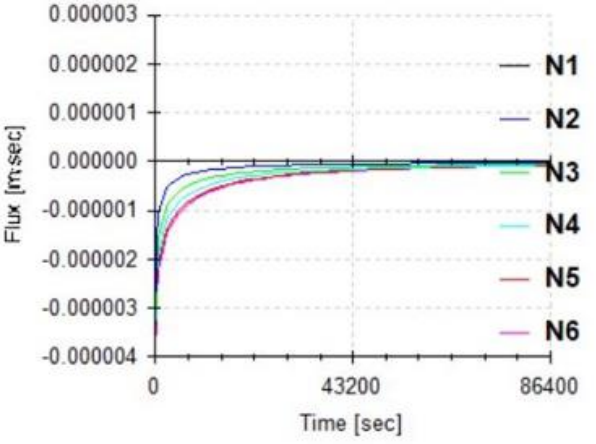
4.1. Water Flow Validation

In this section, two setups are modeled using the developed model and tested against HYDRUS. Both setups represent drying of a fully saturated soil column; the first one has no flux at the surface while the second includes time-dependent water application. The runs are made for a day (86400 seconds). The developed code used time increments of 1 second and HYDRUS has variable time increments between 1 and 1000 seconds depending on stability. In both cases, the soil column is 50 cm in length, divided into 25 nodes which gives Δx = 0.02 m. Input variables are given in the Table 2. Note that porosity equals to saturated water content.

Table 4.1. Water flow validation input parameters

	First Run	**Second Run**
θ_r (VG Parameter)	0.1	
θ_s (VG Parameter)	0.39	
a (VG Parameter)	5.9 (1/m)	
n (VG Parameter)	1.48	
Initial Conditions	$h(0,x) = 0$ (Fully Saturated)	
K_s (Hydraulic Conductivity)	3.64×10^{-6} (m/s)	
Surface Application	$q_{surface}(t) = 0$	$q_{surface}(35000:37000) = 8.64 \times 10^{-7}$(m/s) $q_{surface}(39000:41000) = 8.64 \times 10^{-7}$(m/s) $q_{surface}(43000:45000) = 8.64 \times 10^{-7}$(m/s) $q_{surface}(47000:49000) = 8.64 \times 10^{-7}$(m/s) $q_{surface}(51000:53000) = 8.64 \times 10^{-7}$(m/s)

Water flow is the core part of the model built. In reality many factors influence the movement of water such as heat flow. However, this run focuses on testing Richard's equation. . For this purpose, the solutions of a simple model with no surface flux are compared. The result of this run is given in the Figure 4.1. The results consisting of hydraulic head, moisture content, water flux and hydraulic conductivity as a function of depth and time are almost identical. This suggests that the flow module is modelled correctly.

MATLAB	HYDRUS
	
	
	

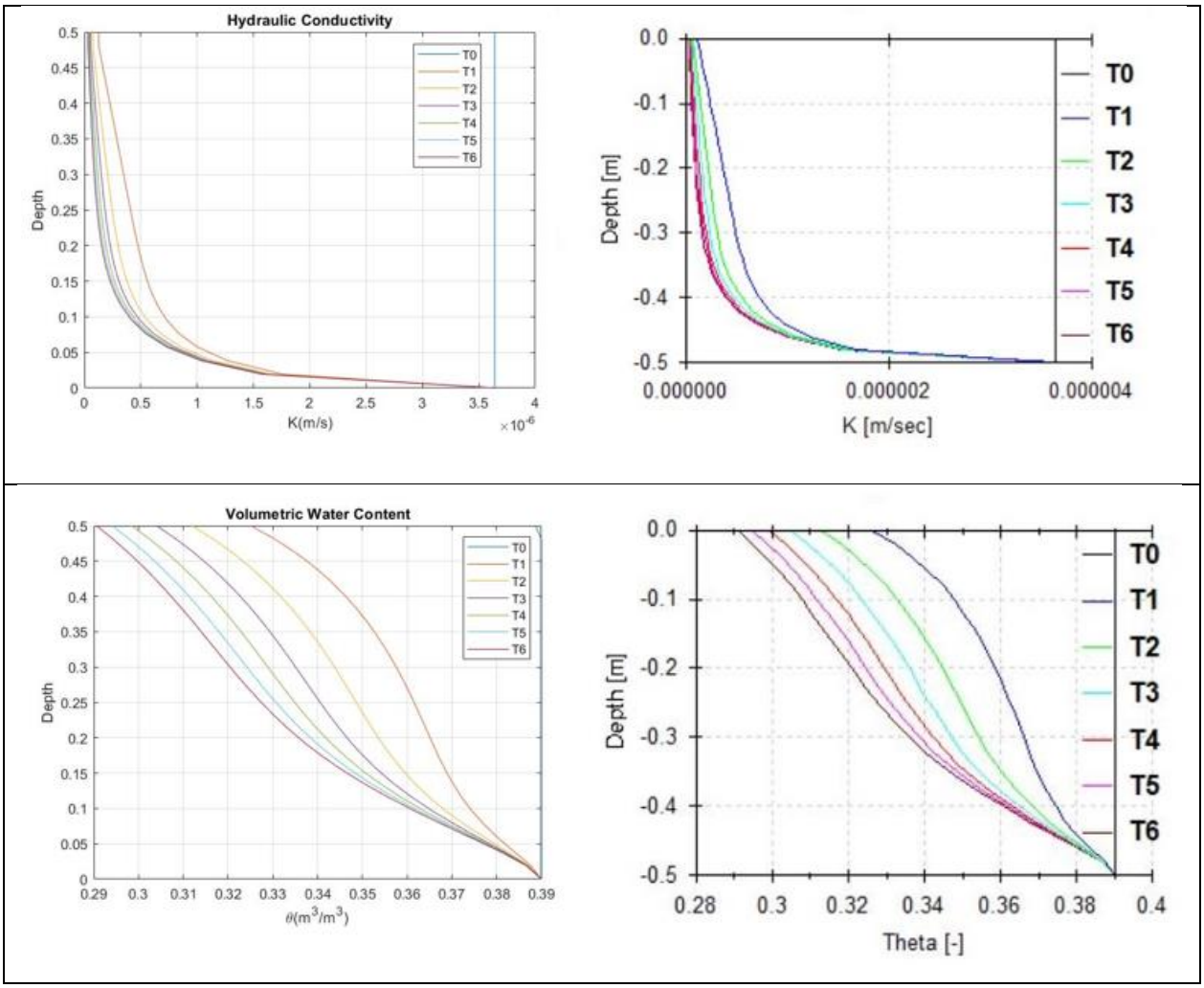
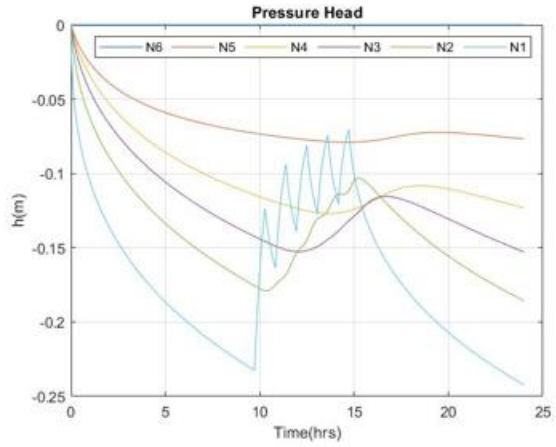
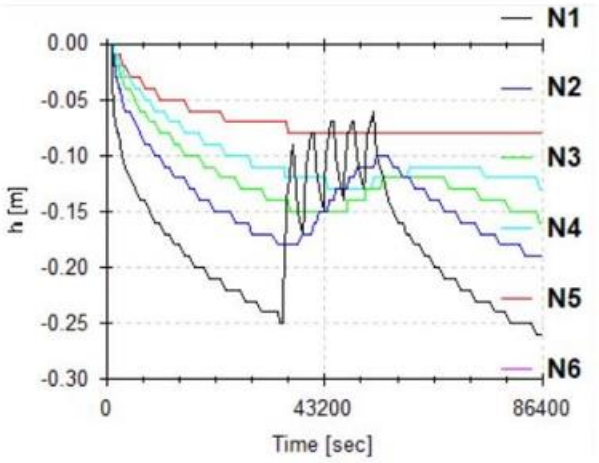
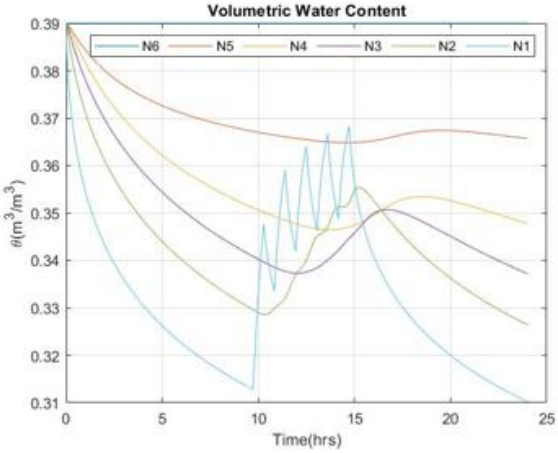
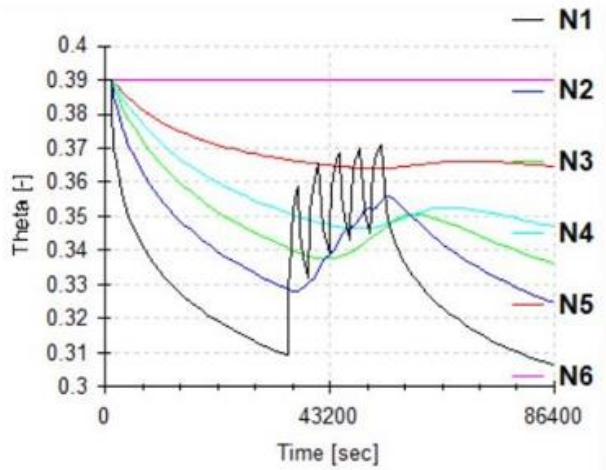
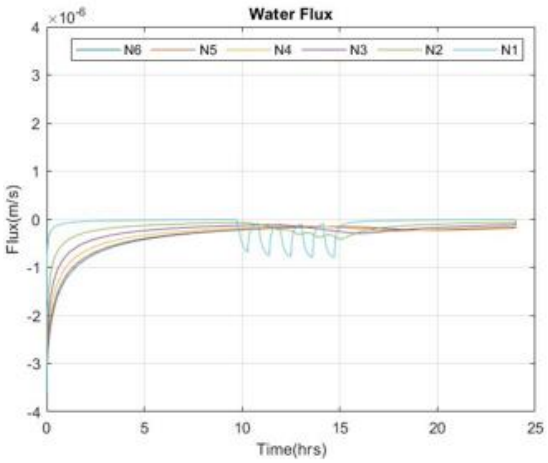
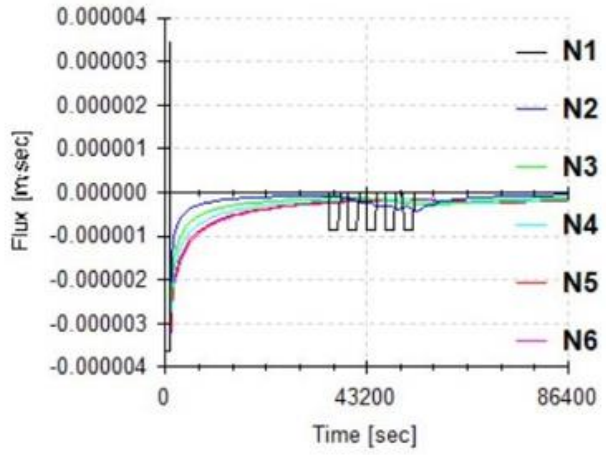


Figure 4.1. Validation results of 1st run (N_i =50, 40, 30, 20, 10, 0 cm and T_i=0, 14400, 28800, 43200, 57600, 72000, 86400 s)

Flux along a soil column varies as a function of evapotranspiration, evaporation, irrigation and precipitation. So, a variable surface flux is added to the same model and compared. Effects of this application can be seen in the Figure 4.2. The results are quite similar despite the sharply changing surface conditions; Little differences in calculated values and shapes can be observed which stem from numerical methods and time step adjustments. It is noted that the solution obtained with the developed code is quite smooth.

MATLAB	HYDRUS
	
	
	

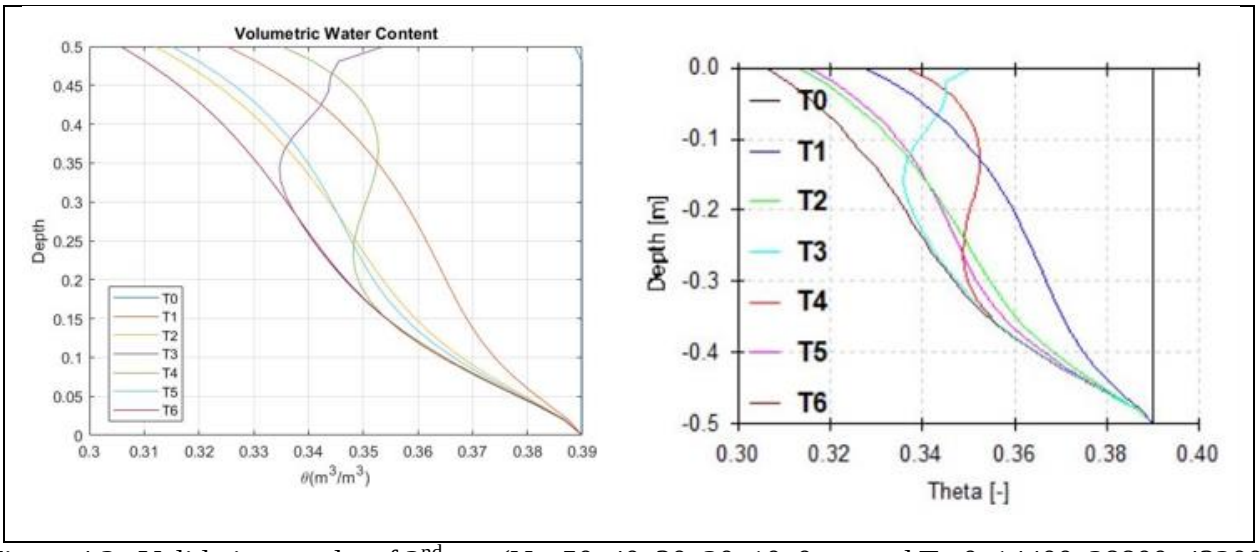
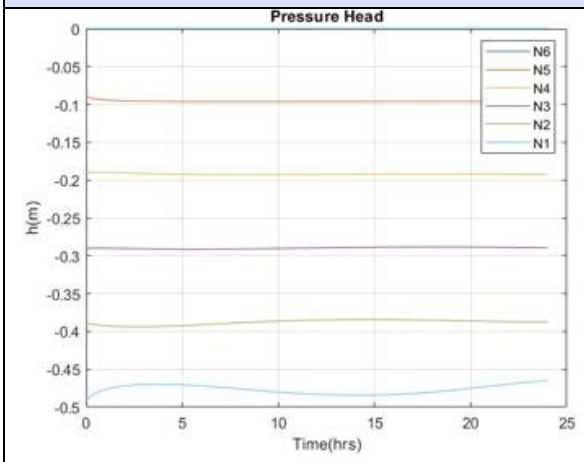
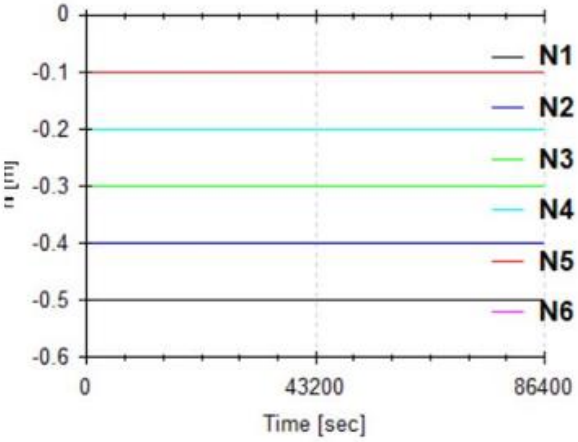
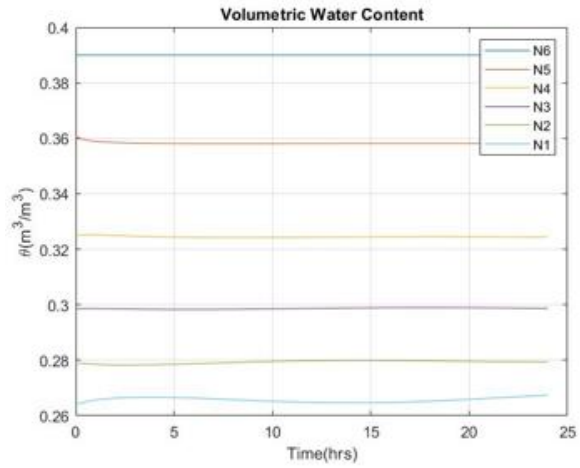
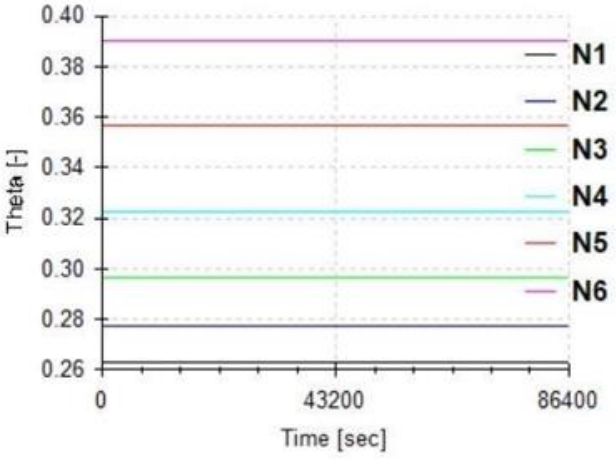
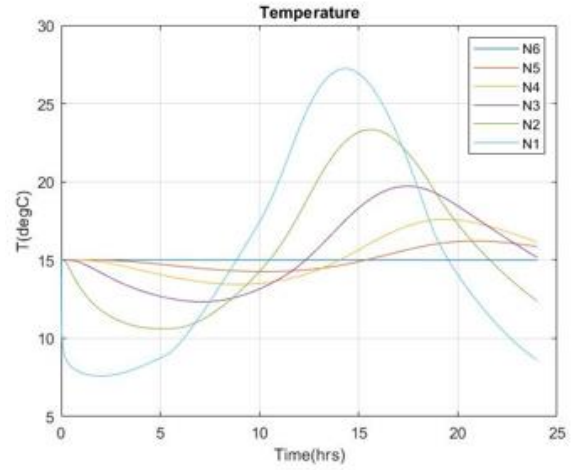
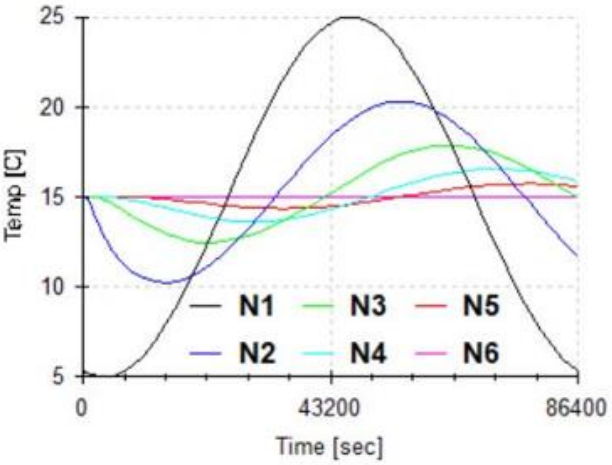


Figure 4.2. Validation results of 2nd run (N_i =50, 40, 30, 20, 10, 0 cm and T_i=0, 14400, 28800, 43200, 57600, 72000, 86400 s)

4.2. Water Flow Coupled with Heat Flow Validation

The next test runs examines the temperature and heat dependency on water flow. For this purpose, no flux water was imposed at the top boundary but with surface temperature fluctuations. As initial conditions, temperature is set to 15°C throughout the column and pressure head is calculated as $h = -x$, as described in Section 4. This condition approximately represents naturally drained soil assuming constant hydrostatic pressure and x is defined as 0 at the bottom, increases towards the surface. Mean air temperature is given as 15°C and the daily temperature variation is given 10°C.

As it is showed in Figure 4.1., results are in good agreement with each other however small sinusoidal fluctuations are seen in MATLAB's water results whereas HYDRUS gives near perfect straight lines. It can be seen from MATLAB graphs, while surface temperature reaches its peak value, water content is decreasing. The shape difference can be a result of HYDRUS' low-resolution solution for efficiency. Note that, it took 4 minutes for MATLAB to solve this problem, whereas HYDRUS calculations lasted less than a second. On the other hand, temperature values are overestimated in MATLAB by less than 5 °C but shape and distributions are in good agreement.

MATLAB	HYDRUS
	
	
	

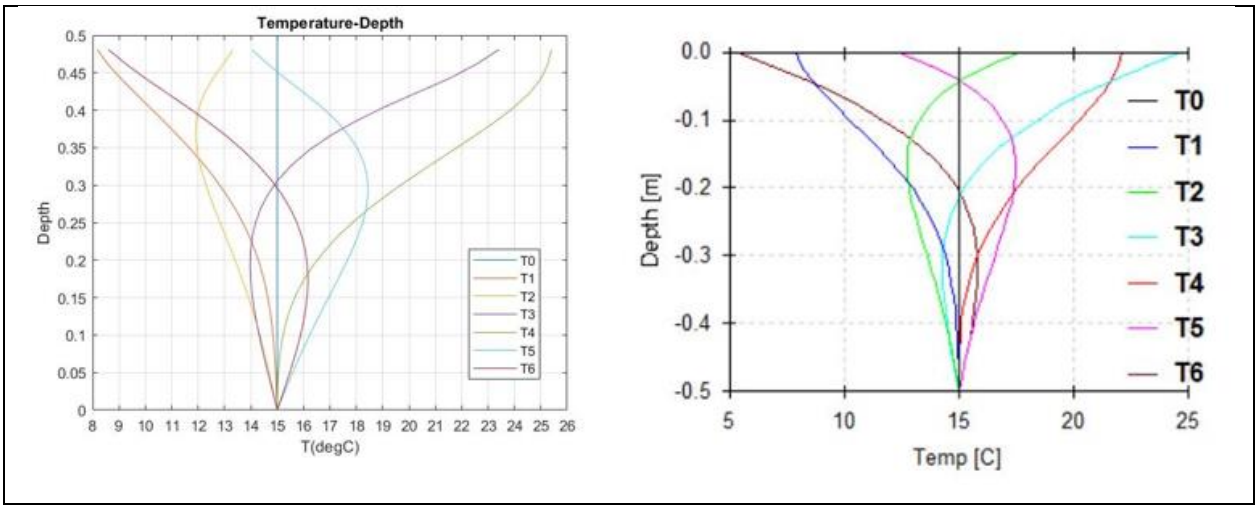
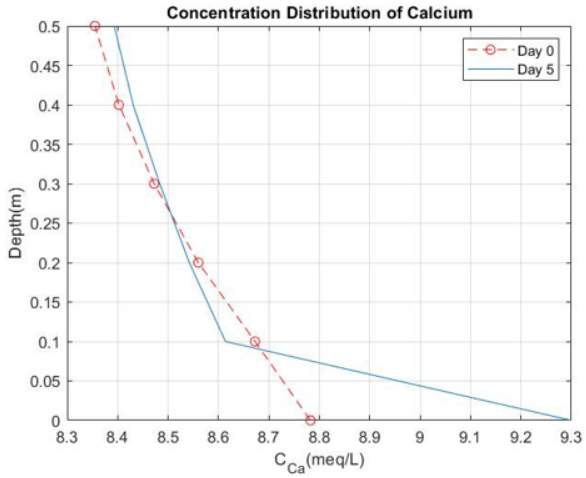
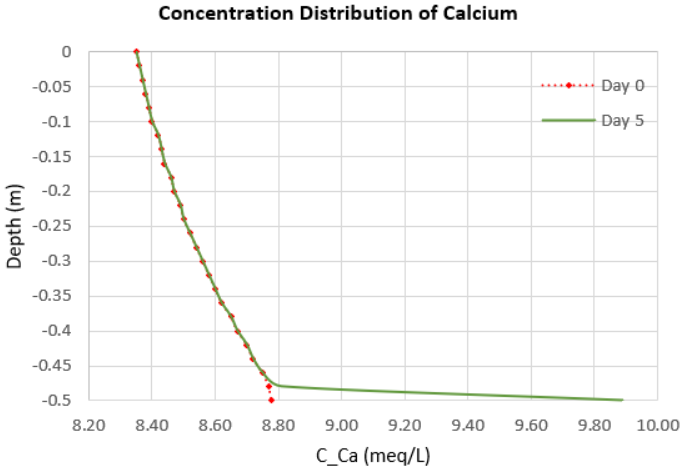
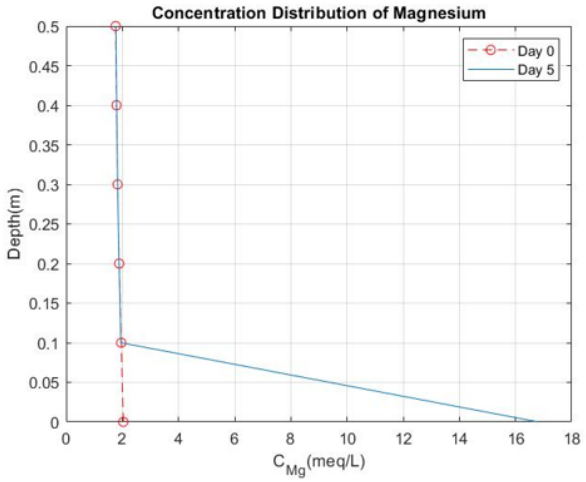
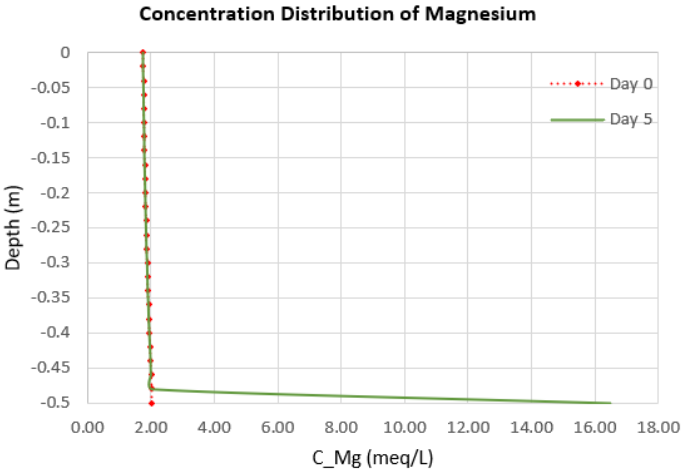
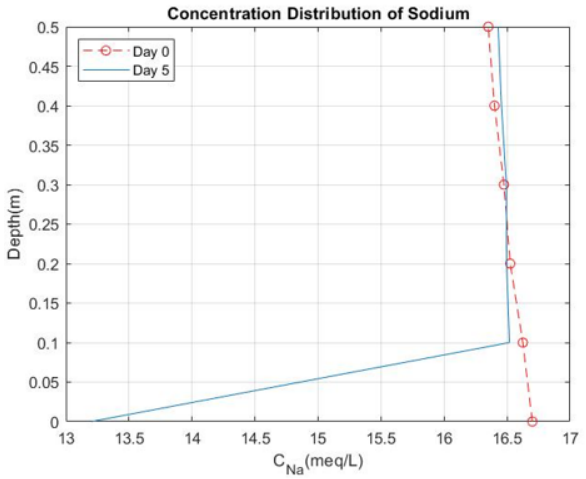
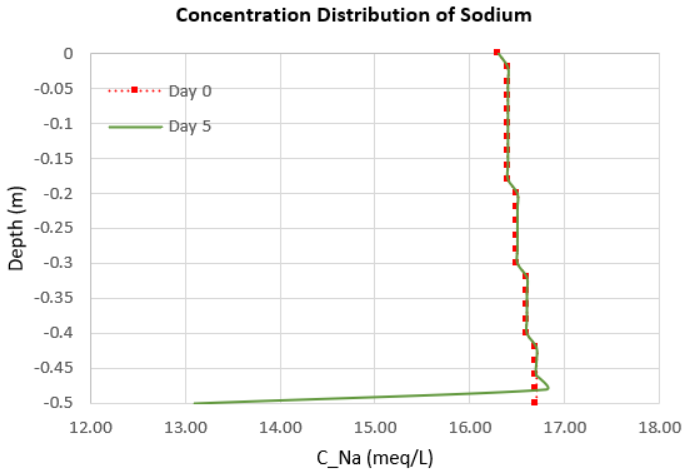


Figure 4.3. Validation results for temperature comparison (N_i =50, 40, 30, 20, 10, 0 cm and T_i=0, 14400, 28800, 43200, 57600, 72000, 86400 s)

4.3. Water Flow with Solute Transport Validation

For solute transport, the same water flow parameters are used as the previous problem: no surface flux and water table at the bottom with saline water. Initial concentrations are calculated by HYDRUS according to equilibrium constants (Gapon Selectivity Constants): K_{13}=0.323, K_{14}=0.106 and K_{14}=4.908. The simulations are 5 days long. The aqueous phase concentrations change with time are presented in Figure 4.4. The shapes look very similar in both models and as expected solute concentrations are increasing at the bottom due to capillary action from water table. Although the behavior of models are similar, the kink in Day 5 occurs at a depth of 40 cm of column in MATLAB whereas it occurs at a depth of 47 cm in HYDRUS. Hence, it can be said that the concentrations are overestimated in MATLAB, and this is a predictable result of the concentration calculation technique described in Section 3.3. Also, it is seen that, HYDRUS shows no change in concentrations for upper levels between Day 0 and Day 5 but in MATLAB these values slightly deviated from start. The reason is that HYDRUS uses given Gapon Constants for calculating values for Day 0 whereas MATLAB calculates these constants from given initial concentrations. Although algebraically these constants should be the same, when it is used in numerical methods rounding errors leads to these negligible differences. In addition, the way HYDRUS calculates solute distributions includes some other major ions such as $(HCO3)^{-1}$, $(SO3)^{-2}$ and so on. It inevitably creates changes in shapes.

MATLAB	HYDRUS
	
	
	

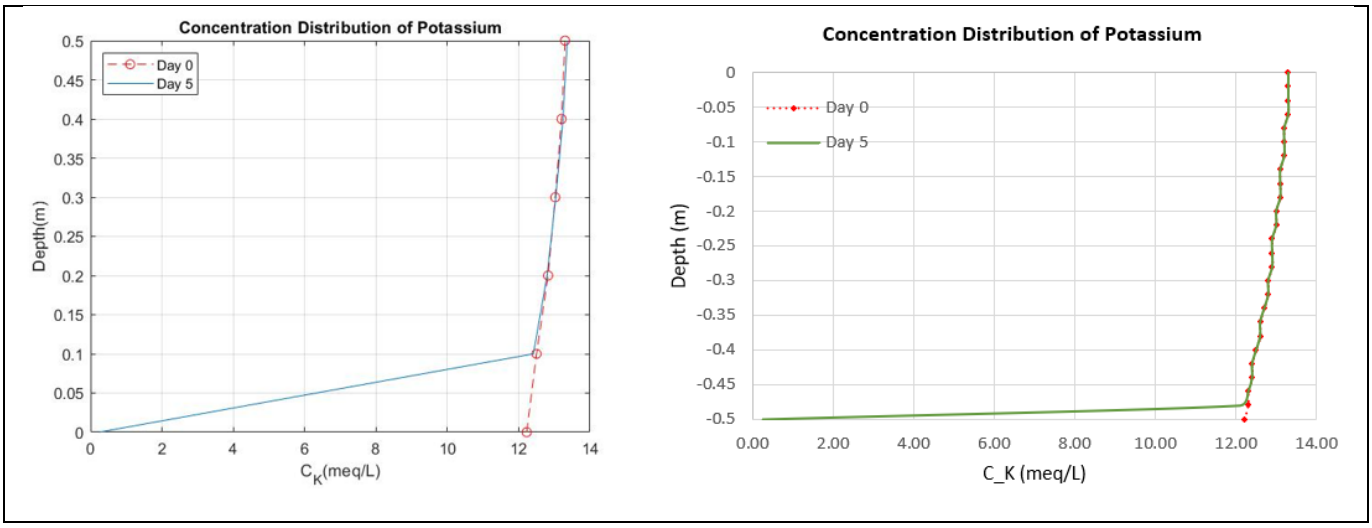


Figure 4.4. Validation results for solute concentration comparison

The total of adsorbed concentrations over the entire length as a function of time are given in Figure 4.5. The adsorbed concentrations are fairly similar in both calculations. The differences are given as percentage in Figure 4.6. with the highest difference (Day 5 - Mg) equal to 1.1 % suggesting good agreement between the two solutions. A significant issue which should be mentioned here is the slight overestimation of adsorbed calcium compared to the HYDRUS solution. The reason is actually embedded in Eq. (46), because it assumes CEC is always attained in the developed model. To assure that, when there is solute deficit, calcium is the element to fill it out. In HYDRUS this necessity is lower due to other cations considered (i.e. H^+). Moreover, HYDRUS includes excess calcium in the system in the form of precipitated calcite, which causes calcium concentration to remain constant. In the MATLAB model, calcium can only be adsorbed so the adsorption concentration increases as the other ions' adsorption decreases.

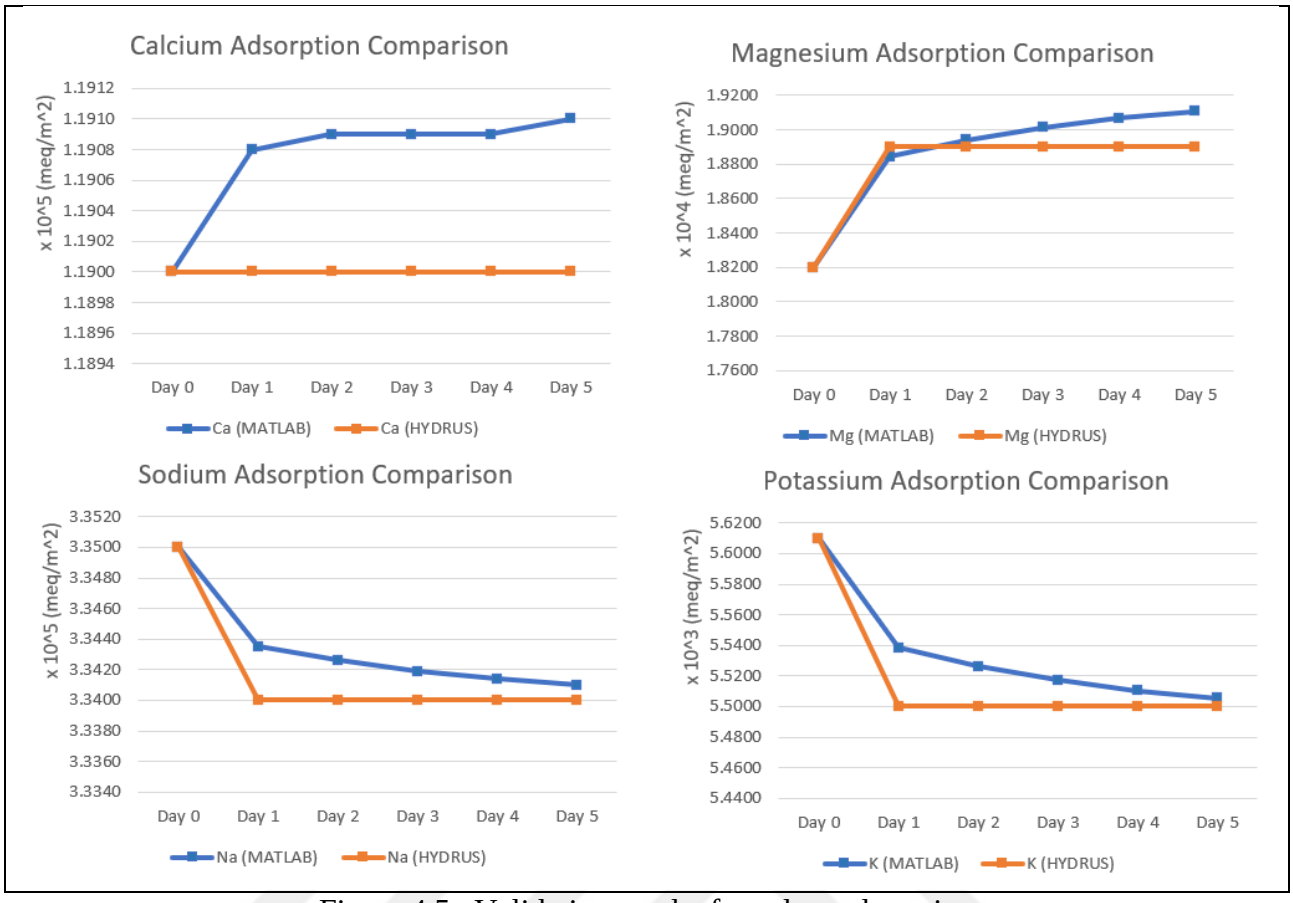


Figure 4.5. Validation results for solute adsorption

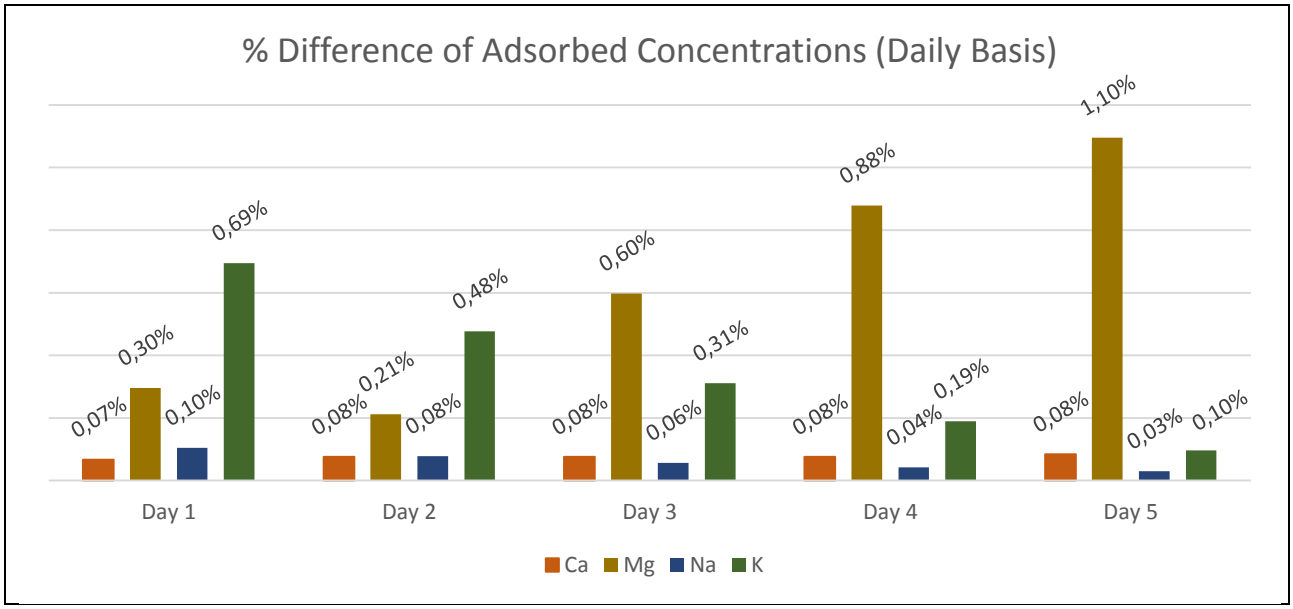


Figure 4.6. % Difference of adsorbed concentrations (daily basis)

All in all, the code developed in MATLAB is tested by considering the water flow by itself and as well the flow coupled with heat and solute transport. for Various initial and boundary conditions are considered. When compared to HYDRUS, which is a commercial tool that is widely used and tested to model coupled mechanisms in soil, the results are acceptable. Some differences occur

inevitably due to different assumptions. The results of the test problems provides some confidence that the code is simulating the coupled mechanisms accurately.

In the following chapter, the program will be used to simulate more realistic problems and to assess the interdependence of the different processes that are occurring simultaneously Although the code has not be optimized numerically and is less efficient that a commercial software such as HYDRUS, having the code in hand gives more opportunity to evaluate the interdependence of the different modules of the code (water flow, heat flow and solute transport) than what is afforded by a commercial tool. Moreover, it provides the flexibility to include or exclude any module, thereby allowing us the ability to impact any particular mechanism on soil properties and water and solute transport.

5. RESULTS AND DISCUSSION

The agricultural topsoil present in the Konya closed basin, a significant agricultural area of Turkey, is prone to salt accumulation as the slope grades are low and the area lies at high pressure belt of the globe. If left unaddressed, the over exploitation of the existing groundwater resources is likely to have detrimental effects in the future. It is imperative that crop type and irrigation systems used be consistent with the available water resource. Modeling predictions show that climate change in the coming decades will likely exacerbate these problems.

The developed model can be used as a tool to assess the impact of different cases. The primary benefit of the code is that it can jointly simulate various processes which are water, solute and heat flow and their impact on salt accumulation and soil sodification. Because the code simulates various coupled processes jointly, it can be used to assess under which conditions certain mechanisms such as heat flow or vapor flow are significant.

5.1. Ambient Conditions

For demonstration purposes, the meteorological data used is the simulations are those provided from meteorological service of Turkey for the Çumra Station in the Konya basin for 2019. The model can be readily applied to other locations in Turkey or elsewhere. The meteorological data needed by the model include air temperature, relative humidity, wind, rainfall, ambient air pressure, soil temperatures in 10, 20, 50 and 100 cm depths. These parameters for year 2019 are given in Figures 5.1-5.3. Monthly irradiance values are taken from the public statistics provided from the same institution. Although the data is available for the entire year, the time of interest regarding to this model is provided for year 2019 in the figures below (Figure 5.1 to 5.4). Note that these figures are for daily average values but while implement them into the code, hourly distributions are made by using Eq. (80-85). Radiation has a different state here as daily average data is randomly generated from the monthly total values given in Table 5.1.

Table 5.1. Average Monthly Solar Radiation (TSMS, 2018)

Months	Jan	Feb	Mar	Apr	May	June	July	Aug	Sep	Oct	Nov	Dec
kWh/m²	56.3	78.6	117.3	155.2	178.4	206.8	217.7	195.2	154.3	105.9	66.6	51.2

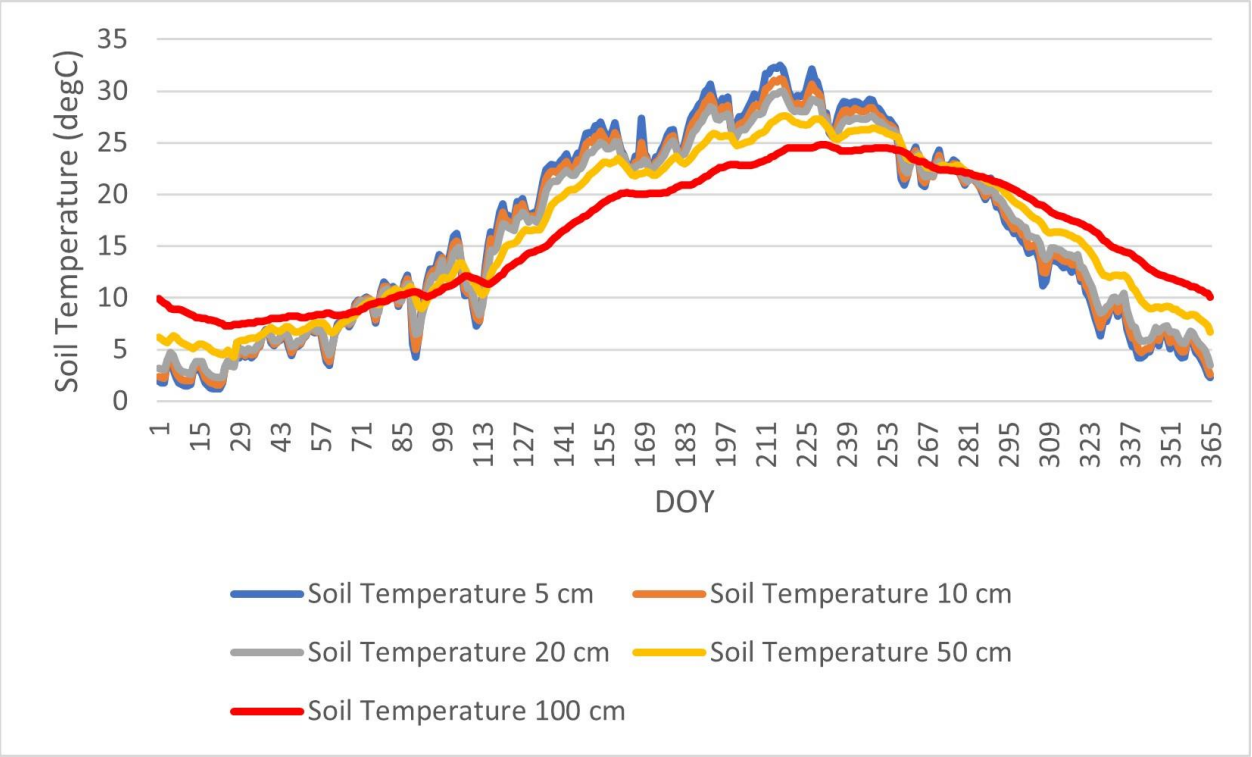


Figure 5.1. Soil Temperatures as a function of time at different depths

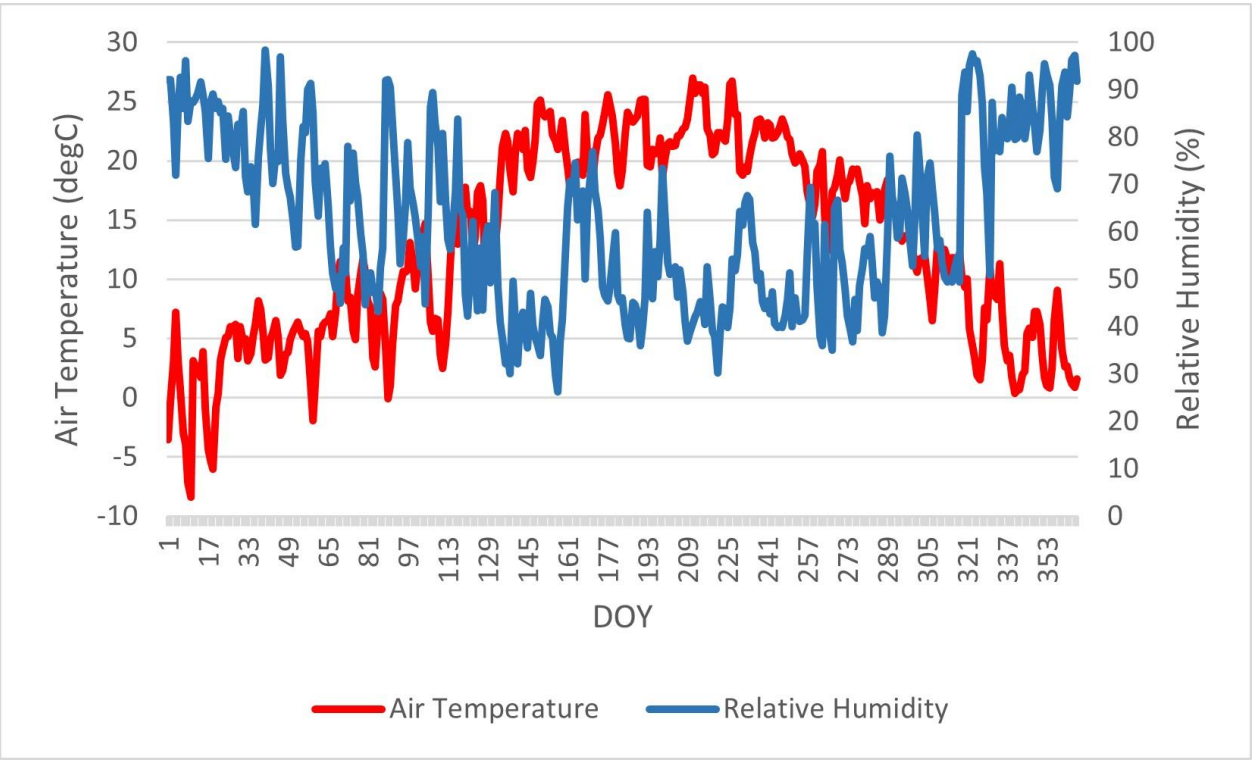


Figure 5.2. Air Temperature and relative humidity as a function of time

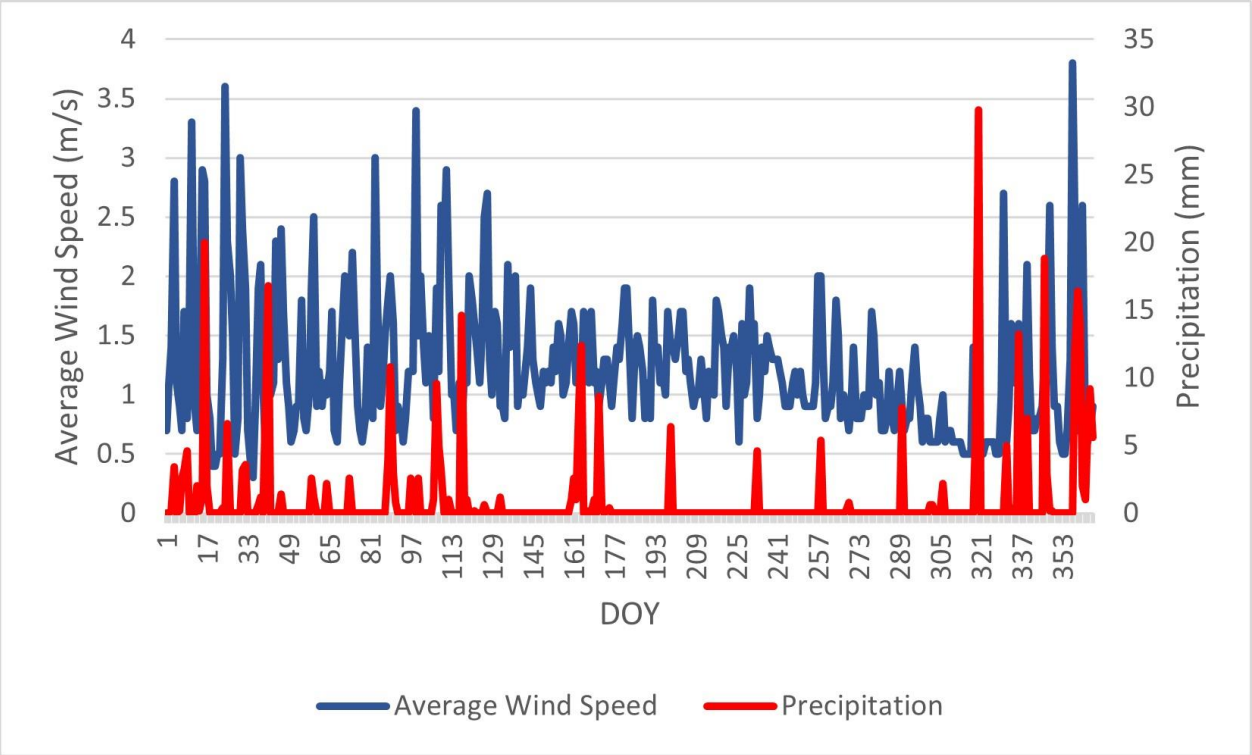


Figure 5.3. Average wind speed and precipitation as a function of time

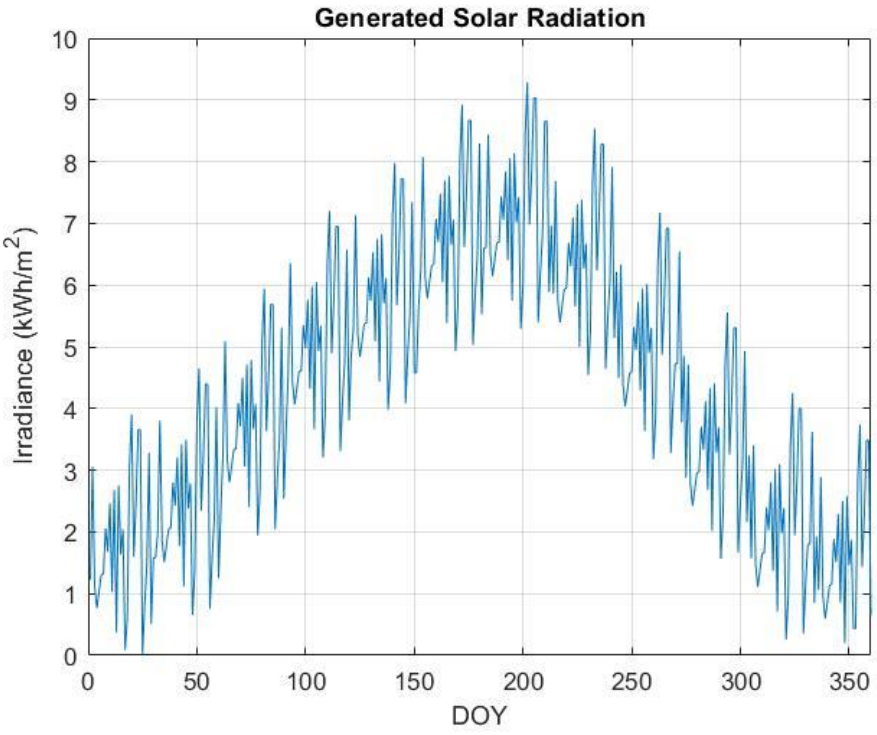


Figure 5.4. Daily distributed generated solar radiation from Table 5.1

Calibration parameter in Eq. (81), f, is found 3.687. Daily variations of temperature and relative humidity are given for smooth transitions between days. The ones used in base run are provided below along with hourly distributed radiation.

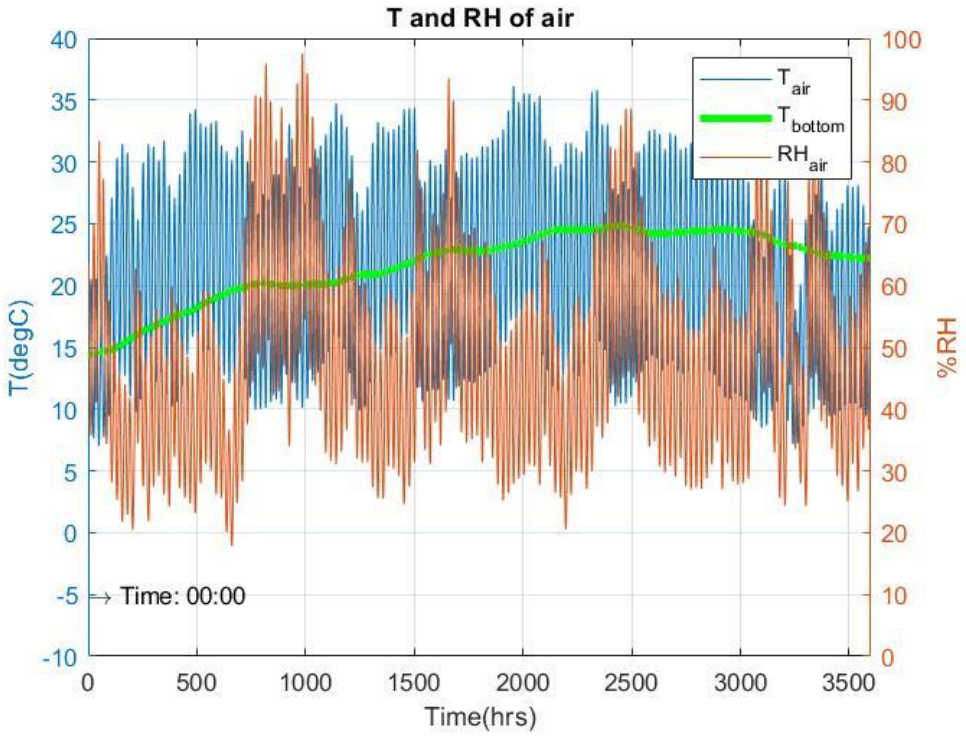


Figure 5.5. Hourly distributions of air temperature, relative humidity and soil temperature at bottom boundary (Start Time: DOY: 130 Hour: 00:00)

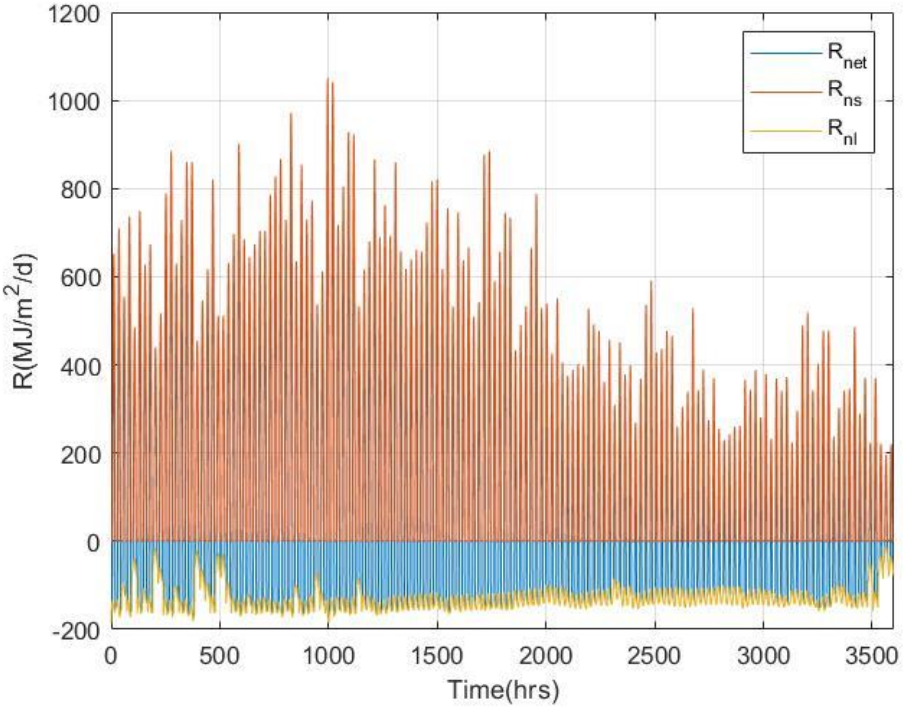


Figure 5.6. Hourly distributions of incoming shortwave radiation, outgoing longwave radiation and net radiation

Figures 5.5 and 5.6 cover a period of 3600 hours (150 days) To better visualize the hourly data, Figure 5.7 shows the temperature, relative humidity and radiation over a much smaller period. These figures clearly show the day and night variations that are incorporated into the model.

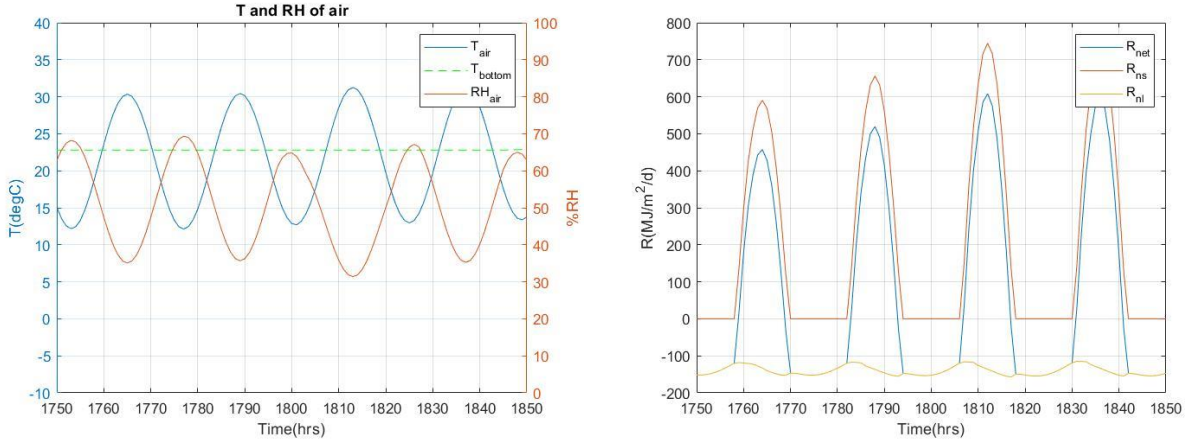


Figure 5.7. Hourly temperature, relative humidity and radiation (data are from Figure 5.5 and 5.6)

Note that hour 1800 on the horizontal axis corresponds to the midnight of the day in the middle of given period (DOY 205), so the previous and next two days can be seen. From left-hand side, it is seen that highest temperatures and lowest relative humidity occur in the afternoon.

Obviously, the bottom temperature at the bottom boundary of the soil column can be taken as constant for short periods. And on the right-hand side of Figure 5.7, it is seen that incoming shortwave is only available when sun is up, roughly between 06:00 and 18:00. It must be mentioned that variations in daylight hours are not included in this model. Outgoing longwave is always observable and it is accounted for in the cooling of the air and soil surface. Therefore, the net radiation used in the energy balance equation has cooling effect when negative (night hours) and heating effect (daytime hours) when positive at the surface.

5.2. Base Run

A base run is first conducted for the purpose of showing the salt accumulation within the soil in a single plant growth season. In this run, the selected crop type is maize as it is one of the most common crop types in the region. As most of the growth season of maize is summer, it requires a significant amount of irrigation. On the other hand, the source of irrigation is mostly groundwater as surface water sources are not enough in dry season. Therefore, the base run shows how the soil structure changes due to increased sodicity over a single season. The initial sodicity in the soil is assumed to be low. Soil hydraulic parameters are selected for sandy clay loam. Soil hydraulic parameters are provided in Table 5.2. Irrigation water quality is selected to be sodic (high SAR) adopted from the study of (Bozdağ, 2014) which examined groundwater quality data at various locations of the Konya Basin, is the water quality data used in the model for irrigation are given in Table 5.3. Similar to validation runs, porosity equals to saturated water content.

Table 5.2. Soil hydraulic parameters used in Base Run

Parameter	**Value**
θ_r (VG Parameter)	0.1
θ_s (VG Parameter)	0.39
a (VG Parameter)	5.9 (1/m)
n (VG Parameter)	1.48
Initial Conditions	$h(0,x) = -x$ (Constant hydrostatic pressure) $T(0,x) = T_{soil(100\,cm)}$
K_s (Hydraulic Conductivity)	3.64×10^{-5} (m/s)

Table 5.3. Irrigation Water Parameters (Bozdağ, 2014),

EC ($dS\ m^{-1}$)	Ca (mg/L)	Mg (mg/L)	Na (mg/L)	K (mg/L)	SAR
3.372	186	201.60	303.61	9.44	3.65

A growth period selected for maize starts from early May to late September (TAGEM, 2017). This corresponds to DOY (day of the year) 130 to 280. The irrigation water requirement is determined by using evapotranspiration values given in (TAGEM, 2017) and average rainfalls given in Table 3.2. For simplicity, the length of maize is taken as constant for four different period as given in Table 5.4. Evapotranspiration values for maize are given in Table 5.5.

Table 5.4. Average maize height during growth season

Crop: Maize	DOY: 130-170	DOY: 171-200	DOY: 201-230	DOY: 231-280
Crop Height (m)	0.5	1.0	1.5	2.0

Table 5.5. Evapotranspiration values of maize in 10 days interval (TAGEM, 2017)

DOY	130 - 140	141 - 150	151 - 160	161 - 170	171 - 180	181 - 190	191 - 200	201 - 210	211 - 220	221 - 230	231 - 240	241 - 250	251 - 260	261 - 270	271 - 280
ET (mm)	11	13	15	21	36	51	66	72	79	69	66	66	49	21	8

The irrigation scheduling is done by subtracting the values of evapotranspiration from expected total average monthly rainfall, divided to three parts, indicating irrigation is carried out in 10 days of intervals. The result is given in Figure 5.8.

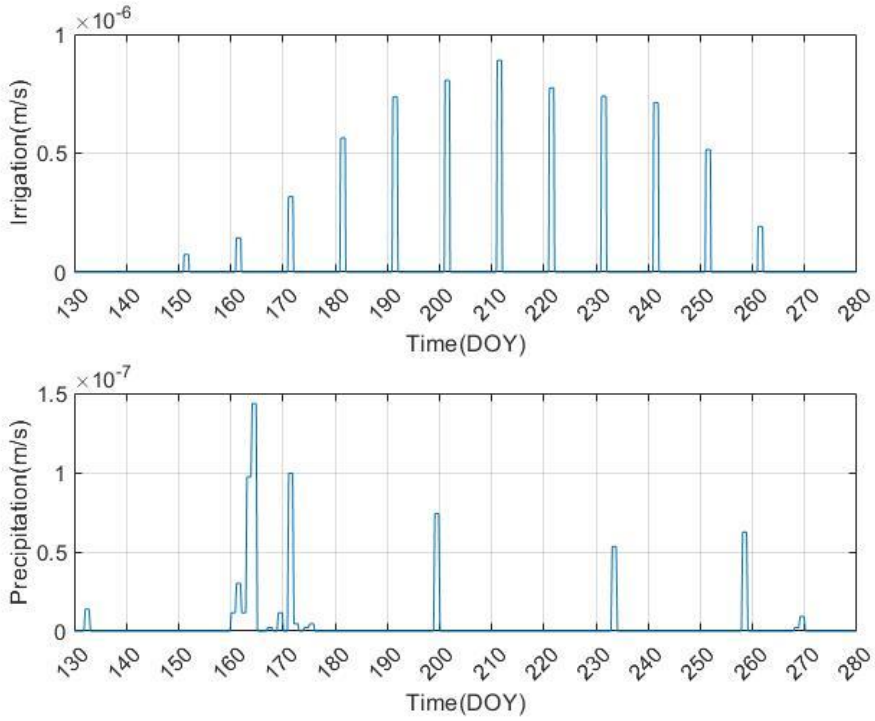


Figure 5.8. Irrigation scheduled from expected rain and evapotranspiration, actual precipitation

As it can be seen, days with high rain expectancy (Table 3.2) irrigation requirement is low and vice versa. Observed precipitation shows a few peaks throughout the season and these two elements are the water supplies from the surface to the soil column. Note that irrigation water contains solutes.

To better evaluate the impact of using high sodic water for irrigation purposes, the initial ESP and SAR values are assumed to be low indicating an initially suitable soil for agriculture. However, the application of saline groundwater as irrigation water showed a significant deterioration of soil structure in one growth season. The sodicity of the soil is expressed in terms of a rise in ESP and SAR values as presented in in Figure 5.9. The values shown in this Figure are the average for the entire soil column. There is a general trend for increase in ESP and SAR due to the use of sodic water for irrigation. The drops in ESP and SAR observed in these graphs correspond to precipitation events as shown in Figure 5.8. The corresponding decrease in the hydraulic conductivity at two different locations of the column is shown in Figure 5.10.

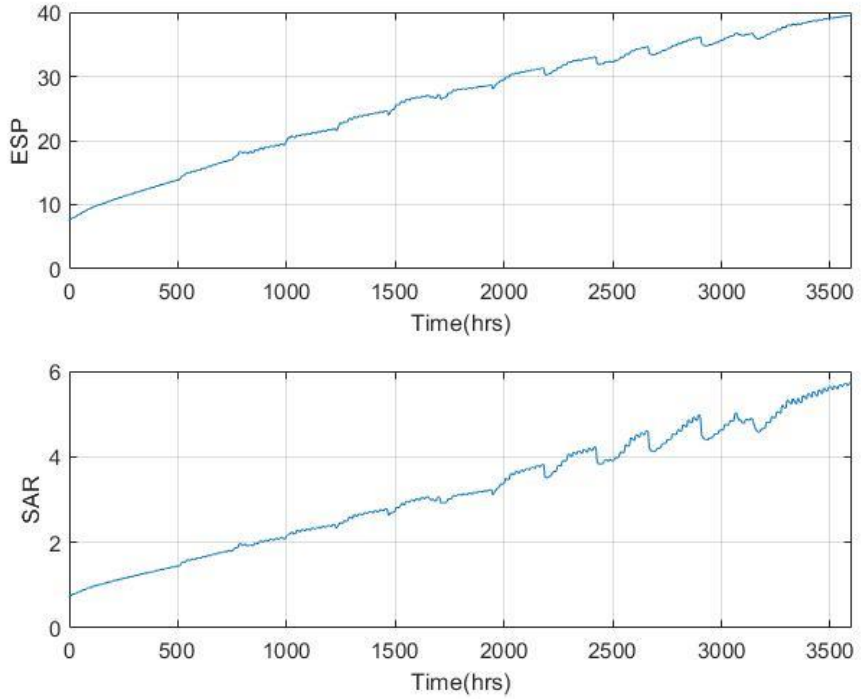


Figure 5.9. ESP and SAR values for the Base Run

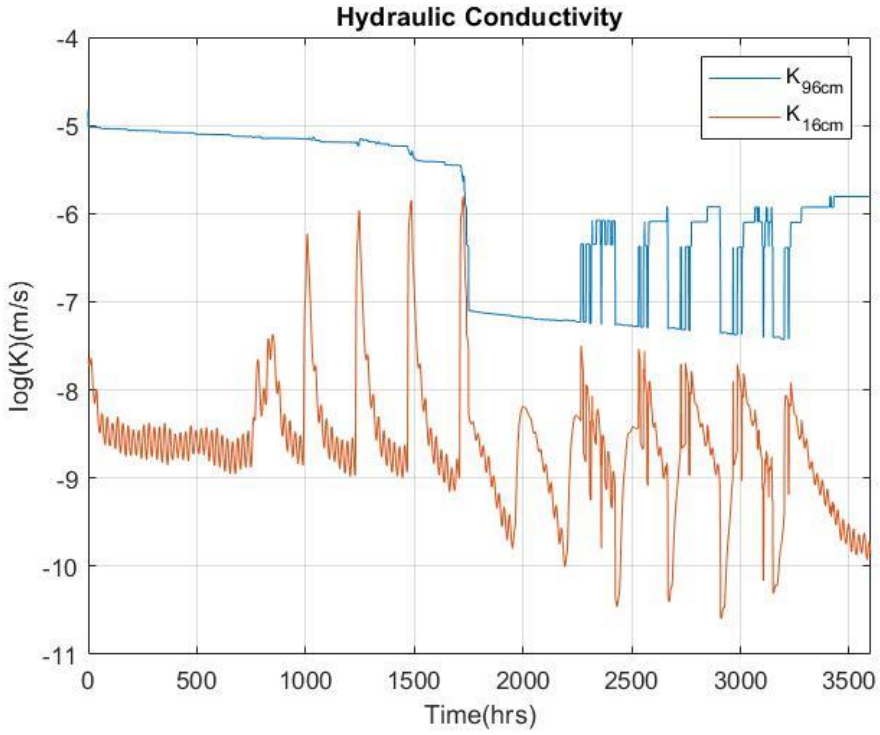


Figure 5.10. Changes in hydraulic conductivity as a function of time at two different elevations for the Base Run

It is observed that ESP passes a value of 15 around 700 hours (~1 month) which corresponds to sodic conditions (Table 1.1). Based on the permeability reduction model adopted in this study,

ESP=25 is an important threshold for clogging which is passed around 1700 hours (~2.5 months). This corresponds to a sharp decrease in hydraulic conductivity values.

The model shows salt accumulation at the surface as well as above the water table. Salt accumulation in the bottom part is mostly due to capillary action from the saline water table whereas the salt accumulating at the surface is due to the combined effect of precipitation/irrigation and evaporation. Higher fluctuations in salt concentrations are observed at the surface due to the discrete irrigation events whereas the change in concentrations are more gradual above the water table. Also at the surface, even though the irrigation water is saline, the higher water content causes an increase in the relative permeability. The high water content also causes small drops in the ESP and SAR curves. However, after the irrigation events as water content decreases due to evapotranspiration the ESP and SAR gradually increase. Overall, a gradual increase in these parameters is observed in time and is accompanied by a decrease in the hydraulic conductivity.

Separate plots of the main cations are shown in Figure 5.11 and 5.12. It is seen that although calcium in soil water increases, the adsorbed calcium decreases. Since the soil is assumed to be at CEC, the decrease in the sorbed Ca concentration is accompanied by accumulation of other ions especially sodium. On the other hand, soluble magnesium increases slowly compared to its increase in adsorbed state. This is attributed to the high content of potassium in aqueous and adsorbed phase, and it looks like magnesium replaces potassium with its higher affinity. However, particularly after the hydraulic conductivity underwent a significant reduction, exchangeable sodium is the primary element that continues to rise and this is attributed to the high sodium content of irrigation water.

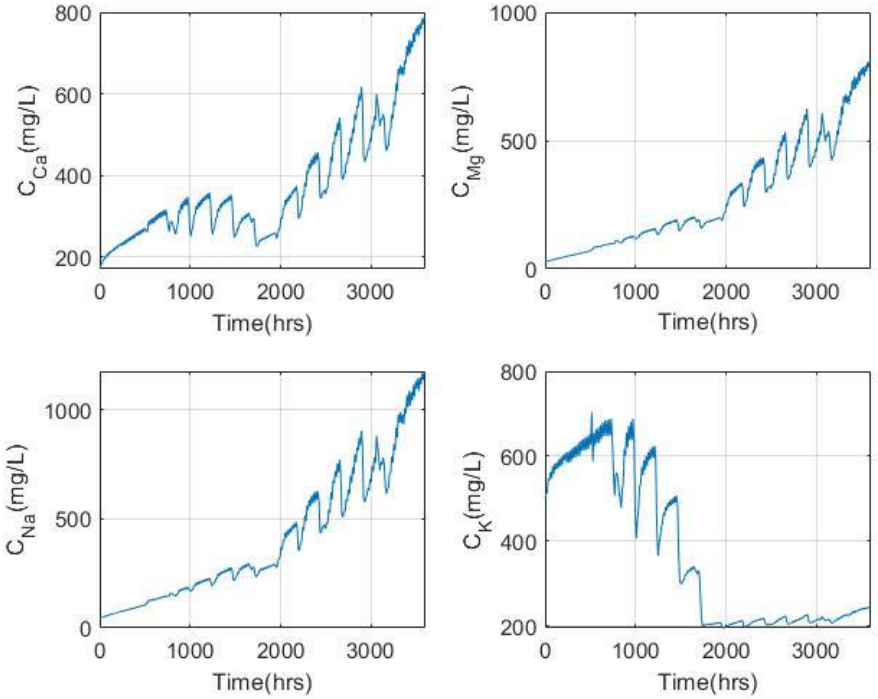


Figure 5.11. Soluble concentrations as a function of time for the Base Run

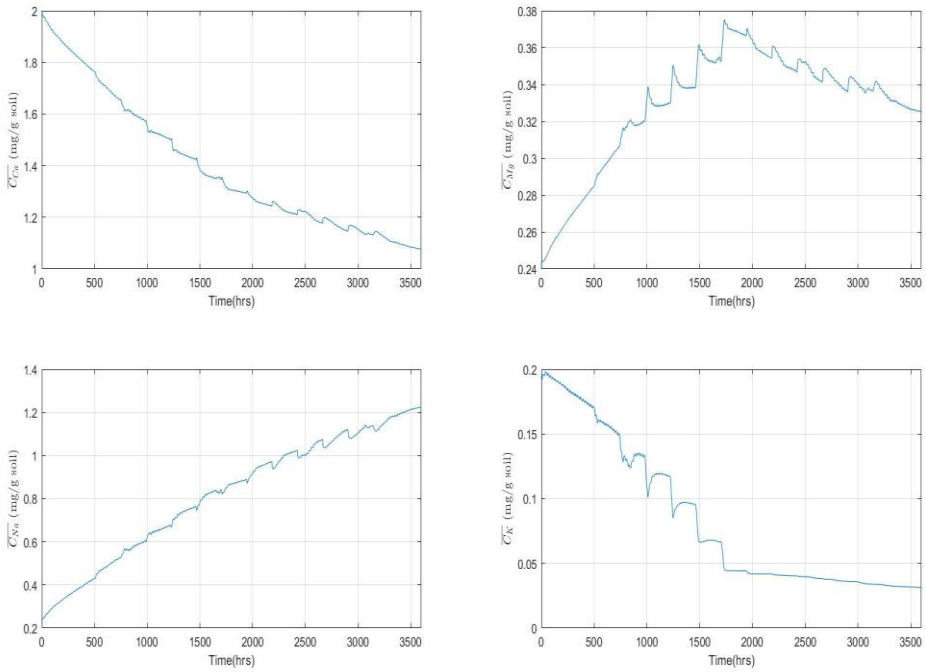


Figure 5.12. Exchangeable cation concentrations (sorbed concentrations) as a function of time for the Base Run

As expected, evaporation at the surface increases all the concentrations in the summer months. This effect can be clearly seen in Figure 5.13. The concentrations are highest at the surface. An

important result from here is that calcium, magnesium and sodium concentrations keep increasing whereas potassium concentration decreases as time goes. Again, it is due to high initial content of potassium and low potassium content in the irrigation water. A secondary shallow increase is seen around 0.3 m depth from the bottom caused by solute rise due to capillary action. The upward flux can be seen in Figure 5.14. Positive flux shows solute mass transporting upwards in the column. Exchangeable concentrations are also presented in Figure 5.15. The distributions over the depth show that, in terms of sodicity, sodium is supplied from up and down with lower adsorbed sodium in the middle of the soil column at the end of the 1st month. However, after 5 months, adsorbed sodium is equal to that at the bottom boundary with an increasing trend.

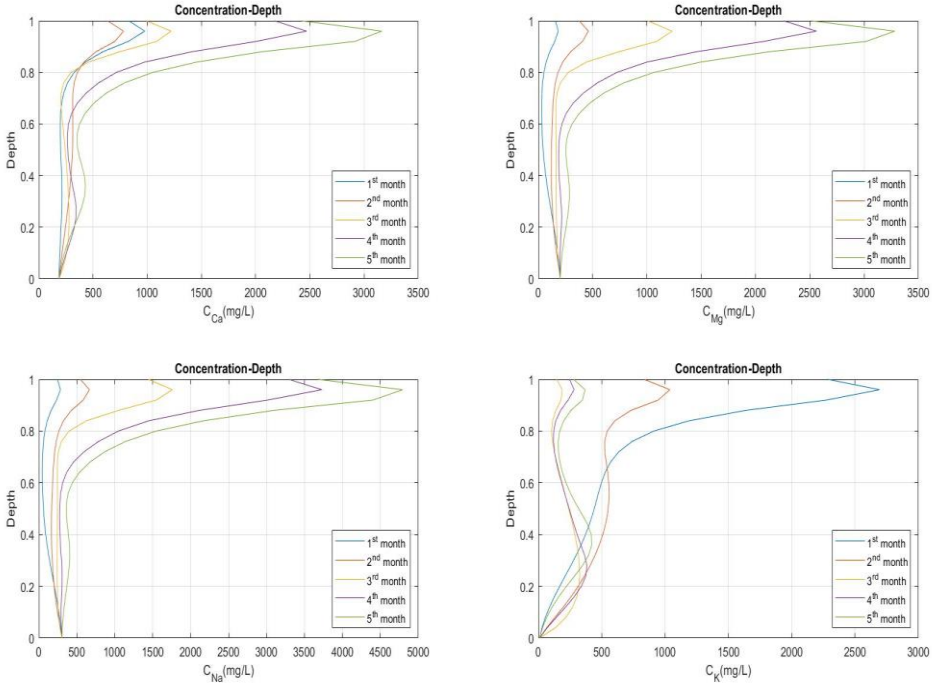


Figure 5.13. Soluble concentrations as a function of time and depth for the Base Run

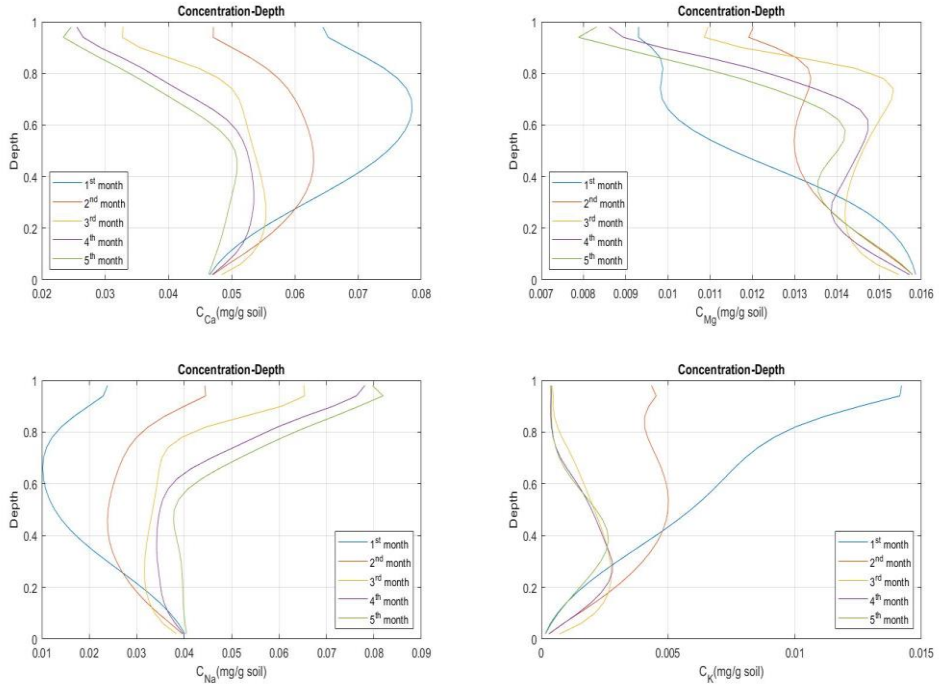


Figure 5.14. Exchangeable cation concentrations as a function of depth and time for the Base Run

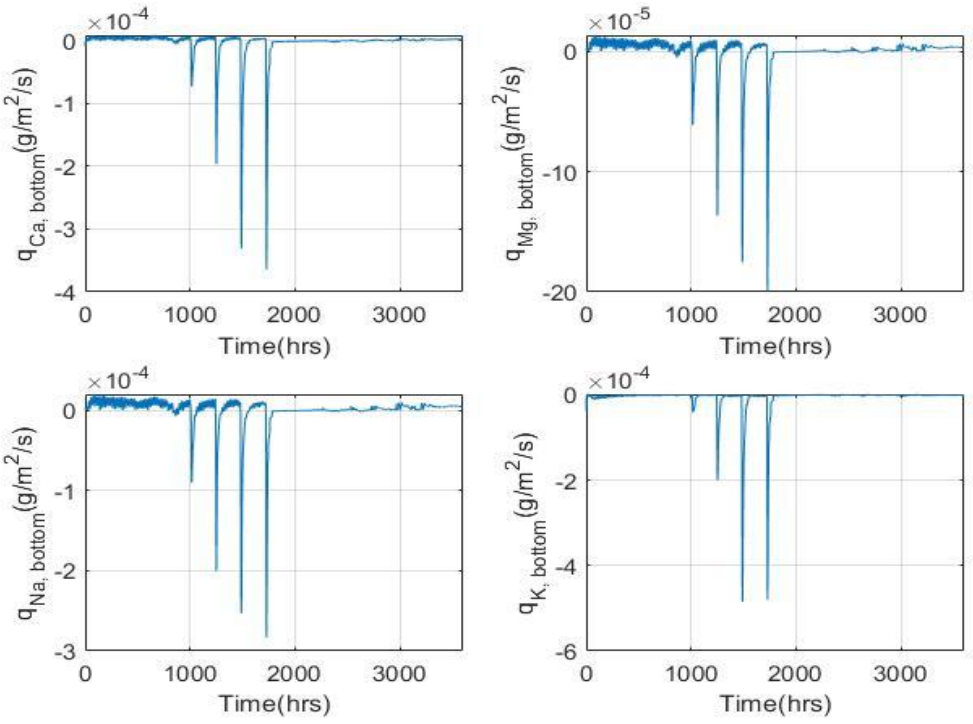


Figure 5.15. Cation fluxes at bottom of column as a function of time for the Base Run

Pressure head and water content data show that until the hydraulic conductivity undergoes the dramatic decrease around the 1700th hour, the applied water from the surface creates higher changes near the surface zone. At later times, because of the decrease in hydraulic conductivity, water content remains higher on average. At the bottom pf the soil column water content is steady governed by the

presence of the water table and the evaporation at the ground surface.. These effects can be seen in Figure 5.16 and Figure 5.17. The corresponding total liquid water content and vapor content as a function of time is presented in Figure 5.18.

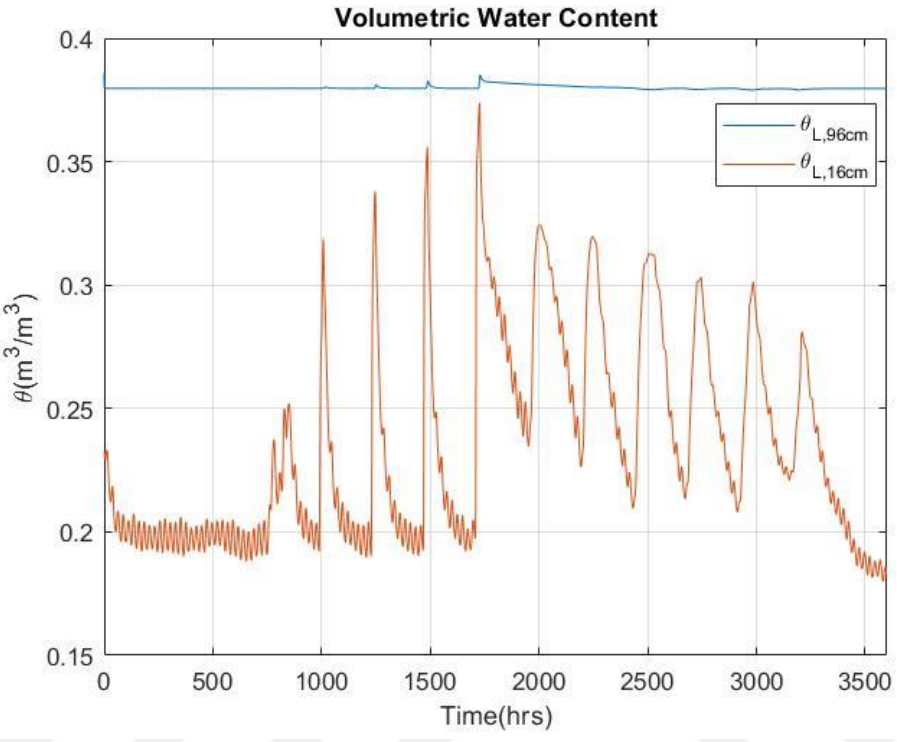


Figure 5.16. Water content as a function of time for the Base Run

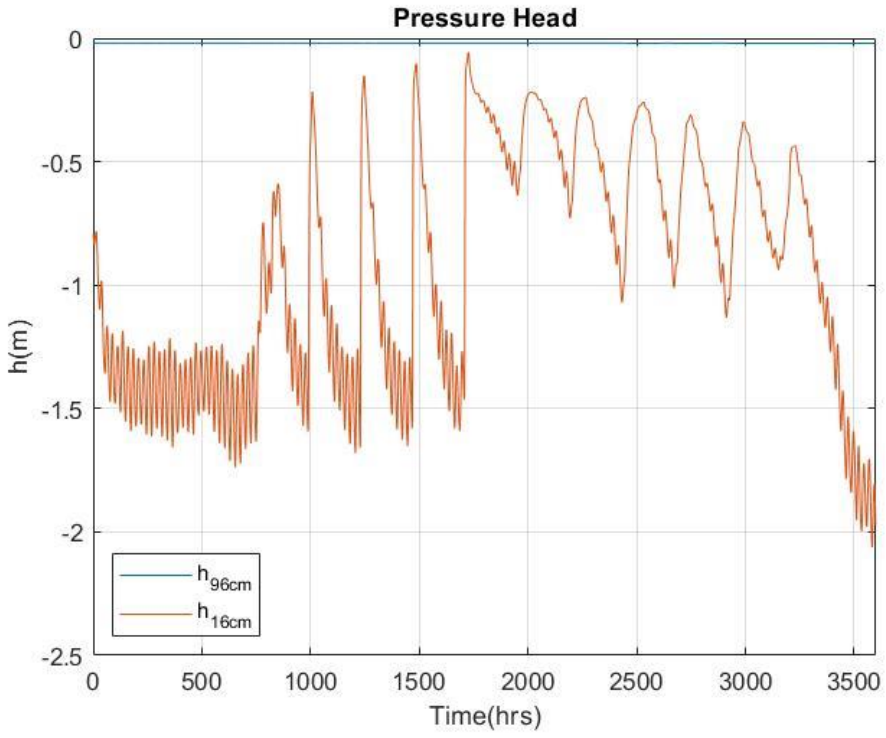


Figure 5.17. Pressure head as a function of time for the Base Run

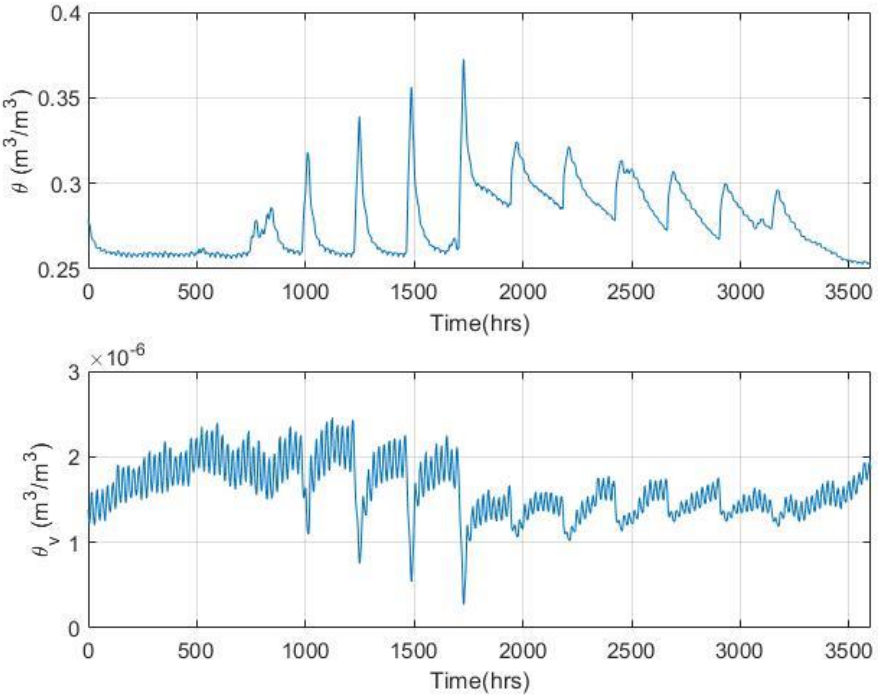


Figure 5.18. Liquid Water and vapor content over the entire column as a function of time for the Base Run

The variation of the water content in the soil column as a function of time over the duration of the base case is presented in Figure 5.19. At the end of the first two months the water contents are the same although the fluctuations are observable from Figure 5.16. However, at the end of the 3rd month, even though the surface is dry, the water accumulation can be seen in the middle. These movements of water content are in good agreement with what is seen in concentration distributions. Figure 5.19 also shows that those the highest subsurface evaporation rates are located in the top 30 cm from the surface where water content is highest. This effect is confirmed in Figure 5.20 which sows the evaporation rate Similarly, high summer temperatures in the soil lead to high evaporation rates and because of this, almost no condensation is observed within the soil. As expected, the highest peak is seen at the end of 3rd month which is the middle of the summer and irrigation rate is the highest.

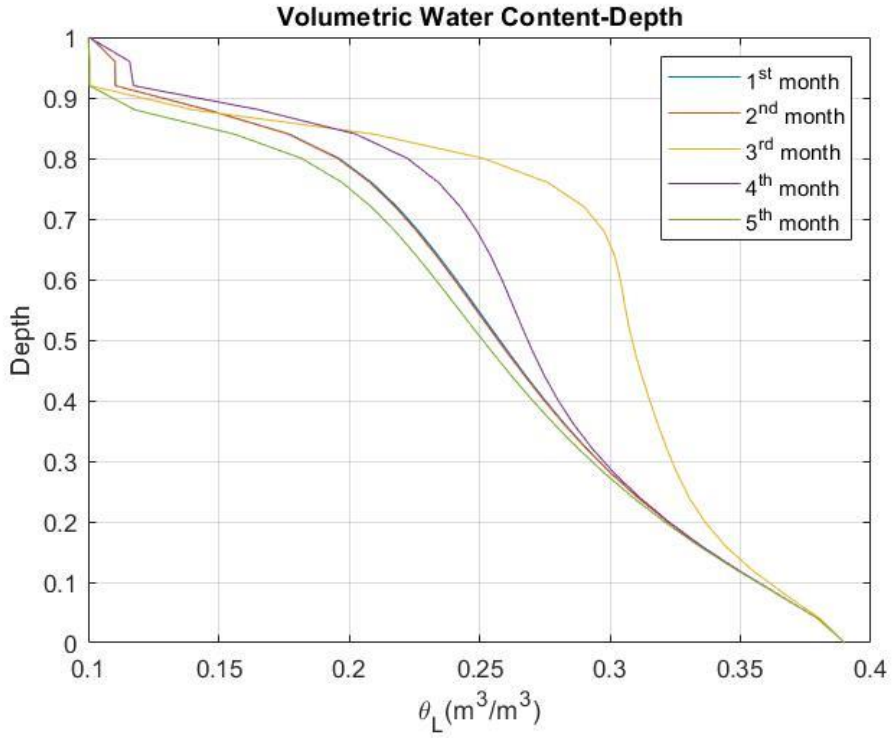


Figure 5.19. Water Content as a function of time and depth for the Base Run

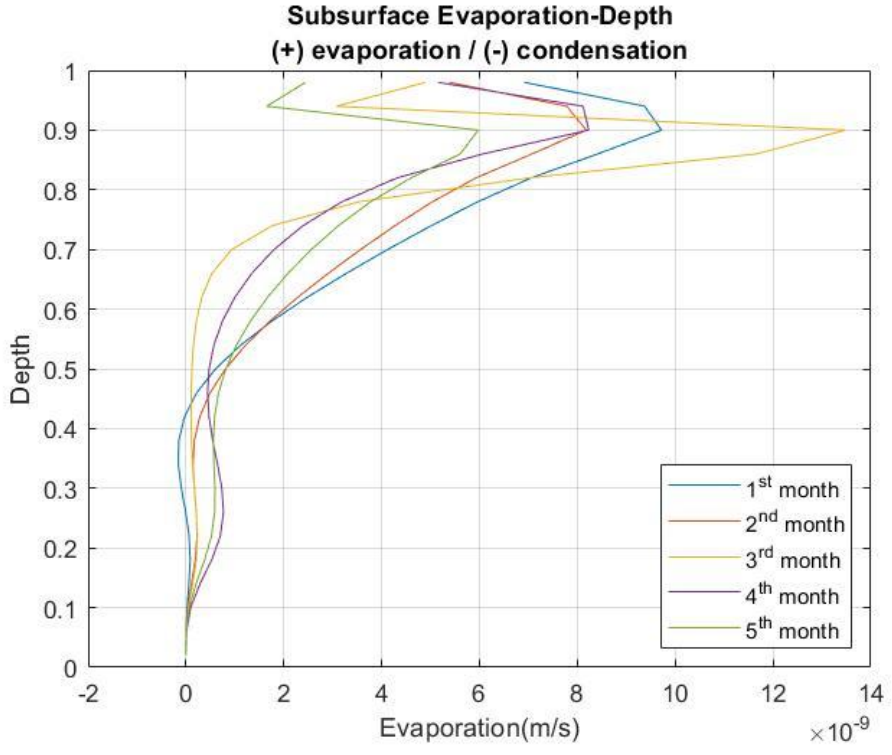


Figure 5.20. Subsurface evaporation rates as a function of time and depth for the Base Run

The temperature is a key element in all of these mechanisms, as many parameters are temperature dependent Figure 5.21 shows the distribution of the temperature as a function of time for two depths. The results indicate that near the surface zone large fluctuations are observed that are directly

influenced by the ambient atmospheric temperature. The daytime and nighttime temperatures are clearly observed. On the other hand, the temperature in the bottom part of the domain is much smoother. An interesting result at this point is that the highest evaporation rates are not seen in at the highest temperatures. Instead, high evaporation rates leads to evaporative cooling and even if the air temperature is higher at the middle of summer, the soil temperatures are lower than the ones in previous months. Figure 5.21 is also comparable to Figure 5.1 and without evaporative cooling due to irrigation, the temperatures would have reached to 30 °C. Note that the temperature of irrigation water is not considered in these calculations as it is taken as 15 °C which equals to reference temperature of entire model including the groundwater temperature.

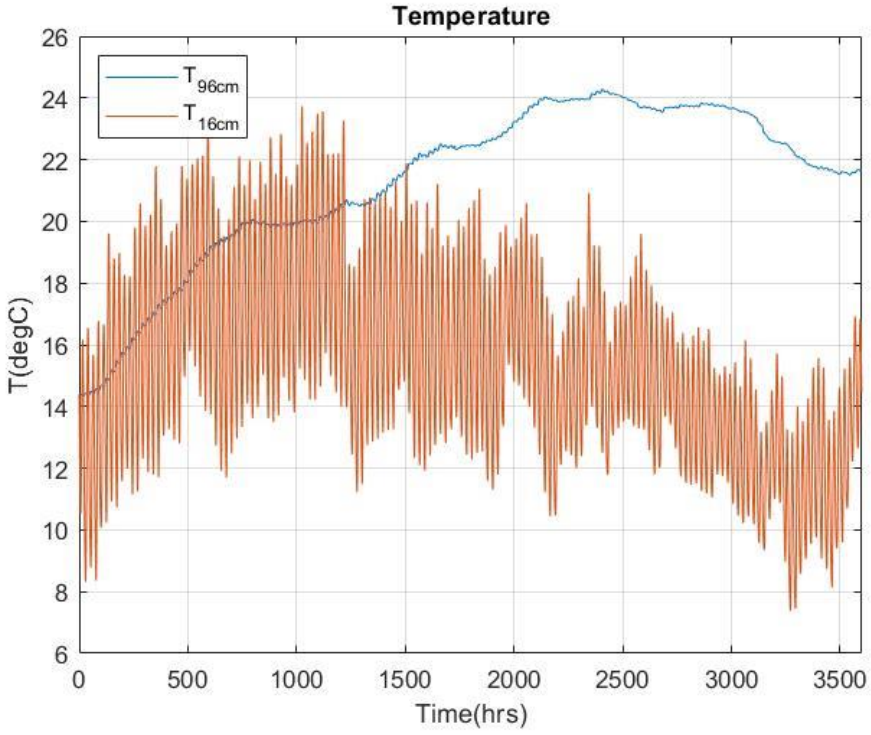


Figure 5.21. Temperature variations as a function of time for the Base Run

5.3. Case 1 – Non-Saline Groundwater Non-Sodic Soil

The results of the base case case show that the complexity of the mechanisms occurring during soil irrigation, namely the transport of water, heat and solute within the soil column. The risk of soil sodification is observed when high salinity water is used for irrigation coupled with high evaporative rates. In the following sections the results of the base case are compared to those for different cases. In case 1 we examine the impact of irrigation water quality. Specifically, the same initially healthy soil is irrigated with a non-sodic groundwater. The irrigation water quality is taken from (Bozdağ, 2014) for a well located close to a river. The parameters are given in Table 5.6.

Table 5.6. Irrigation water parameters in Case 1 (Bozdağ, 2014)

EC (dS m^{-1})	Ca (mg/L)	Mg (mg/L)	Na (mg/L)	K (mg/L)	SAR
0.69	80	25.21	25.33	4.68	0.63

The soil is assumed to planted with maize with the precipitation and irrigation schedule. And the rest of the parameters are the same with base run. Note that, in this model water flow driven by osmotic pressure is not included so the changes in water content stems from solute effects on hydraulic conductivity. However, significant changes are observed in ESP-SAR values as seen in Figure 5.22. Although some fluctuations in daily, ESP and SAR is observed, these two parameters remain close to their values at the beginning of the simulation. As a consequence, hydraulic conductivity values vary with water content but not due to sodicity variations shown in Figure 5.23.

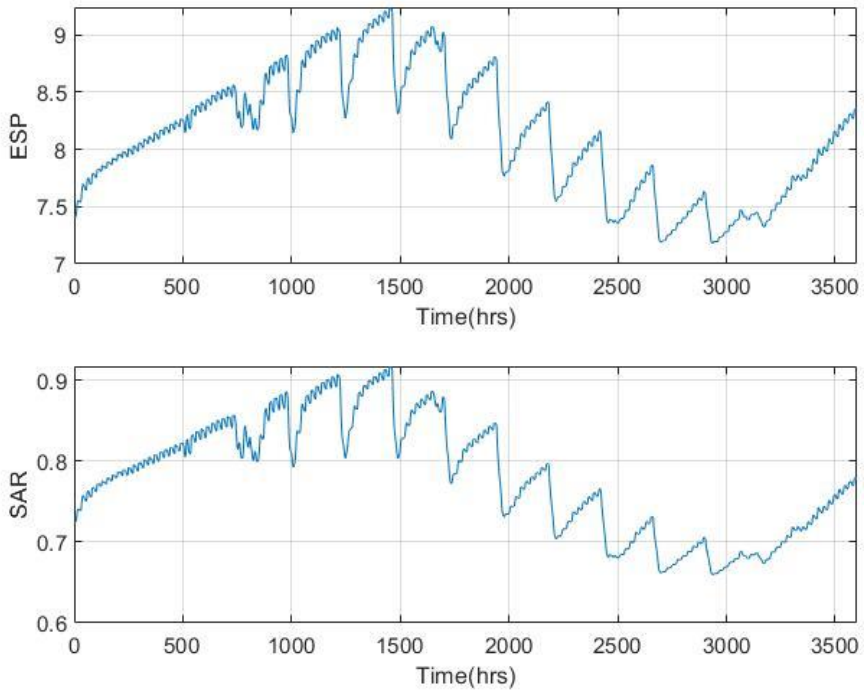


Figure 5.22. ESP and SAR values for Case 1

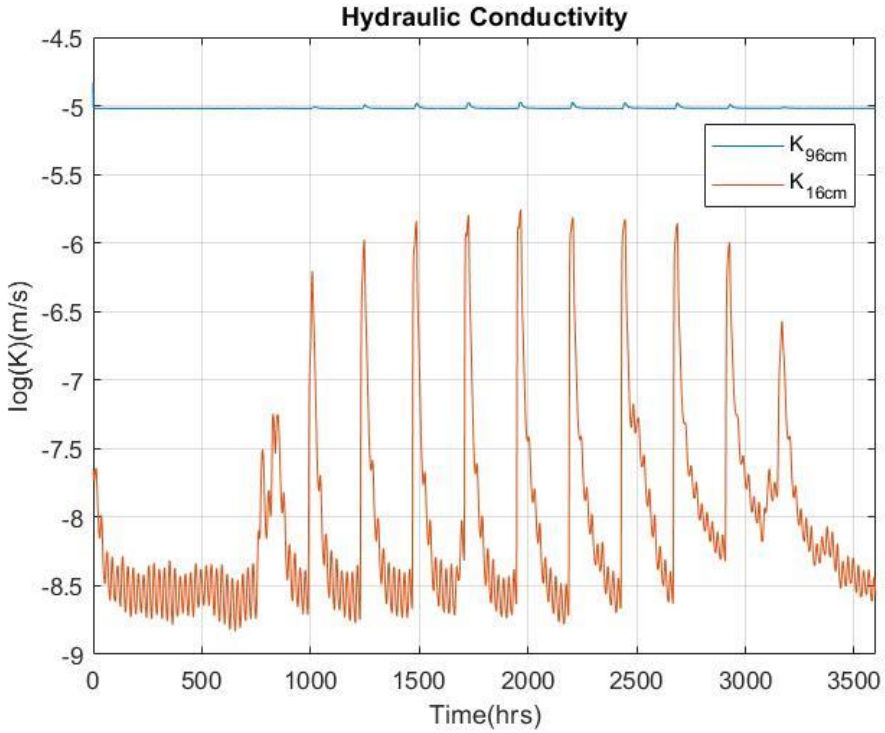


Figure 5.23. Hydraulic conductivities as a function of time at two depths for Case 1

The soluble and exchangeable concentrations for Case 1 are presented in Figure 5.24 and Figure 5.25. In contrast to the base run, the groundwater has less sodium than the soil, so as a result, some of the sodium is desorbed and is leached out from the soil to water table. The leaching rate is depicted in Figure 5.26.

The clogging effect can be easily seen when Figure 5.18 and Figure 5.27 are compared. The water quantity increases more in base as well as the concentrations. It is also validated from almost no bottom flux after clogging in Figure 5.15. This water accumulation creates root stress due to osmotic pressure and gives less space for soil aeration. On the other hand, the soil in Case 1 has time for aeration between irrigation cycles.

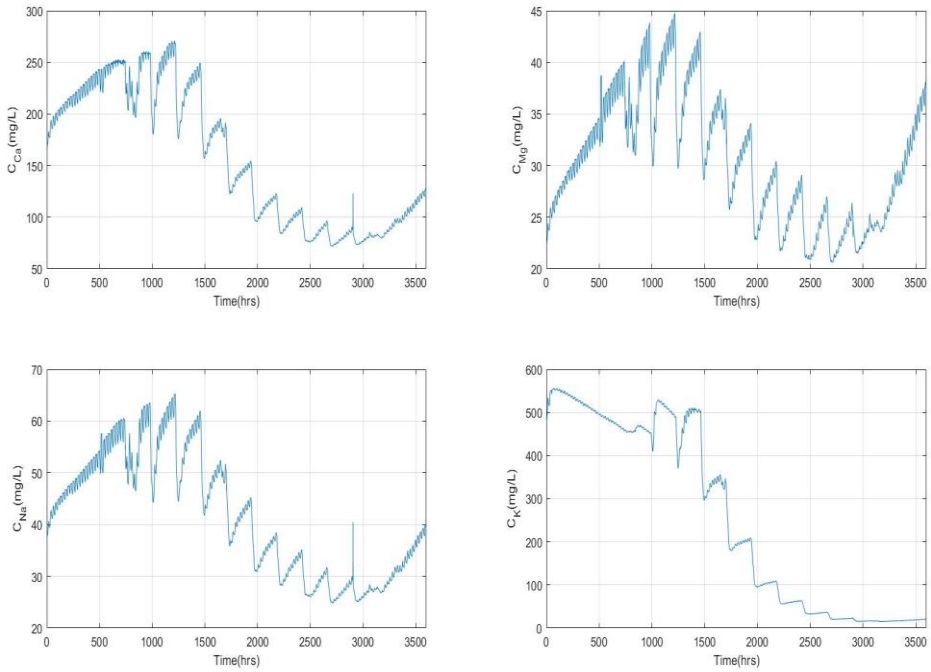


Figure 5.24. Soluble concentrations for Case 1

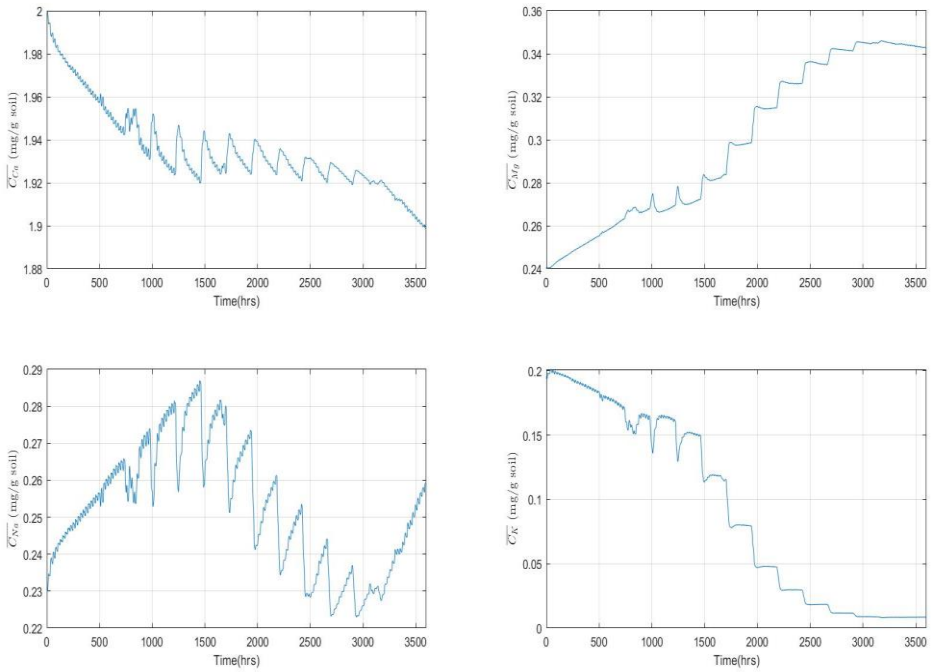


Figure 5.25. Exchangeable cation concentrations for Case 1

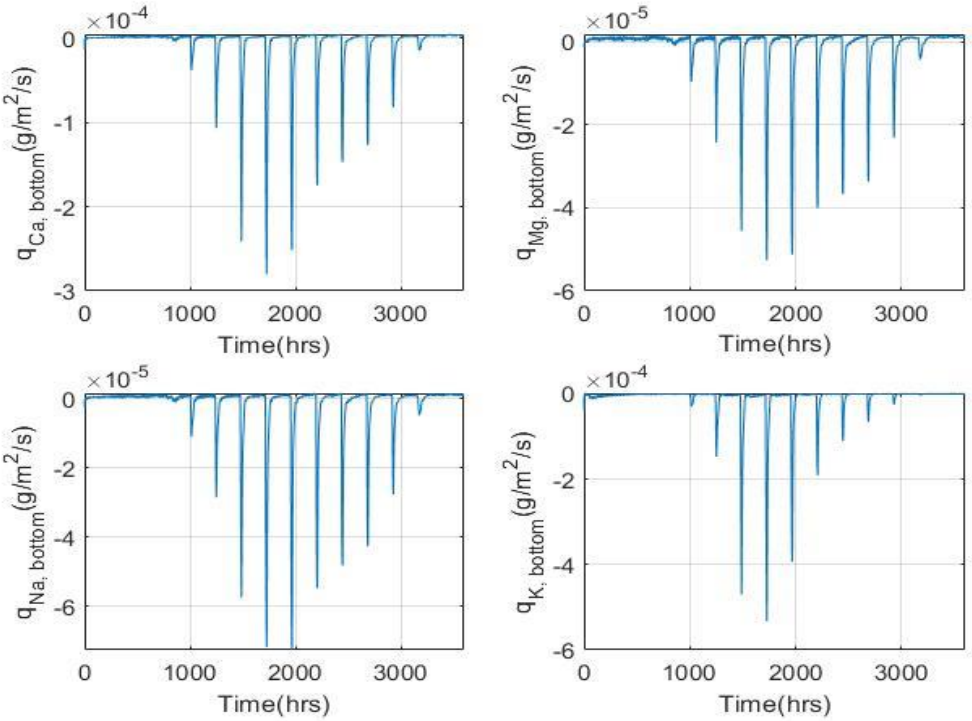


Figure 5.26. Solute bottom flux for Case 1

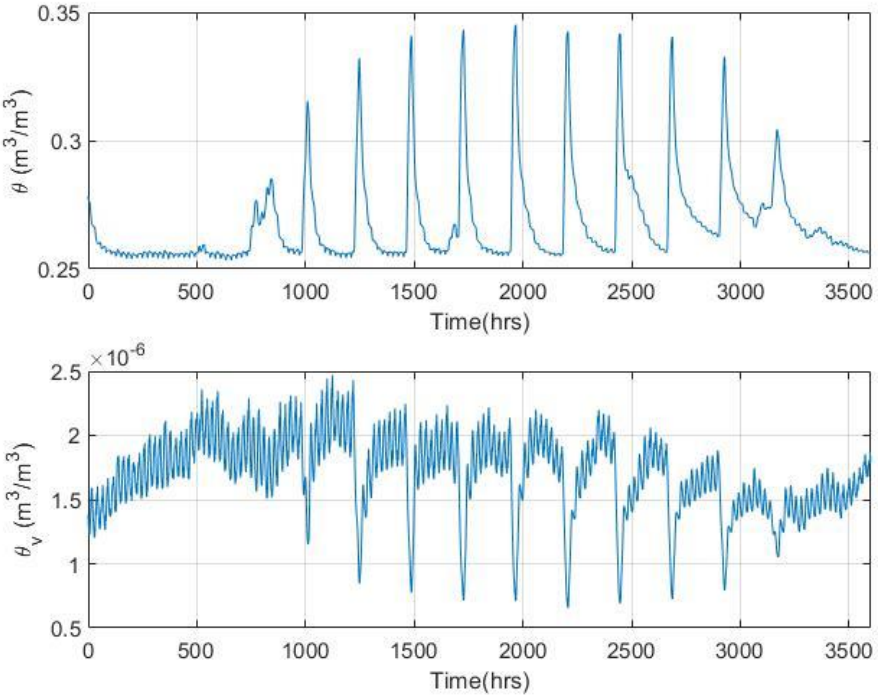


Figure 5.27. Liquid water and vapor content of the entire column as a function of time for Case 1

5.4. Case 2 – Climate Change Effects

According to recent IPCC report (IPCC, 2014), temperature and precipitation amounts over subtropical region are expected to change due to increase greenhouse gas emissions. For the region where Konya is located, as much as 3 °C of increase in surface temperatures and 20 decrease in yearly total precipitation are expected by the end of the century. It is also predicted that saline-sodic regions are prone to more drastic soil deterioration combined with extended periods of drought. To investigate this influence, Case 2 is similar to the base case except that the temperature is increased by 3 degrees while the precipitation is decreased by 20% with all other input parameters unchanged from the base run.

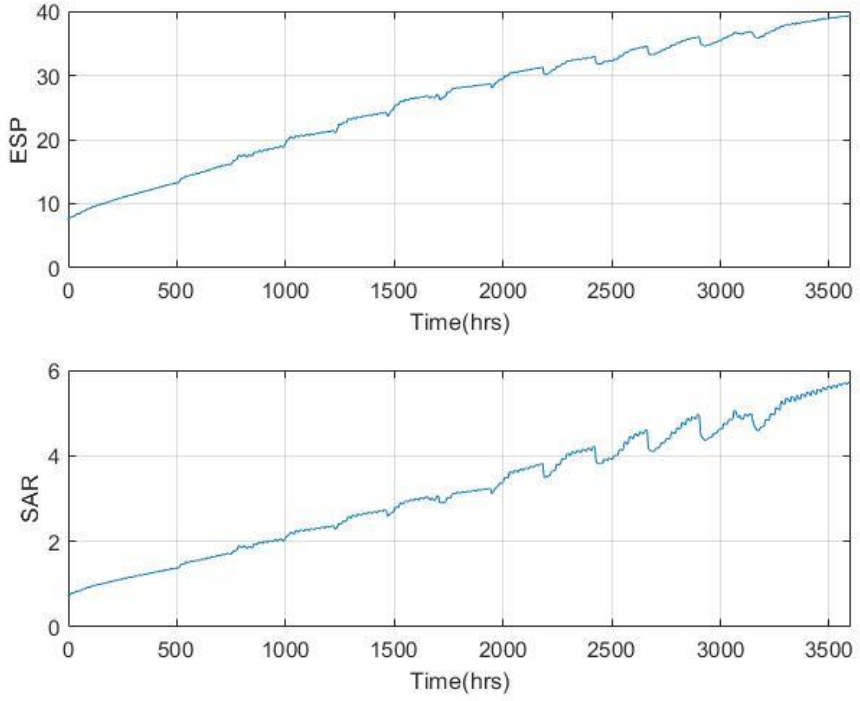


Figure 5.28. ESP and SAR as a function of time for Case 2

Figure 5.28 shows the ESP and SAR values as a function of time for Case 2. The results do not show significant changes on these two parameters over 1 season of crop growth. Figures 5.29 and 5.30 show the water content (liquid and vapor) and fluxes at the bottom boundary, respectively as expected slightly higher vapor content is observed because of the higher temperature. At the 3rd month, lower water content compared to Base Run is more obvious than the other months as shown in Figure 5.31. Hence, it can be said that the effects of summer on soil structure is enhanced with increasing drought. However, since irrigation is defined as the difference between the precipitation and crop water demand, irrigation compensates for the decrease in precipitation. Hence little

difference is observed between these two cases. Nevertheless, it can be seen, the liquid water content within the soil is higher with higher irrigation.

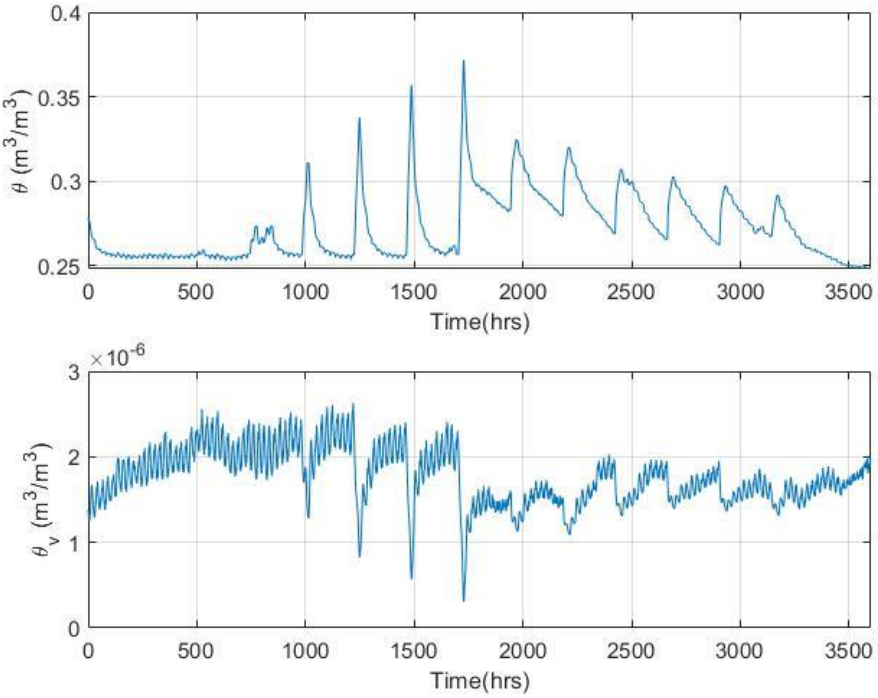


Figure 5.29. Liquid water and vapor content of the entire column as a function of time for Case 2

Another factor that makes the two cases similar is the presence of a shallow water table at the bottom boundary which increases the availability of water in the soil column.. Lower leaching rates after irrigations show this effect clearly in Figure 5.30. Hence the primary difference between Case 2 and the increased temperature due to climate change which tends to increase evaporation.

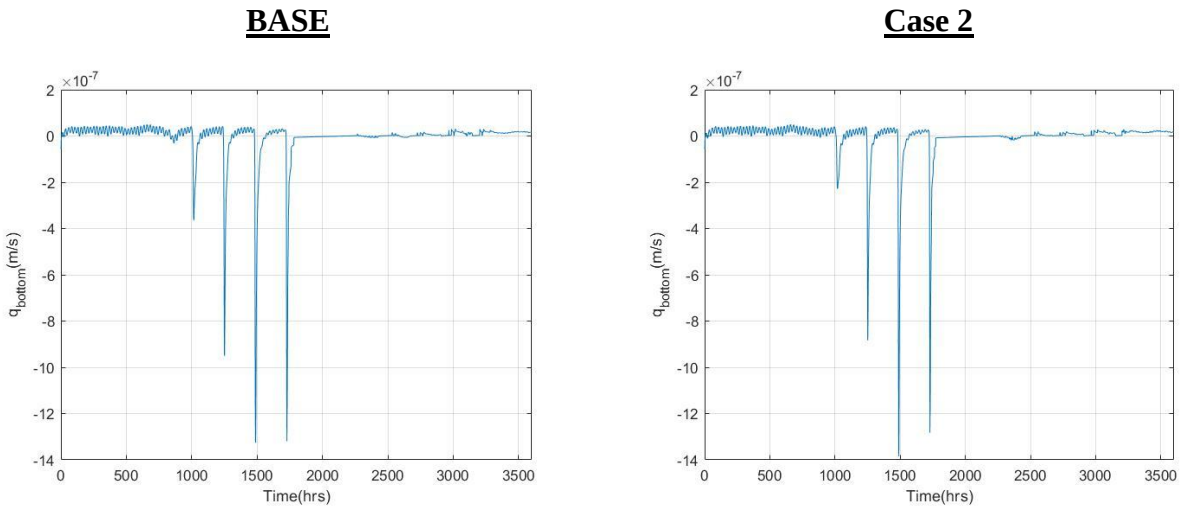


Figure 5.30. Water flux at the bottom of the domain for the Base Run and Case 2

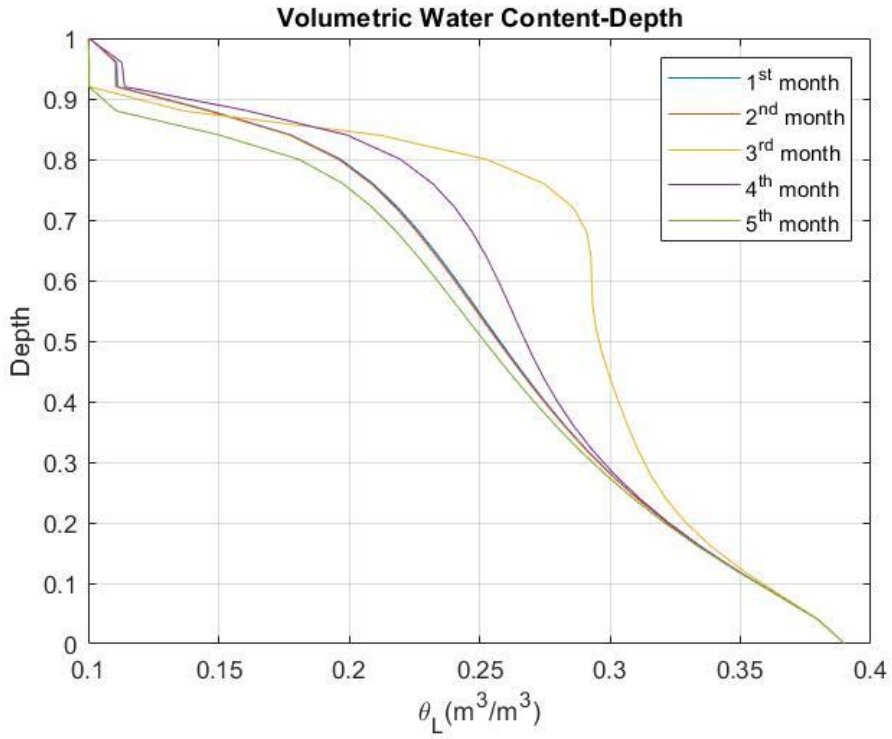


Figure 5.31. Water content as a function of depth and time for Case 2

5.5. Case 3 – Crop Type Effects

Crop type selection is another aspect that is thought to be affecting soil sodicity. As the crop type changes, most important parameters altered are irrigation scheduling and evapotranspiration rates. Hence, Case 3 examines the impact of the selected crop on salt accumulation. Specifically, the selected crop for Case 3 is sugar beet as it is one of the most common agricultural products in the Konya region which extensive agroindustry built around its production. The crop height is set to a

constant value of 30 cm and growth season is kept the same Hence, the irrigation is applied over the same period. However, water demand for sugar beets is greater than that for maize. The evapotranspiration rates used for irrigation are given in Table 5.7 based on the water requirements for the Konya region (TAGEM, 2017). All other parameters are kept as for the Base Case.

Table 5.7. Evapotranspiration rates of sugar beet in 10 days interval (TAGEM, 2017)

DOY	**130 - 140**	**141 - 150**	**151 - 160**	**161 - 170**	**171 - 180**	**181 - 190**	**191 - 200**	**201 - 210**	**211 - 220**	**221 - 230**	**231 - 240**	**241 - 250**	**251 - 260**	**261 - 270**	**271 - 280**
ET (mm)	13	19	31	38	51	64	70	71	77	68	65	65	52	31	22

The resultant irrigation pattern is shown in Figure 5.32. Although the growth season is longer, in order to not create difference due to meteorological data, the same part of the year is used. The effect of planting sugar beet instead of maize eventually increased ESP and SAR values to a higher level because of the saline groundwater used for irrigation. The ESP and VAR plots over one growth season are given in Figure 5.33.

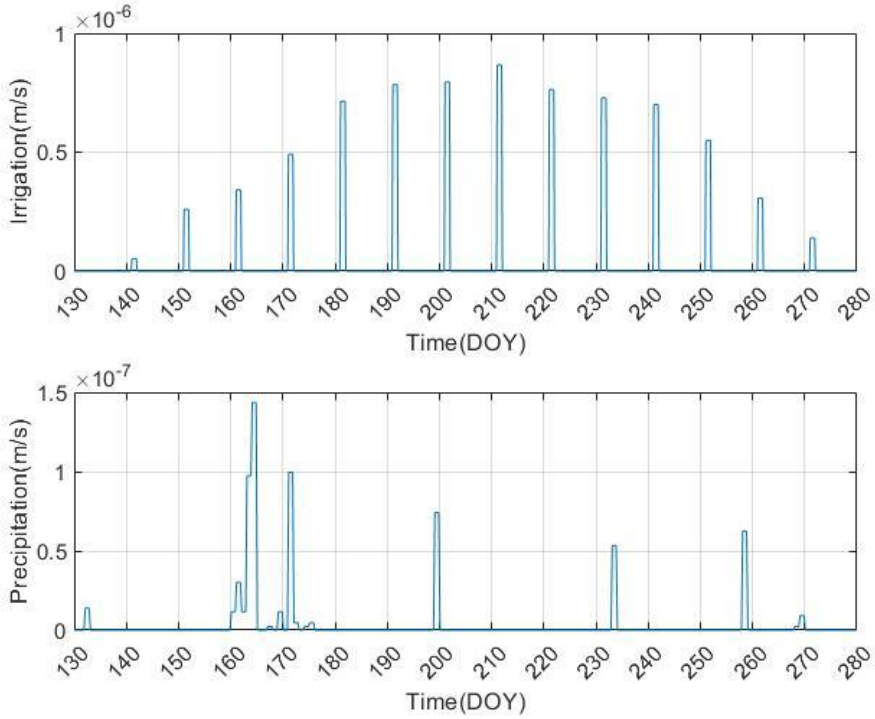


Figure 5.32. Irrigation and precipitation of Case 3

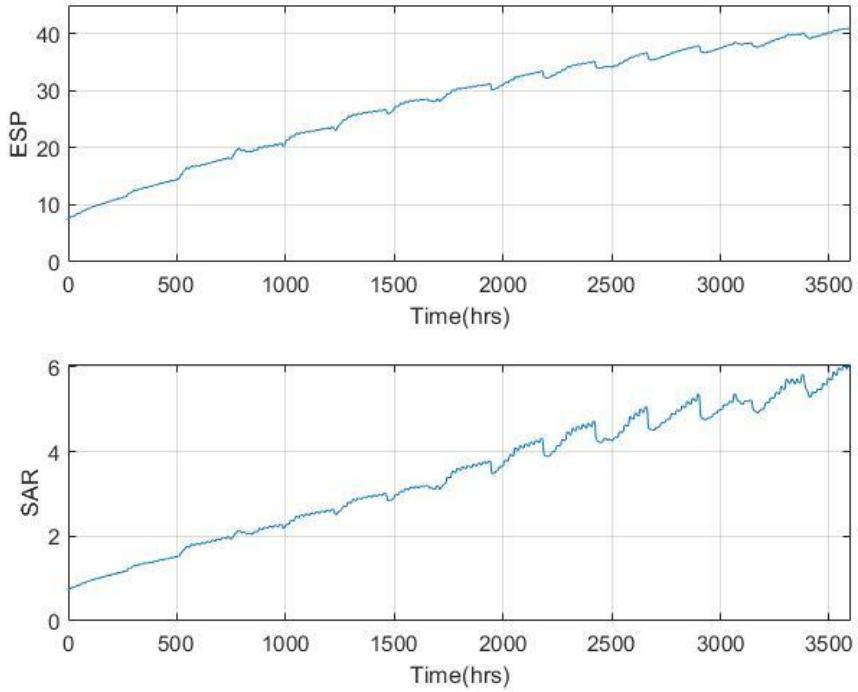


Figure 5.33. ESP and SAR values for Case 3

5.6. Case 4 – Vapor Flow Effects

Water flow in the soil can occur in two phases, liquid and vapor. As it can be seen from the equations including vapor transport brings extra complexity to the system. In this case we examine the significance of including vapor transport in the conservation equations. for this purpose, in Case 4, the vapor terms from the flux equation are excluded with only liquid water flow retained. All other input parameters are identical to that of the Base Case.

Figures 5.34 and 5.35 show the ESP and SAR values for Case 4 and the water content (now only liquid water) obtained for this case. Comparison with the Base Case shows that ignoring the vapor water flow leads to overestimation of water content in the soil and lower ESP and SAR values. Also, it is noticeable that the daily fluctuations observed in water content in base run are much lower in this case. So, it can be said that, for the conditions considered in these cases, vapor flow can have a significant impact on the simulated results..

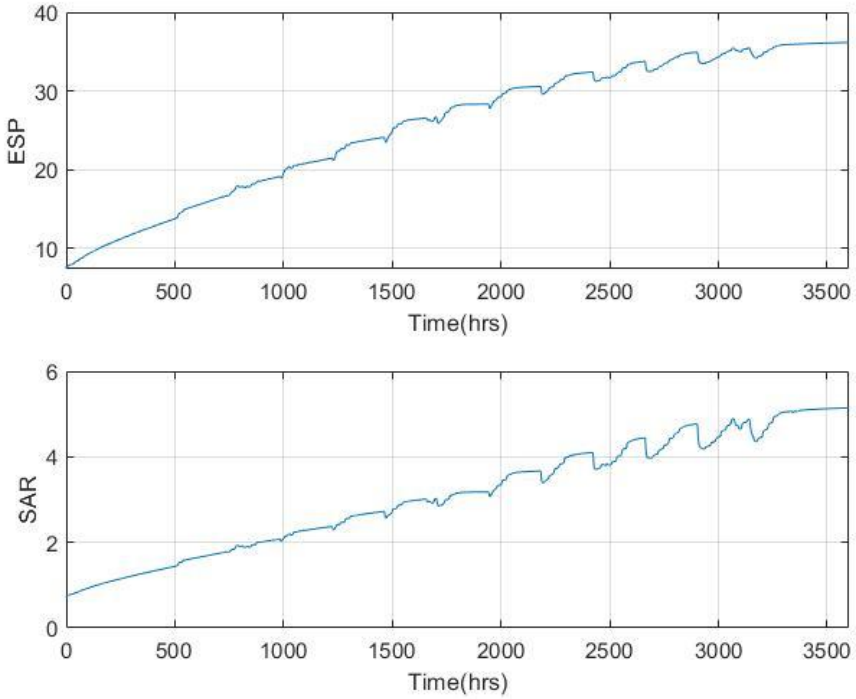


Figure 5.34. ESP and SAR values for Case 4

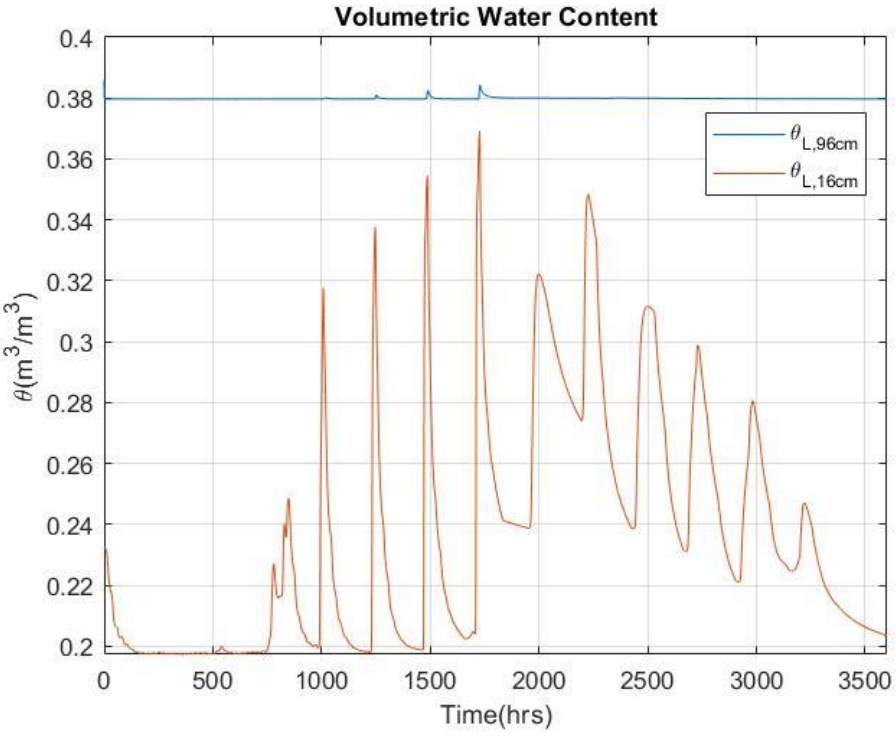


Figure 5.35. Water content as a function of time for Case 4

Also, before and after irrigation, profile plots of flux terms are provided in Figure 5.36 and Figure 5.37 from the base run and Case 4, respectively. The selected irrigation day is DAY 191 as it is one of the days with high water application. It is clearly seen that majority of water flow consists of vapor

flow at the upper parts of soil column when conditions are dry, and it is almost entirely liquid flow when conditions are wet. It is also noticeable from comparing near surface flux values that the vapor flow is replaced with liquid water flow in Case 4.

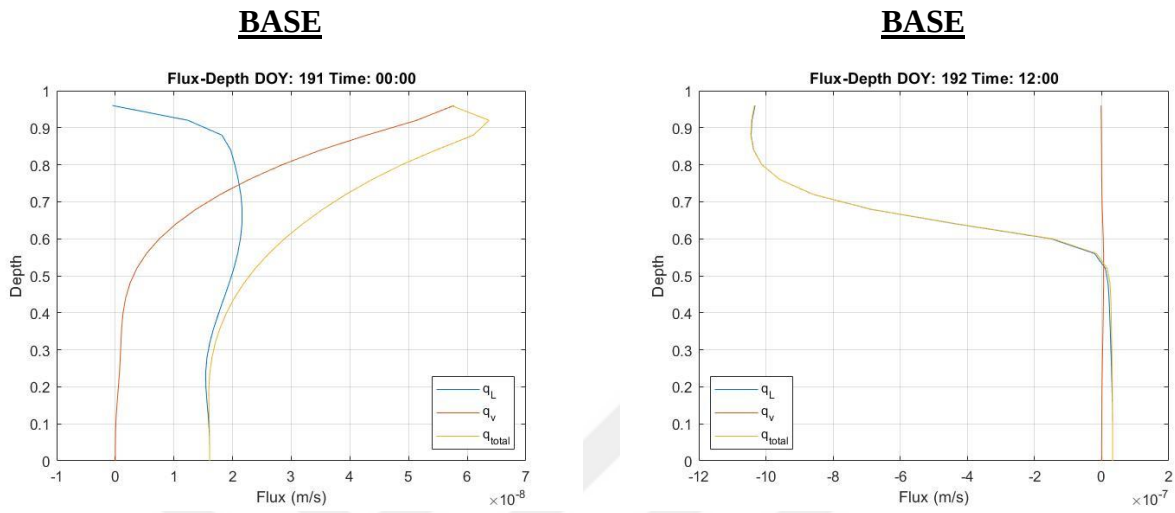


Figure 5.36. Flux distributions over depth before and after irrigation event on day 191 in Base Run for given time

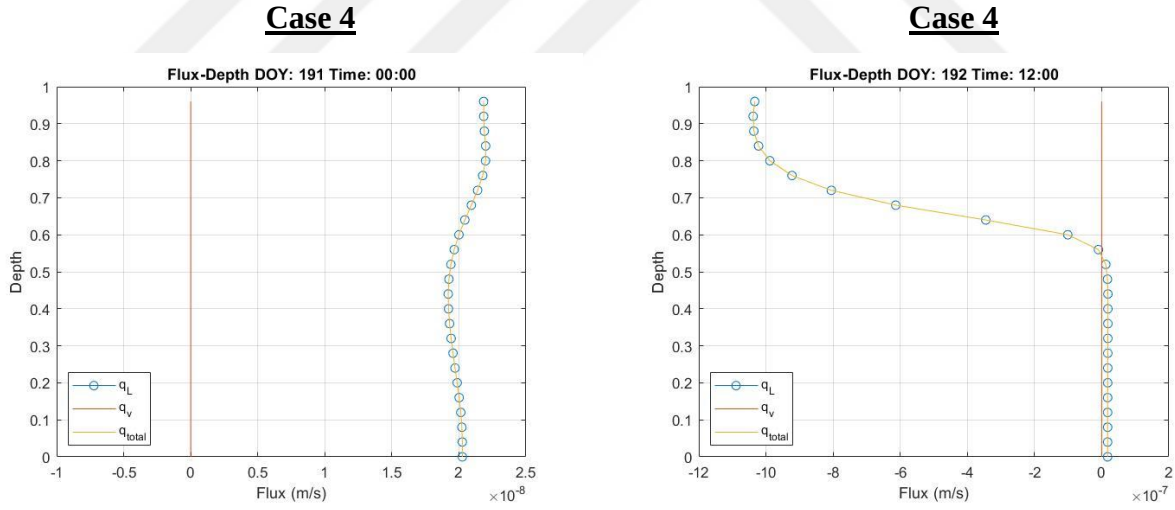


Figure 5.37. Flux distributions over depth before and after irrigation event on day 191 for Case 4

Finally, the partition of flux terms at the surface are shown in Figure 5.38 and Figure 5.39 from the base run and Case 4, respectively. The time shown is during and after the irrigation at DOY 231 and precipitation. While the soil surface is drying, which is interpreted by positive liquid flux at the surface, some of the resultant vapor travels inwards. This term is missed when vapor flux is not included.

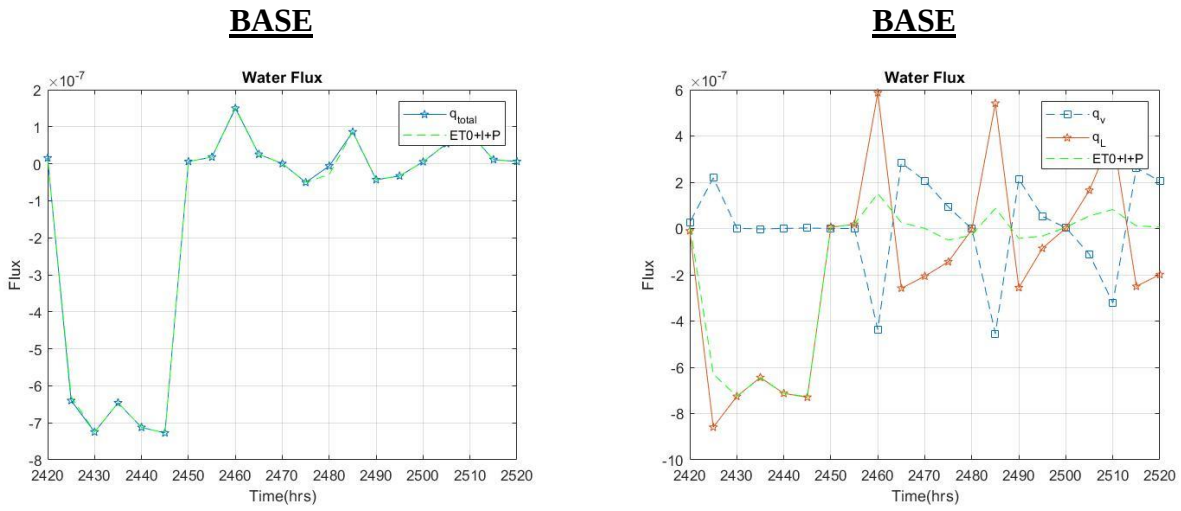


Figure 5.38. Total surface flux, liquid surface flux and vapor surface flux for the Base Run

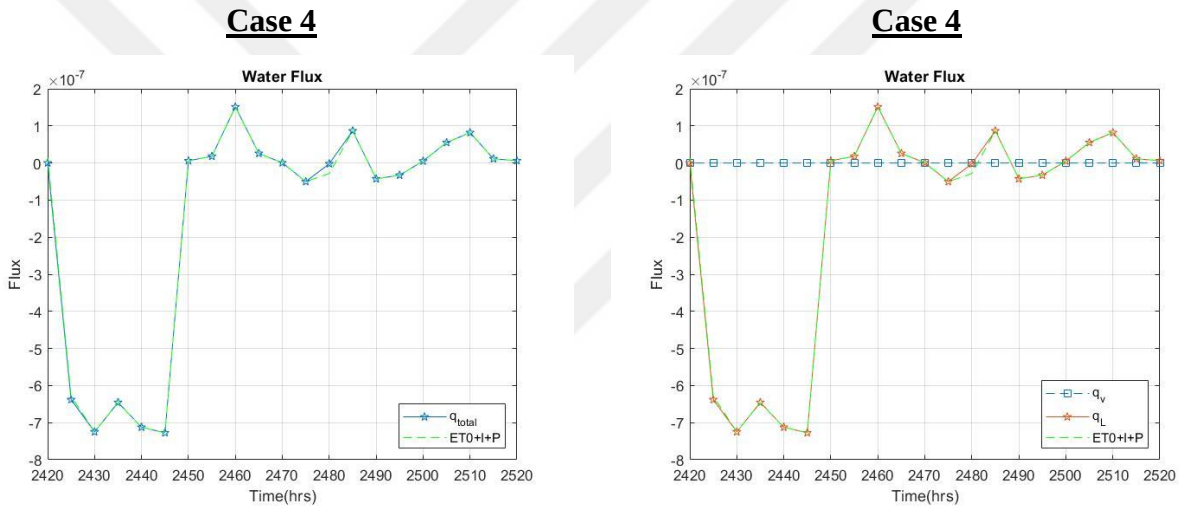


Figure 5.39. Total surface flux, liquid surface flux and vapor surface flux for Case 4

Another important outcome of excluding vapor flux is seen in temperature changes in the soil. The heat is transported in the form of latent heat along with vapor flux. So, when it is not taken into account, lower temperatures are seen. This can be observed Figure 5.40 with its counterpart in the base run. Apart from this, without vapor transport, the vapor occurring at a level cannot leave its place, so the behavior of subsurface evaporation becomes mostly condensation which is the opposite of the base run, although the order is much lower. This effect can be seen in Figure 5.41.

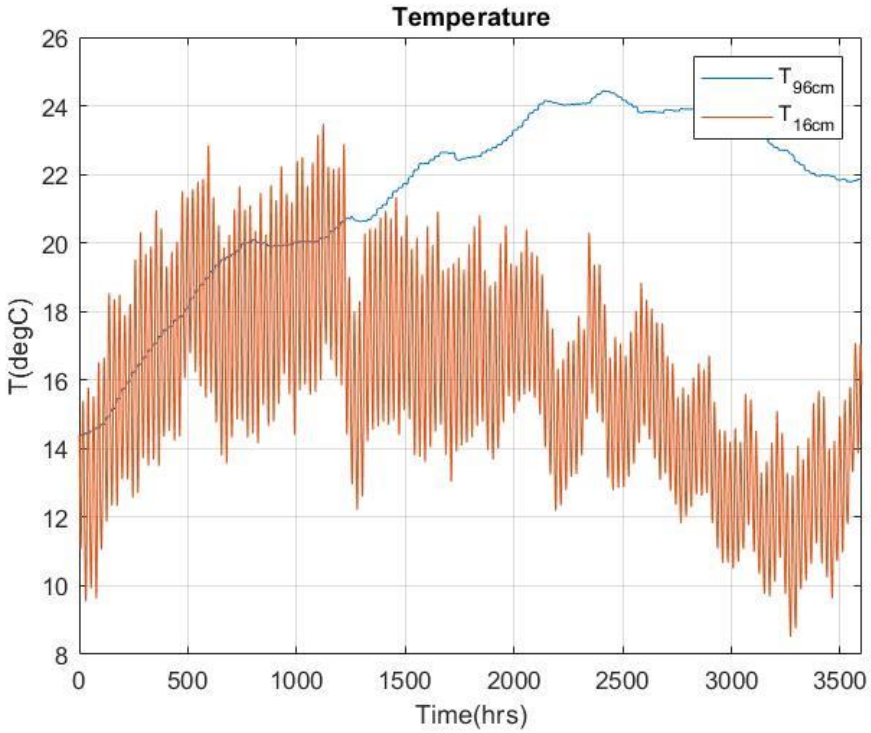


Figure 5.40. Changes in temperature at different levels for Case 4

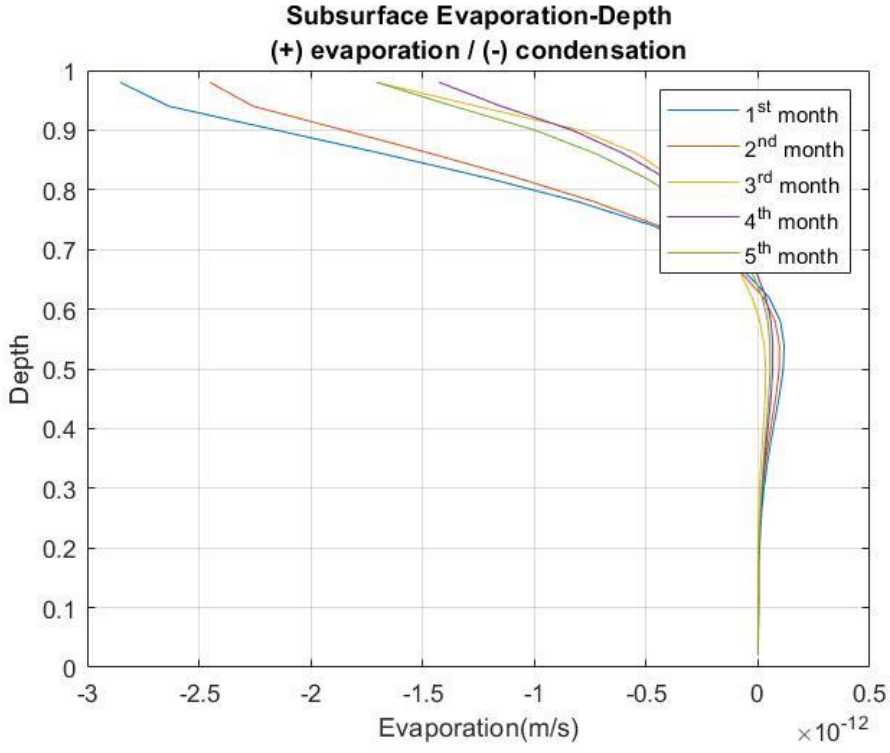


Figure 5.41. Subsurface evaporation / condensation in Case 4

The overall quantities of water and vapor content are also given in Figure 5.42 and liquid content shows noticeable increase. On the other hand, the vapor content is the same. The reason to that is,

although there is less space in soil for moist air in the Case 4, the relative humidity values are found to be higher as given in Figure 5.43.

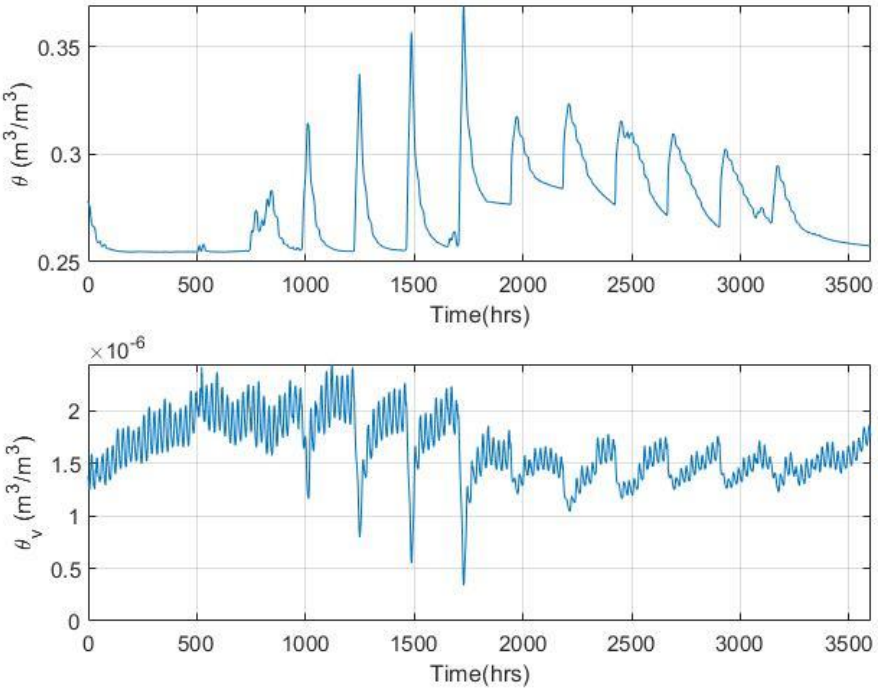


Figure 5.42. Liquid water and vapor content of entire column as a function of time for Case 4

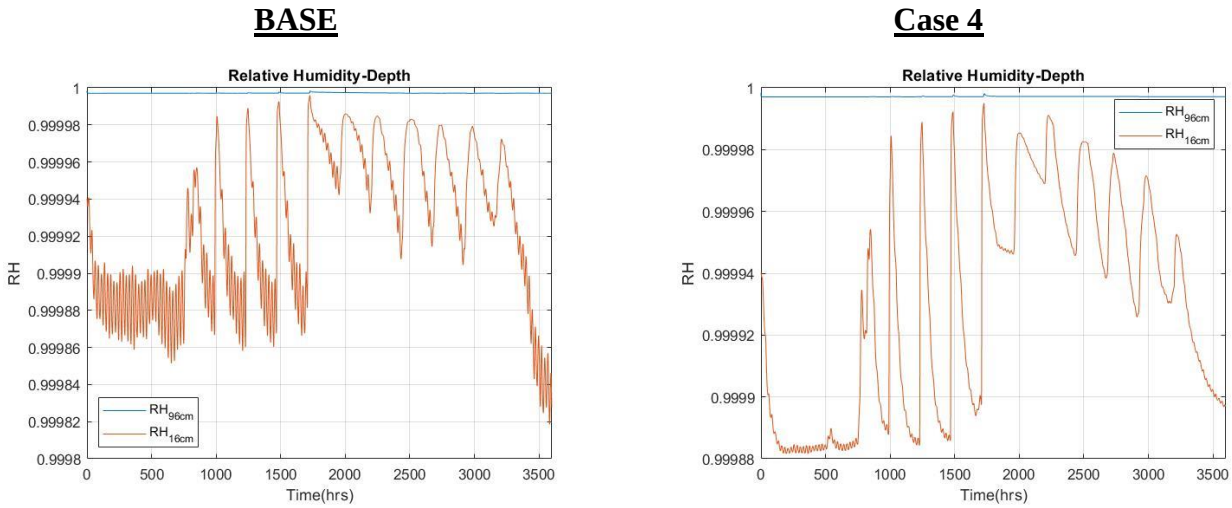


Figure 5.43. Relative humidity values for the Base Run and Case 4

6. CONCLUSIONS AND FUTURE RESEARCH

Large fractions of the agricultural soils, particularly in arid and semi-arid regions of the world suffer from the problem of soil sodification due to the use of groundwater with levels of solutes for irrigation purposes. The processes leading to the accumulation of salts in the soil are complex governed by the flow of water, and the transport of heat and solutes in the soil column. In theory, these processes are fully coupled and must be solved simultaneously to accurate predict the flow of water and solutes in the soil due to irrigation. However, often models are simplified by focusing on particular processes while ignoring the other.

In this study a coupled physically based model of water flow (both liquid water and vapor), heat transport and solute transport is developed. The developed code also allows for detailed analyses for short and long term changes in soil structure due to agricultural processes. As one of the important findings, including daily variations may not be as important as for short periods. Similarly, if the water availability is questioned in the long run, the vapor flow may be excluded but if the solute distribution is examined vapor flow has a certain effect. Another important result is about the importance of selecting crop type. However, the most significant result of this study is showing the clogging effect due to sodicity and how this situation makes the soil ineffective for agricultural purposes.

The different modules of the model were first validated by comparing its out to the output from HYDRUS a widely used software for water and solute transport in soil. Overall, the model results were found to be consistent with HYDRUS results. For demonstration purposes the model was then applied to hypothetical agricultural area planted with maize. Meteorological and water quality data were adopted from the Konya region. However, the model could readily be applied to other regions or conditions. Besides the based case, the model was used to simulate water, heat and solute transport for 4 different cases. The main findings of this study are:

- The base case demonstrated the interconnectedness of the different processes, highlighting the need to develop a physically-based couple system for the accurate simulation of water and solute within agricultural soils. For the conditions considered, this run showed the potential for accumulation of salts within the soil and the increase of the ESP and SAR parameters and the corresponding risk of soil clogging which can be detrimental to crop yields.

- Case 1 considered the impact of water quality on the SAR and ESP values. It is observed that these parameters can be maintained under control with limited decrease in hydraulic conductivity if better groundwater is used for irrigation.

- Case 2 considered the effect of expected changes in temperature and precipitation due to climate change. The result is that these effects are not as important as irrigation water quality while assessing sodicity, at least for regions with shallow water table.

- Case 3 showed the direct effect of crop type as it changes the irrigation pattern and evapotranspiration values. Expectedly, the crops are selected in a way that the farmer is willing to make the highest profit. However, disregarding the sodicity inducing effects of a crop type may be costly as it can result in agricultural soil loss.

- Case 4 was actually about the importance of including vapor flow in the calculations. The increased workload comes with heat and vapor calculations is undeniable however it is clearly shown that using water flow only underestimates the sodicity level. As most of the vapor flow occurs near surface, the uncalculated quantity of adsorbed solute is located at this layer and this situation may lead to underestimation of stress that the roots experienced.

The model was then to examine the problem of sodicity and was applied to a hypothetical field where the meteorological conditions are not favorable in terms of drought. As presented here, the main focus was to assess the sodicity risk associated with irrigation of agricultural lands over a single crop growth season. However, the model can also be applied to specific field problems to identifying optimal crop selection and for managing salinity and sodicity impacts for longer time periods and variable climatic conditions.

The work conducted in this study can help identify future lines of research. In the future, the code can be expanded to include other ions' effects, such as pH sensitivity and so on. Similarly, precipitation of salts can be a significant thing to add as it changes porosity and thermal conductivity of the soil and needless to say the ESP and SAR values. In addition, water flow due to osmotic pressure can be a key element especially for saline-sodic soils. The root stress is another phenomenon which comes hand in hand with osmotic pressures as the plants may not be able to get the water from the soil and this effect can be added. Apart from this, plant growth can be modeled as a function of

water and nutrients available to them. The impact of soil heterogeneity could be readily examined with the developed code as soils are often recognized to vary spatially and with depth.

The definition of soil column can be expanded from 1D to 2D or 3D depending on the calculation technique used. In this model, the explicit method is used to solve the governing partial differential equations which is well-known for its instability problems although it is easier to program. Future research can incorporate the option of other numerical schemes such as the implicit or semi-implicit methods. For example, the software, HYDRUS referred here, uses a computational technique called Picard iterations which allows for much larger time steps and is therefore computationally more efficient than the explicit scheme used in this study.

An advantage of developing a modular code like this is that it is possible to replace any of the models used with updated ones. For example, the hydraulic conductivity reduction equations are quite old dating back to 1968. Based on specific experiments the reduction terms could be modeled differently. Doing this type of work is not an option with commercial software.

Overall, this study underscores the complex mechanisms that govern the flow of water and solutes in agricultural soils. Numerical models can serve as an important tool for the simulation of these mechanisms and their impacts on crop yields and for identifying best practices to alleviate their adverse effects.

REFERENCES

Allen, R. G., Pereira, L. S., Raes, D., & Smith, M. (2006). FAO Irrigation and Drainage Paper No. 56 Crop Evapotranspiration.

Alley, W. M., Reilly, T. E., & Franke, O. L. (1999). General Facts and Concepts About Ground Water. In Sustainability of Ground-Water Resources (p. 6). Denver, Colorado: U.S. Geological Survey Circular 1186.

Ayers, R., & Tanji, K. (1981). An application from Ayers and Westcot's 1985 "Use of treated municipal wastewaters for irrigation. ASCE 1981 Water Forum Conference Proceedings.

Berke, M. Ö., Dıvrak, B. B., & Sarısoy, H. D. (2014). Konya'da Suyun Bugünü Raporu. WWF-Türkiye.

Beyer, M. (2016). Quantitative Studies Along The Soil –Vegetation – Atmosphere Interface Of Water – Limited Environments: Practice-Oriented Approaches Based On Stable Water Isotopes, Modeling And Multivariate Analysis.

Bozdağ, A. (2014). Combining AHP with GIS for assessment of irrigation water quality in Çumra irrigation district (Konya), Central Anatolia, Turkey. Environ Earth Sciences,73:8217-8236.

Brooks, R. H., & Corey, A. T. (1964). Hydraulic Properties of Porous Media, Hydrology Papers, Colorade State University, No:3.

Brutsaert, W. (1982). Evaporation into the atmosphere: Theory, history, and applications. D. Reidel Publ.: Dordrecht, the Netherlands.

Campbell, G. S., & Norman, J. M. (1998). An Introduction to Environmental Biophysics., Edition 2, Springer, New York, NY.

Cass, A., Campbell, G., & Jones, T. (1984). Enhancement of thermal water vapor diffusion in soil. Soil Science Society American Journal, 25-32.

Chaudhari, S. K. (2001). Saturated Hydraulic Conductivity, Dispersion, Swelling, And Exchangeable Sodium Percentage Of Different Textured Soils As Influenced By Water Quality. Communications in Soil Science and Plant Analysis.

Chung, S.-O., & Horton, R. (1987). Soil Heat and Water Flow With a Partial Surface Mulch, Water Resources Research, Vol:23, No:12, 2175-2186.

Daamen, C. C., & Simmonds, L. P. (1996). Measurement of Evaporation from Bare Soil and its Estimation Using Surface Resistance. Water Resources Research, 1396-1402.

Davis, J., Waskom, R., & Bauder, T. (2007). Managing Sodic Soils. U.S. Department of Agriculture and Colorado CSU Extension.

Dıvrak, B. B., İş, G., & Ayas, C. (2007). Complementary financing for Environment in the context of Accession – Innovative Sources. WWF Türkiye.

Dogan, S., Berktay, A., & Singh, V. P. (2012). Comparison of multi-monthly rainfall-based drought severity indices, with application to semi-arid Konya closed basin, Turkey. Journal of Hydrology,470-471,255-268.

GENUCHTEN, M. T. (1980). A Closed-form Equation for Predicting the Hydraulic Conductivity of Unsaturated Soils. Soil Science Society of America Journal,44:892-898.

Genuchten, M. T. (1980). A closed-form equation for prediction they hydraulic conductivityof unsaturated soils. Soil Science Society America Journal, 44, 892-898.

Griend, A. A., & Owe, M. (1994). Bare soil surface resistance to evaporation by vapor diffusion under semiarid conditions. Water Resources Research, Vol. 30, No. 2,181-188.

Griffin, R. A., & Jurinak, J. J. (1973). Estimation of Activity Coefficients from the Electrical Conductivity of Natural Aquatic Systems and Soil Extracts. Soil Science, Vol.116, No. 1, 26-30.

Grifoll, J., & Josep Ma. Gasto, Y. C. (2005). Non-isothermal soil water transport and evaporation. Advances in Water Resources, 1254.

H. Frenkel, J. O. (1978). Effects of Clay Type and Content, Exchangeable Sodium Percentage, and Electrolyte Concentration on Clay Dispersion and Soil Hydraulic Conductivity. Soil Science Society of America Journal, 42, 32-39.

Hanson, B. R., Grattan, S. R., & Fulton, A. (1999). Agricultural Salinity and Drainage. Water Management Series publication 3375, 47.

Hem, J. D. (1961). Calculation and Use of Ion Activity. Geological Survey Water-Supply Paper 1535-C.

Ingrid Y. Padill, a. T., & Conklin, M. H. (1999). The effect of water content on solute transport in unsaturated porous media. Water Resources Research, 3303-3313.

IPCC. (2014). Climate Change 2014: Synthesis Report. Geneva, Switzerland.

M. Seilsepour, M. R. (2009). Prediction of Soil Exchangeable Sodium Percentage Based on Soil Sodium Adsorption Ratio. American-Eurasian Journal of Agricultural & Environmental Sciences, 01-04.

McNeal, B. L. (1968). Prediction of the Effect of Mixed-Salt Solutions on Soil Hydraulic Conductivity. Soil Science Society of America Journal,Vol. 32, No.2,190-193

Meterological Service Of Turkey. (2021, December). Retrieved from https://mgm.gov.tr/veridegerlendirme/il-ve-ilceler-istatistik.aspx?k=undefined&m=KONYA, Retrieved Dec. 25, 2021.

TSMS. (2018). Türkiye Yillik Global Güneş Radyasyonu. T.C. Tarim Ve Orman Bakanliği Meteoroloji Genel Müdürlüğü.

Miller, G. R., Rubin, Y., Mayer, K. U., & Benito, P. H. (2008). Modeling Vadose Zone Processes during Land Application of Food-Processing. Journal of Environmental Quality, 37, S-43.

Monteith, J. L. (1965). Evaporation and Environment. Symposia of the Society for Experimental Biology, 205-224.

Mualem, Y. (1976). A new model for predicting the hydraulic conductivity of unsaturated porous media. Water Resources Research, 513-522.

Narasimhan, T. N. (2005). Buckingham, 1907: An Appreciation. Vadose Zone Journal, 434.

Nassar, I., & Horton, R. (1992). Simultaneous transfer of heat, water, and solute in porous media: I. Theoretical development. Soil Science Society of America Journal, 1350-1356.

Noborio, K., McInnes, K. J., & Heilman, J. L. (1996a). Two-Dimensional Model for Water, Heat, and Solute Transport in Furrow-Irrigated Soil: I. Theory. Soil Science Society of America Journal, 1001-1009.

Noborio, K., McInnes, K. J., & Heilman, J. L. (1996b). Two-dimensional model for water, heat, and solute transport in furrow-irrigated soil: II. Field evaluation. Soil Science Society of America Journal, 1010-1021.

Penman, H. L. (1948). Natural evaporation from open water, bare soil and grass, Proceedings of the Royal Society A,193: 120-145.

Philip, J. R., & Vries, D. A. (1957). Moisture Movement in Porous Materials under Temperature Gradient. American Geophysical Union, 222-232.

Quirk, J. P., & Schofield, R. K. (1955). The Effect Of Electrolyte Concentration On Soil Permeability. Journal of Soil Science, Vol. 6, No.2, 163-178.

Reeve, R. C., Bower, C. A., Brooks, R., & Gschwend, F. B. (1954). A Comparison of the Effects of Exchangeable Sodium and Potassium upon the Physical Condition of Soils. Soil Science Society of America Journal, 130.

Richards, L. A. (1931). Capillary Conduction of Liquids Through Porous Mediums. American Institute of Physics, 318-333.

Richards, L. A. (1954). Diagnosis and Improvement of Saline and Alkali Soils. Washington: U.S. Government Printing.

S. Siebert, J. B. (2010). Groundwater use for irrigation – a global inventory. Hydrology and Earth System Sciences, 1863-1880.

Saito, H., Simunek, J., & Mohanty, B. P. (2006). Numerical Analysis of Coupled Water, Vapor, and Heat Transport in the Vadose Zone. Vadose Zone Journa, 784-800.

Sakai, M., Toride, N., & Simunek, J. (2009). Water and Vapor Movement with Condensation and Evaporation in a Sandy Column. SSSAJ.

Simunek, J., & Suarez, D. L. (1994). Two-dimensional transport model for variably saturated porous media with major ion chemistry. Water Resources Research., Vol.30, N. 4, 1115-1133.

Simunek, J., Genuchten, M. T., & Sejna, M. (2006). The HYDRUS Software Package for Simulating the 2D/3D Movement of Water, Heat and Multiple Solutes in Variably Saturated Media Technical Manuel. Prague: PC Progress.

Šimůnek, J., Šejna, M., Saito, H., Sakai, M., & Genuchten, M. T. (2013). The HYDRUS-1D Software Package for Simulating the One-Dimensional Movement of Water, Heat, and Multiple Solutes in Variably-Saturated Media., Version 4.17, California.

Stankovich, J. M., & Lockington, D. A. (1995). Brooks-Corey And Van Genuchten Soil-Water-Retention Models. Journal Of Irrigation And Drainage Engineering, 121: 1-7.

Suarez, D. L., & Simunek, J. (1993). The UNSATCHEM-2D code for simulating two dimensional variably saturated water flow, heat transport, carbon dioxide transport, and solute transport with major ion equilibrium and kinetic chemistry. Riverside, CA: U.S. Salinity Lab.

TAGEM. (2017). Türkiye'de Sulanan Bitkilerin Bitki Su Tüketimleri. Ankara.

Truesdell, A. H., & Jones, B. F. (1974). Wateq, a computer program for calculating chemical equilibria of natural waters. Journal of Research of the U.S. Geological Survey, 233-248.

Valiantzas, J. D. (2011). Combined Brooks-Corey/Burdine and van Genuchten/Mualem Closed-Form Model for Improving Prediction of Unsaturated Conductivity. Journal Of Irrigation And Drainage Engineering, 223.

van Bavel, C., & Hillel, D. I. (1976). Calculating potential and actual evaporation from a bare soil surface by simulation of concurrent flow of water and heat. Agricultural Meteorology,Vol. 17, 453-476.

Wang, C., & Yang, K. (2018). A New Scheme for Considering Soil Water-Heat Transport Coupling Based on Community Land Model: Model Description and Preliminary Validation. Journal of Advances in Modeling Earth Systems,10, 1-24.

Whitaker, S. (1985). Flow in Porous Media I: A Theoretical Derivation of Darcy's Law, Transport in Porous Media 1, D. Reidel Publishing Company, 3-25.